Downloaded from orbit.dtu.dk on: Aug 22, 2022

DTU Library

Positron lifetimes in water and ice, and in frozen aqueous solutions

Eldrup, Morten Mostgaard

Publication date:
1971

Document Version
Publisher's PDF, also known as Version of record

Link back to DTU Orbit

Citation (APA):
Eldrup, M. M. (1971). *Positron lifetimes in water and ice, and in frozen aqueous solutions*. Risø National Laboratory. Denmark. Forskningscenter Risoe. Risoe-R No. 254

General rights
Copyright and moral rights for the publications made accessible in the public portal are retained by the authors and/or other copyright owners and it is a condition of accessing publications that users recognise and abide by the legal requirements associated with these rights.

- Users may download and print one copy of any publication from the public portal for the purpose of private study or research.
- You may not further distribute the material or use it for any profit-making activity or commercial gain
- You may freely distribute the URL identifying the publication in the public portal

If you believe that this document breaches copyright please contact us providing details, and we will remove access to the work immediately and investigate your claim.

Risø Report No. 254

Risø Report No. 254

Danish Atomic Energy Commission

Research Establishment Risø

Positron Lifetimes in Water and Ice, and in Frozen Aqueous Solutions

by Morten Eldrup

November 1971

Sales distributors: Jul. Gjellerup, 87, Sølvgade, DK-1307 Copenhagen K. Denmark

Available on exchange from: Library, Danish Atomic Energy Commission, Risø, DK-4000 Roskilde, Denmark

U.D.C.
539.124.6:539.189.2:546.212

Positron Lifetimes in Water and Ice, and in Frozen Aqueous Solutions*)

by

Morten Eldrup

Danish Atomic Energy Commission
Research Establishment Risø
Chemistry Department

and

Laboratory of Applied Physics II
Technical University of Denmark
Lyngby

Abstract

An introduction to the subject is given, the principle of lifetime measurements is discussed and the experimental apparatus described. A computer program used for data analysis is described and the problems involved in the analysis discussed. All lifetime spectra are resolved into three components. For H_2O the long lifetime, attributed to ortho-positronium, is 0.68 nsec in ice between -196°C and -100°C, increases to 1.12 nsec at 0°C and abruptly to 1.86 nsec upon melting. Its relative intensity is 52% in ice and 27% in water. Spectra for heavy ice are identical with those for light ice, whereas heavy water gives 2.01 nsec, 22%. The increase in lifetime in ice above -100°C is attributed to trapping of positronium in temperature-created defects. Spectra for frozen aqueous solutions of concentrations above 10^{-7} mole fraction contain at -160°C a long-lived component attributed to the trapping of positronium. Very good agreement with the trapping model is obtained for HF solutions, both fast frozen and annealed. An irreversible change in the spectrum takes place by heating a fast frozen HF solution above approx. -125°C.

*) This report is submitted to the Technical University of Denmark in partial fulfilment of the requirements for obtaining the lic. techn. (Ph. D.) degree.

ISBN 87 550 01 25 4

CONTENTS

Page

Page

1. INTRODUCTION

1.1. Annihilation of the Positron

The story of the introduction of the positron into the world of physics known to man is one of the many exciting ones in modern physics. It is the story of a theoretical development and of carefully analysed and interpreted experiments, which both, completely independently, lead to the same conclusion, the existence of a "positive electron"[1].

Already in 1926 Gordon and Klein had formulated a relativistic quantum mechanical theory, but it gave solutions with negative energy for the electron[2]. Dirac in 1928 removed another difficulty of the Klein-Gordon equation: its dependence on time in a nonlinear way, but the problem of the negative energy solutions for the electron still existed in Dirac's equation[3]. Such solutions could be associated with positive particles, and Dirac tried to combine them with the properties of the proton, the only positively charged elementary particle known at that time, but it was soon shown that the solutions had to be connected with particles with a mass like that of the electron. Some attempts were made to construct theories which did not contain the negative energy solutions, but they failed. So in 1930, Dirac postulated his famous "hole" theory, stating the possible existence of what would seem to be a positive electron, namely a missing negative electron in the otherwise filled infinite number of electron states with negative energy[4].

In the years around 1930, many investigations were carried out with Wilson chambers in order to study the different reactions which high-energy cosmic radiation might undergo with matter. In a magnetic field, the tracks of charged particles were curved in the chamber in such a way that it was possible to distinguish positive particles from negative ones (e. g. protons from electrons, which were the only charged particles believed to exist at that time). Furthermore, by studying the ionisation produced by each particle in the chamber, it was possible to estimate its energy and mass. Sometimes tracks were seen, however, that did not fit into the accepted picture accounting for the behaviour of protons and electrons. Such tracks were always rejected as "spurious" or "dirt effect", or, on a few occasions, as electrons "curving the wrong way", "coming up from the floor" or "moving backwards". In 1932, however, after a careful analysis of a photographic plate Anderson came to the conclusion that the track observed must originate from a positive particle, the mass of which was much closer to that of the electron than to that of the proton[5].

This observation was a pure experimental result. Anderson did not know the theory of Dirac, and not until the beginning of 1933, in a paper by Blackett and Occhialini[6], which gave further experimental evidence of positive electrons, was it demonstrated that the experimentally observed properties of the new particle were those predicted by the Dirac theory. This beautiful harmony between theory and experiment swept away nearly all doubt. The existence of the positron was established.

As shown in Dirac's theory, an electron with positive energy may fall down in a "hole" in the "sea" of electrons with negative energies. Thus both the electron and the positron (or "hole") disappear emitting as γ-quanta the transition energy:

$$E = 2m_o c^2 + E_+ + E_-$$

where $m_o c^2$ is the rest mass energy of an electron or positron (= 0.511 MeV) and E_+ and E_- are the kinetic energies of the positron and the electron. This process is called annihilation of the electron and the positron. The properties of the γ-quanta depend upon the electron - positron state at annihilation. Information may therefore be gained about this state by investigating the annihilation photons. The number of photons emitted are limited in several ways. Firstly, the probability of a certain number of photons being emitted decreases rapidly when this number increases. On the other hand, emission of only one photon requires a third body to take part in the process in order to conserve momentum, and this leaves only annihilation with emission of two or three γ-quanta to be significant. Due to conservation of charge parity in the annihilation process, further limitations are imposed on the number of photons emitted. If the spins of the annihilating particles are antiparallel, only an even number of photons (e.g. 2γ annihilation) can be emitted. If the spins are parallel, only an odd number (e.g. 3γ annihilation) can be emitted. (These statements are not strictly correct since some annihilation processes which are normally of very low probability have been ignored, viz. processes in which the orbital quantum number $l \neq 0$). The rate of annihilation is for low positron and electron energies directly proportional to the electron density felt by the positron[7].

When 2γ annihilation is taking place at low energies, the two quanta, each with an energy of 0.511 MeV, will be emitted in almost opposite directions in order to conserve momentum. The deviation, θ, from the angle π is determined by

$$\theta \simeq \frac{p}{m_o c} ,$$

where p is the total momentum of the annihilating pair perpendicular to the direction of photon-emission, c the velocity of light, and m_o the electron rest mass.

When a positron enters a condensed material it will be slowed down by ionising the molecules and by exciting the electrons and the molecular vibrations. Usually it reaches thermal or nearly thermal energies before annihilating. The slowing down time is generally assumed to be less than 10^{-11} sec.[7,9].

The subsequent annihilation can take place from different states of the positron. It may annihilate as a free particle (free annihilation) or from some bound state within a molecule or a defect, or it may annihilate from a state where it is bound to one electron only.

This bound state is the so-called positronium atom. The positron mean lifetime is for all states, except for the positronium state (and maybe some defect states), of the order of 10^{-10} sec to $5 \cdot 10^{-10}$ sec. The positronium lifetime may be several nanoseconds (1 nsec = 10^{-9} sec) as described in the next section.

The theory of the annihilation process comes within the Quantum Electrodynamics field[10]. The characteristics of the annihilation process are summarized in ref. [7].

1.2. Positronium

The positronium atom is a bound state of an electron and a positron. It is an analogy to the hydrogen atom, only that the proton is replaced by the positron. This again means that it is treated quantum mechanically in lowest order like a hydrogen atom with a reduced mass of $\frac{m_o}{2}$.

The binding energy in the ground state will then be equal to half of that of the hydrogen atom:

$$E_B = 6.8 \text{ eV}.$$

The radius in the relative movement of the electron and the positron is the double of the Bohr radius, resulting in a diameter of the positronium atom like that of the hydrogen atom (1.06 Å).

A chemical symbol, Ps, has also been proposed for the positronium atom, and is now generally accepted.

The positronium ground state splits into two different states:

1) The singlet or para state (p-Ps), where the spins of the electron and the positron are antiparallel. This gives for the angular momentum the quantum numbers $J = 0$ and $m = 0$.

2) The triplet or ortho state (o-Ps), where the spins of the electron and the positron are parallel. This state has $J = 1$ and is divided into three substates with $m = -1, 0, +1$.

Having antiparallel spins, p-Ps can only undergo 2γ-annihilation. For the free p-Ps, the mean lifetime is $1.25 \cdot 10^{-10}$ sec.

The free o-Ps on the other hand can only undergo 3γ-annihilation with a mean lifetime of $1.4 \cdot 10^{-7}$ sec.

The energetical conditions for the formation of Ps in a gas are described in the so-called Ore gap model[11]. A highly energetic positron will be slowed down primarily by ionisation of the gas. When its energy reaches values below the ionisation potential (V), the slowing down will take place with electronic excitation of the molecules, slowing down having higher probability than Ps-formation. Below the lowest excitational level (E^x), elastic collisions and excitation of vibrations in the molecules are responsible for the slowing down. In this energy region the Ps formation probability is higher than the slowing down probability, but when the positron reaches energies below V-6.8 eV, Ps formation is energetically impossible, since the kinetic energy of the positron plus the Ps binding energy is not sufficient to overcome the binding energy of the electron in the molecule. Hence only positrons with energies in the interval between E^x and V-6.8 eV can form Ps. This interval is known as the Ore gap.

In condensed materials the affinities of the positron and the Ps in the materiel should be taken into account. These quantities are difficult to estimate, and thus the value of the model is reduced in such cases. In some solids (metals, and maybe ionic crystals), no Ps has been observed. This has been correlated with the reduction of the Ore gap to zero[12].

When Ps is formed in a condensed material the ratio of ortho to para is assumed to be 3 to 1 (3 ortho states, 1 para state). The lifetime of the ortho state will be drastically reduced from that of free o-Ps owing to the so-called pick-off annihilation. This process takes place while the Ps moves around in the material frequently colliding with the molecules. During such collisions the positron wave function will overlap the wave function of the electrons of the material. This gives a high probability for the positron of annihilating with an electron that has opposite spin, under the emission of

2 γ-quanta. This pick-off reduces the o-Ps lifetime to a few nanoseconds or less.

If the o-Ps is trapped in some region of the material with more space (i. e. smaller electron density), the pick-off will be reduced and the lifetime increased.

Other processes may reduce the lifetime of o-Ps. Paramagnetic species may cause conversion, i. e. the spin of one of the particles in o-Ps is flipped changing the o-Ps to p-Ps followed by rapid annihilation. Like other atoms, Ps may take part in chemical processes, such as oxidation of Ps to free positrons or formation of a compound with another atom (e. g. PsCl). In such cases the lifetime of o-Ps will be reduced. o-Ps is said to be quenched.

When a magnetic field is applied to Ps, a mixing will take place between the para and the ortho state with m = 0. This results in an increase of the shorter Ps lifetime and a decrease of the longer one. Furthermore the total number of Ps-atoms annihilating from the para state will increase. This phenomenon is called magnetic quenching of Ps.

The subjects dealt with in this paragraph are treated in considerable detail in refs. 7 and 13.

1. 3. Experimental Techniques

In all the experimental techniques described here, a radioactive material emitting positrons is used as positron source. The most commonly used is Na^{22}, which has a half-life of 2. 6 years. Its decay scheme is shown in fig. 1.

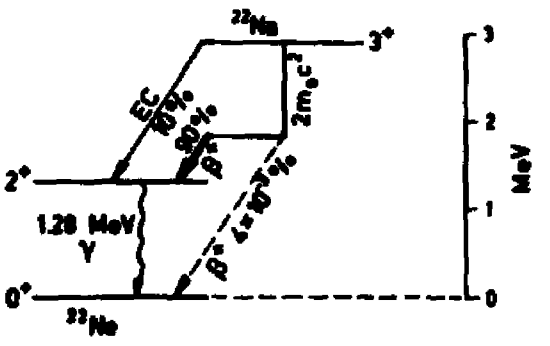

Fig. 1. Decay scheme of Na^{22}.

The two most commonly used experimental techniques are the positron lifetime technique and the angular correlation technique. Also used are the techniques of measuring the 3 γ-annihilation rate, and in a few cases the Doppler broadening of the 0.511 MeV annihilation line caused by the velocity of the annihilating pair has been measured.

1.3.1. Positron Lifetime Technique

In the positron lifetime technique a so-called delayed coincidence technique with two detectors is used. One detector records the birth of the positron by detecting the pratically simultaneous emission of a 1.28 MeV quantum from the Na^{22}-source. The other detector records the moment of annihilation by detecting one of the annihilation quanta. The time difference between the two events is the positron lifetime. This time difference is converted into an electric signal, the height of which is proportional to the time difference. The height of the signal is analysed and stored in a multi-channel analyser. In this way, distribution of the lifetimes of positrons is obtained, the so-called lifetime spectrum.

If positron lifetime was governed by one single annihilation rate, the lifetime spectrum recorded would be a single decaying exponential function (a straight line in a semilogarithmic plot). However, on account of the different possible annihilation processes, the spectrum will often consists of a sum of several exponentials. Such a spectrum is shown in figs. 13, 15, and 16. The component with the longest lifetime is normally ascribed to annihilation of o-Ps, while the short-lived components are due to free annihilation and p-Ps annihilation. The ratio between the area under each component and the total area is the relative intensity of the component. The positron lifetime technique will be described in more detail in the next chapter.

1.3.2. Two-Photon Angular Correlation Technique

In a two-photon angular correlation set-up the angular correlation between the photons from a 2γ-annihilation is measured. The principle of this technique is shown in fig. 2. The distance from the sample to the two detectors is typically 2 m. One detector is fixed, the other can be turned by a small angle, θ, and the number of coincident photons is then measured as a function of θ. If θ is different from zero the sum of the momenta of the two coincident photons, $\bar{k} = \bar{k}_1 + \bar{k}_2$, must be different from zero. If momentum is conserved at the annihilation, $\bar{k}$ is equal to the momentum $\bar{q}$ of the centre of mass of the annihilating electron-positron pair. Since the

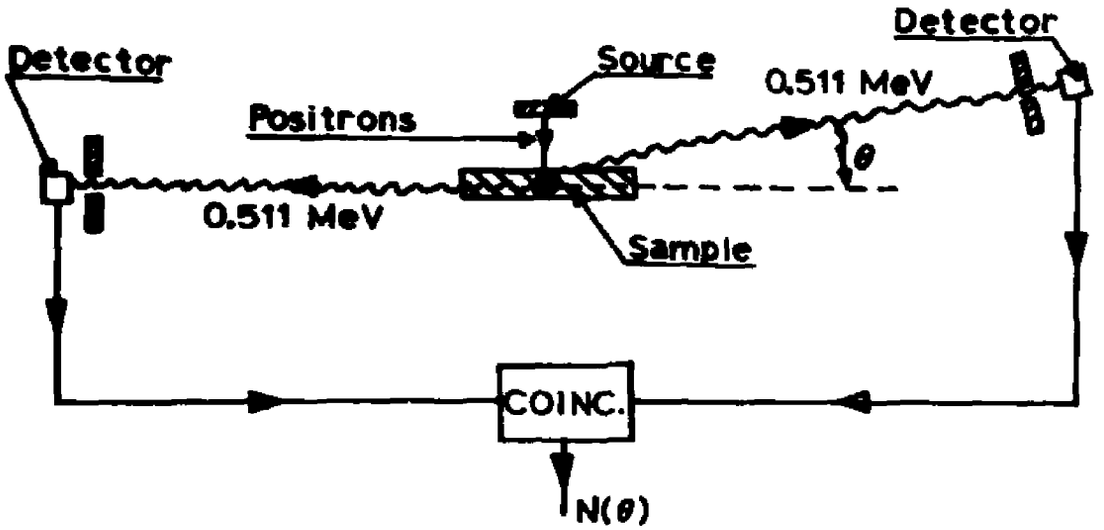

Fig. 2. Principle of typical angular correlation equipment. The number of coincidences, N (θ) between annihilation γ-quanta recorded by the fixed detector (left) and by the movable detector (right) is measured as function of the angle θ .

effective detector areas are usually long slits of a width approx. 1 mm (perpendicular to the plane of the drawing, fig. 2), the component of $\bar{k}$ perpendicular to the slits, say k_z, is measured. Hence:

$$\theta = \frac{k_z}{m_0 c} = \frac{q_z}{m_0 c} .$$

In most cases, the positron will be thermalized before annihilation, while an annihilating electron which is bound in the material (free and pick-off annihilation) will have a kinetic energy of the order of 5 eV. Thus $\bar{q}$ will, in a good approximation, be the momentum of the electron. This will give rise to a broad component in the angular correlation curve of a width of 5-10 mrads.

In cases where p-Ps is thermalized before it annihilates, this will give rise to a very narrow component in the curve (width of the order of 1 mrad).

If the annihilation takes place in a crystal where the positron or electron (or both) feel the periodic potential, it can be shown that a sum of the crystal momentum and a reciprocal lattice vector is conserved[16].

The different features of an angular correlation curve are seen on the curve for monocrystalline ice, shown in fig. 3. The angular correlation technique is described in detail in ref. 14.

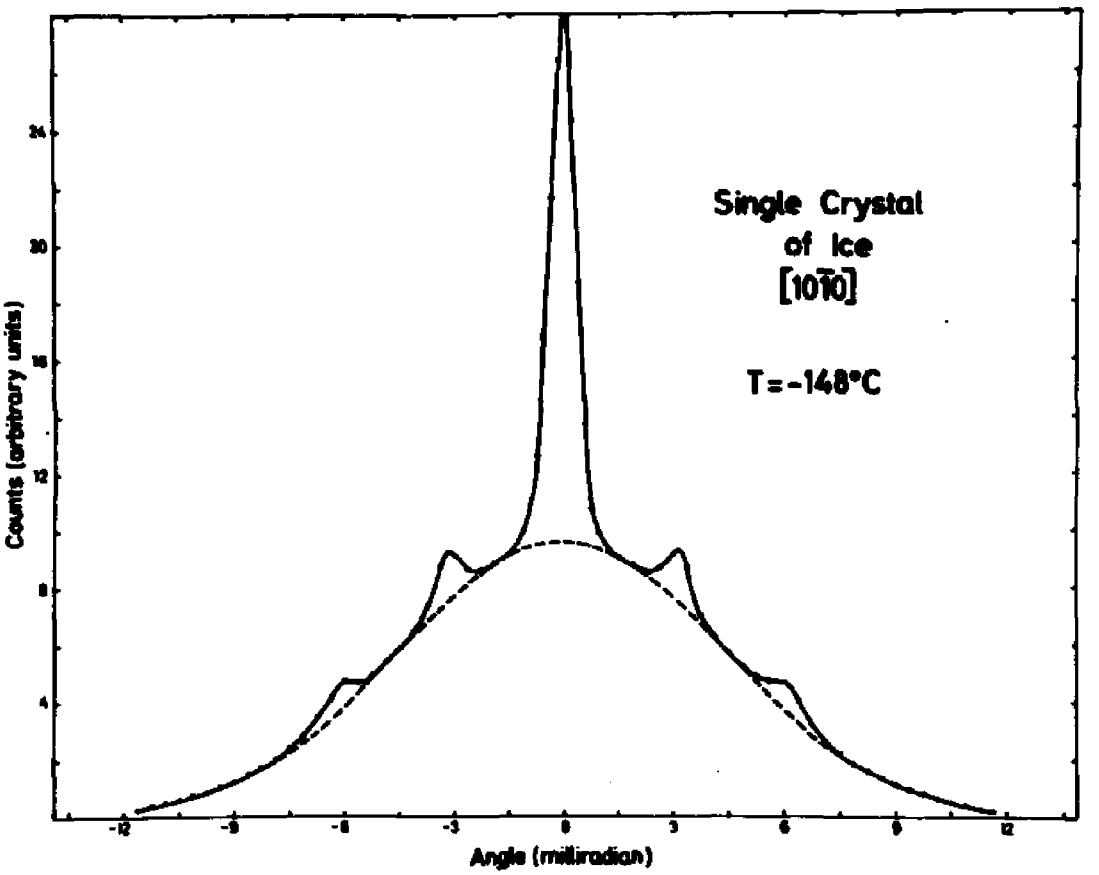

Fig. 3. Angular correlation curve for an ice monocrystal oriented with the [10$\bar{1}$0] axis along the z-direction. The broad component (shown by the broken line) is due to annihilation of "free" positrons and pick-off annihilation of o-Ps. The narrow components are caused by annihilation of p-Ps, the small side peaks being shifted with respect to the central peak by angles equivalent to projections of reciprocal lattice vectors on the z-direction.

1.3.3. 3γ-Annihilation Technique

3γ-annihilation has been detected by means of three detectors, normally placed around the sample with 120° between them and connected to a coincidence circuit. This technique results in one figure only, namely the 3γ-coincidence rate, which in principle may be deduced from lifetime measurements. This fact and the experimental difficulties (e.g. long counting times) are probably the reason why the 3γ-annihilation technique has not been used very much.

1.4. Previous Measurements on Ice and Water

Several review articles about positron annihilation exist, viz. references 7, 8, 12, 13, 15, and chapter 26 in reference 17. In ref. 7, the most recent one, around 300 references are listed, and the same book also contains a table of positron annihilation data for most of the substances investi-

gated up till 1967[79]. Reference 8 is the proceedings of the first international positron conference, held in Detroit in 1965, and ref. 81 a collection of papers presented at the second one, held in Kingston, Canada, in 1971.

Water, in its liquid and solid form, is probably the substance which has attracted more attention than any other in positron annihilation work, mainly because the experimental results have very often been in disagreement with theory or expectations based on experimental results from other substances. Some of the disagreements have been settled through new experiments; however, water and ice still give rise to many unsolved questions.

The first experimental results were found in 1953 by Bell and Graham[18]. Their experiments showed, when going from ice to water, that the long lifetime increased, viz. from 1.2 nsec at -7°C to 1.7 nsec at 20°C. In ice at liquid nitrogen temperature (-196°C), they found a lifetime of 0.85 nsec. They estimated the intensity of the long-lived component which they attributed to annihilation of o-Ps, to be near to 1/3 for all temperatures.

Wagner and Hereford[19] in 1955 measured 3γ-annihilation rates, and found in ice a linear rise with temperature of around 60% going from 4°K to the melting point, but a constant value in water up to room temperature, the value being the same as in ice just below the melting point.

de Zafra and Joyner in 1958[20] measured angular correlation curves for water and ice from -150°C to 90°C and found an unusually narrow component in the ice. They concluded that with certain assumptions the effect of temperature on the measured curves could be explained as from the change of density with temperature. They also pointed out that since the 3γ-annihilation rate, $R_{3\gamma}$, is constant over the ice-water phase transition[19], an anomaly must exist in either the lifetime of o-Ps, τ_2, or its intensity, I_2, at that transition. It can easily be shown that $R_{3\gamma} \propto I_2 \times \tau_2$, which results in an increase in I_2, if τ_2 decreased upon melting, or vice versa. However, since water is denser than ice, the τ_2 should be expected to be smaller (more overlap between electrons and the positron) in water, and so should the I_2 (less space for Ps, therefore less formation probability).

Brandt, Berko and Walker[21] in 1960 put forward a simple, quantitative model to explain the increase of τ_2 with temperature observed in molecular substances. The idea was the same as that mentioned above: the expansion of a substance with rising temperature would leave more free space for Ps and thus reduce the overlap between the positrons and the electrons of the substance. The reduced overlap decreases the pick-off rate, which means an increase of τ_2. This model, which is known as the "free volume model" or "excluded volume model", was compared with measurements on ice and

water, and a reasonable agreement was found in ice. However, at the ice - water phase transition, the model shows a decrease in lifetime in contrast to the experimentally found increase (as qualitatively pointed out in ref. 20).

A magnetic quenching experiment was carried out by Iaci, Quercia and Turrisi in 1962[22]. They compared angular correlation curves for ice and water with and without a magnetic field of 15 kGauss and concluded that in water an enhancement of the narrow component took place when the field was applied. This is what could be expected due to the increased annihilation rate from the para state in a magnetic field, but this effect was not found in ice.

Wilson, Johnson and Stump[23] in 1963 investigated positron lifetime as functions of pressure up to 6000 atm. for several molecular substances in order to separate a possible temperature effect from the density effect owing to the change of density with temperature. The result was in all cases that the long lifetime decreased with increasing density at constant temperature. The magnitude of the change ranged from 2.5% for water to 6.8% for glycerine for a 1% change in density. Furthermore, it was observed that the intensity of the long lifetime was independent of density in liquids but decreased with decreasing density in solids. One of the effects of increasing the temperature, apart from the pure density effect, was a decrease of the long lifetime, a fact which is in agreement with the well-known phenomenon that higher temperatures increase reaction rates. A simple theory was put forward that reproduced the effect of density and temperature.

Fabri, Germagnoli, Quercia and Turrisi[24] made a more detailed search for the effects of the water - ice phase transition on the lifetime spectrum than the one mentioned in ref. 18. Their results show a continuously increasing τ_2, from 1.0 nsec at -20°C to 1.7 nsec at +20°C and decreasing I_2 from around 40% to around 30% in the same temperature interval. The product $I_2\tau_2$ varied in agreement with the 3γ-annihilation rate found in ref. 19. In the same paper the results of a magnetic quenching experiment were reported for the lifetime spectrum of water. They showed a stronger influence of the field than expected for free Ps.

Fabri, Poletti and Randone[25] looked for the influence of the magnetic field on the intensity of the 0.511 MeV photopeak in the γ-spectrum from annihilation in water. Again a stronger effect of the field was found than expected for free Ps.

The authors of ref. 24 and Iaci reported at the Detroit conference (ref. 8 pg. 357) that lifetime magnetic quenching experiments on liquid D_2O were found to be in agreement with theory and that preliminary measurements on

H_2O showed agreement too. The agreement was found in 1968 by Iaci, Lo Savio and Turrisi[26], to be nearly complete. They considered the earlier findings had been affected by impurities.

In the meantime a remarkable result was found in the angular correlation measurements of Colombino, Fiscella and Trossi[27] on ice and water. They demonstrated again the very narrow component in ice, but found that it only existed below around -25°C and that above approx. -18°C the component was considerably broader. Thus the curve narrowed continuously but very rapidly with decreasing temperature in the interval from -18° to -25°C. Furthermore it was found that for angles larger than 4 mrads all curves coincided, and that the narrow peak observed in ice at -4°C disappeared in water at +4°C.

The water - ice phase transition was re-examined in lifetime measurement by Jauho and Virnes[28], who found a discontinuity in both τ_2 and I_2 at +4°C, in ice being 1.1 nsec and 42%, and in water 1.9 nsec and 24%. The product $I_2 \tau_2$ was found constant over the transition in agreement with ref. 19.

Recently, Colombino and Fiscella[29] found by angular correlation magnetic quenching measurements, that both in water and ice magnetic quenching does take place and that its magnitude is in agreement with the theory.

Finally, in a paper by Mogensen, Kvajic, Eldrup, and Milosevic-Kvajic[42] it was demonstrated that angular correlation curves for ice single crystals, apart from the narrow central peak, possessed narrow side peaks at angles equivalent to reciprocal lattice vectors for the ice crystal (fig. 3). This was explained as evidence for Ps being delocalized in ice.

The present work was initiated as an attempt to solve some of the problems raised by the previous experiments. This aim has to some extent been attained but new problems have arisen and remain to be solved.

2. EXPERIMENTAL APPARATUS

2.1. Principle of Lifetime Measurements

2.1.1. Fast-Slow Delayed Coincidence

Measurements of positron lifetimes are generally performed by means of the so-called fast-slow delayed coincidence technique known from Y-ray spectroscopy. (R. E. Bell, chapter 12 in reference 17). A diagram of a typical set-up is shown in fig. 4.

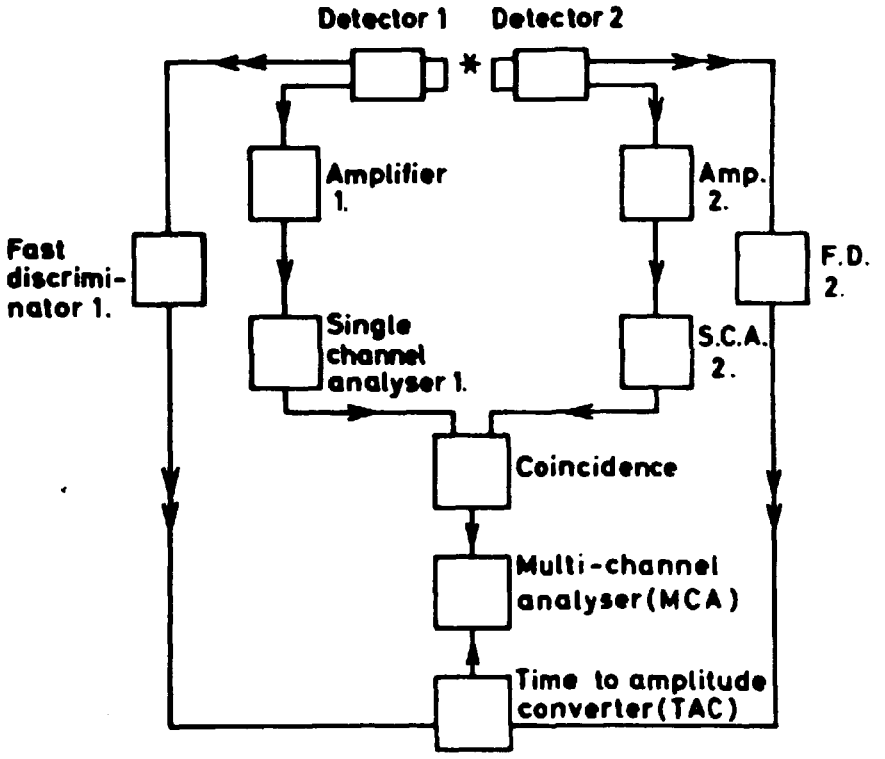

Fig. 4. Diagram of typical equipment for measuring positron lifetimes.

When positron lifetimes are measured, the situation is the following: Very short time (less than 10^{-11} sec) after the emission of the positron, a Y-quantum of 1.28 MeV is emitted (see fig. 1), and on annihilation two quanta of 0.511 MeV are emitted. The problem to be solved is then to detect one quantum of the first kind and one of the second that both are associated with the same positron, and to determine the time difference between their emissions. This is accomplished by using two circuits, one - the energy selecting or slow circuit - ensures that the Y-energies are correct, the other - the timing or fast circuit - records the difference in time between the two quanta.

Each detector consists of a scintillator mounted on a photo-multiplier tube (PM). The scintillator when absorbing a Y-quantum emits light; the light produces from the cathode of the PM a current of electrons that is amplified by the PM. The PM anode signal is used for the fast circuit (marked with double arrows in fig. 4) and is fed into a fast discriminator (FD), the output from which is produced at the very moment when the input signal exceeds a certain discriminator level. This output is fed into one input of the time to amplitude converter (TAC), the other input of which is similarly connected to the other FD. The output of the TAC is a pulse, whose amplitude is proportional to the time difference between the two input signals. This amplitude is analysed and stored in a multi-channel analyser (MCA). In this way the channel number in the MCA becomes proportional to the time difference between the two Y-quanta recorded by the detectors, and the number stored in each channel is the number of events recorded with a certain time difference. (In the positron case, the number of positrons that have lived a certain time).

Now, the energy resolution of the scintillator crystals used in detectors for measurements of small time periods is normally very poor. Hence Y-quanta of a single energy produce output pulses from the detector, the amplitudes of which may cover a wide range (for instance from zero up to a value corresponding to the Compton edge). Because of the finite rise time of the pulses, different amplitude pulses will reach a fixed discriminator level at different times, thus introducing an uncertainty in the time determination. This effect is shown in fig. 5. If, however, only a narrow amplitude range of the output pulses is used, this uncertainty can be greatly reduced. This can be done by means of the slow circuit.

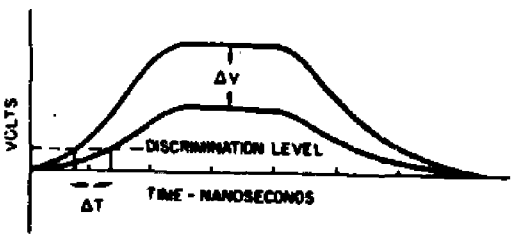

Fig. 5. Uncertainty in time determination caused by differences in pulse height.

In that circuit the pulses from a detector are amplified and then fed into a single channel analyser (SCA) that produces an output pulse only when the

input amplitude lies within certain limits (the so-called window of the SCA). The window of the SCA is then placed in the Y-spectrum from the detector in such a way that it comprises the part of the spectrum which is due to the Y-quanta to be detected (say for SCA1 just below the compton edge of 1.28 MeV and for SCA2 just below that of 0.511 MeV) and secondly is made sufficiently narrow to give a reasonably small time uncertainty.

The two SCA outputs are fed into a coincidence circuit, whose output is used for opening a gate in the MCA which permits the TAC-output to be analysed and stored. In this way only those output pulses from the TAC are recorded that originate from outputs from the detectors with acceptable properties.

2.1.2. Time Resolution

The time resolution of a system like that just described is normally defined as the full width at half maximum (FWHM) of the curve (the so-called prompt curve) obtained from a source emitting two Y-quanta simultaneously (Co^{60} is mostly used). Also the slope of the sides of the prompt curve as given by the apparent half life, $\tau_{1/2}$, is often used to describe the prompt curve. Such a curve is shown in fig. 7.

Several theoretical and experimental investigations have been carried out to clarify the role of different parameters for the time resolution. The most important factors are the width of the light pulse generated by a Y-quantum in the scintillator, the time spread in the collection of this light on the photo-cathode of the PM caused by the finite geometrical size of the scintillator, the transit time spread of pulses travelling from the photo-cathode to the anode of the PM, and the time spread in the rest of the electronic system, the last one mainly from the fast discriminators. All factors mentioned tend to broaden the prompt curve, but a continuous development of faster scintillators and PM-tubes and of better discriminator units steadily reduces the optimal width of the prompt curve that can be obtained.

The different experiments and most of the theories show, in contrast to what one might expect (from fig. 5 for instance), that the optimal discriminator level for the FD is not the lowest possible but is, in most cases, of the order of one tenth of the full amplitude of the pulse. It is also of importance that the more photo-electrons that are produced on the cathode of the PM, i. e. the more light that is produced in the scintillator, the better is the time resolution. The windows of the SCA should, therefore, always be set at the largest possible energies. These problems are treated in review papers by Schwarzschild[30] and by Gatti and Svelto[31]. They also

describe different techniques used to increase the counting rate without decreasing the time resolution. The theory of Hyman[32] has been confirmed by the experiments of Bengtson and Moszynski[33].

2.1.3. Characteristics of a Measured Spectrum

A measured spectrum will normally consist of one decaying exponential function or the sum of a few of these functions somewhat smeared out on account of the finite time resolution and added to a constant background of random coincidences. The decay constants of the exponentials are in the case of positron lifetime measurements the annihilation rates of the different possible annihilation processes, and they (or their reciprocals: the lifetimes) are normally the subject of interest together with the intensities of the different exponentials (i. e. the relative area under each exponential curve). The random background is due to the fact that two positrons may annihilate within such short time interval that they may be recorded as being caused by the same event. The random background counting rate in each channel in the MCA, N_R, can easily be seen to be:

$$N_R = \tau N_1 N_2 = \tau \varepsilon_1 \varepsilon_2 N_o^2 ,$$

where τ is the time interval equivalent to one channel, N_1 and N_2 the counting-rates in detector 1 and 2 respectively (including the single channel analysers), ε_1 and ε_2 the efficiency of these detectors and N_o the source strength. Since the number of counts per sec in each channel associated with the annihilation of only one positron (true coincidences), N_T, is proportional to the source strength, we have

$$\frac{N_R}{N_T} \propto N_o .$$

Thus the background to peak ratio increases proportionally to the source strength.

2.2. Description of the Measuring System

The present work was carried out at the Laboratory of Applied Physics II, of the Technical University of Denmark (LTF II), and at the Chemistry Department, of the Danish Atomic Energy Commission Research Establishment Risö. The experimental set-ups used at the two institutes were almost identical; only the multi-channel analysers and a few other components were different, but their functions were the same in the whole system.

Therefore, only the system used at Risö will be described here. The principle of the system is shown in fig. 4.

As scintillators were used NE111 from Nuclear Enterprise of the dimensions 1" high and 1" in diameter. NE111 was compared with the widely used Naton 136 in reference 33 and found superior to the latter. Its emission spectrum is in the violet and ultraviolet, and in order to take advantage of this fact the PM tube with a quartz window was chosen, namely the tube XP1023 from Philips, which is believed to be the fastest tube currently available. The scintillators were coupled to the PM tubes with silicone oil MS200 from Midland Silicones Ltd., and on the outer surfaces they were covered with titanium dioxide (NE 560 from Nuclear Enterprise). Scintillator and PM were covered with a magnetic shield and connected with the Ortec PM-base model 267. The output to the fast circuit was taken directly from the anode and that to the slow circuit from dynode No. 10 (XP 1023 contains 12 dynodes) of the PM. Adjustment of the potentials of the anode focusing grid and the cathode focusing grid was done to maximize the output amplitude of the detectors at a fixed high voltage. Two Ortec models 446 fixed at 2.2 kV supplied the high voltage for the detectors. As fast discriminators were used Ortec model 417 with discriminator level at 150 mV. The Ortec model 437A set at its highest sensitivity performed the time to amplitude conversion.

Detector output pulses to the slow circuit were amplified by two stages: first by a pre-amplifier, Ortec model 113, close to the detector, and then by the main amplifier, Ortec model 440A. The single channel analysers used were Canberra model 1437. The setting of the SCA windows is shown in fig. 6. The coincidence circuit was that of Ortec, model 414A. 60 nsec was used as resolution time. The standard output pulses from the coincidence unit were shaped to a suitable amplitude and duration in a separate unit to meet the requirements of the gate input of the MCA.

The multi-channel analyser was a Nuclear Data 2200 system with 4096 channels, which could be divided up into a maximum of 16 subgroups. 512 channels were used for recording the spectra. Accumulated data output was received on paper tape via a tally puncher. Spectra stored on paper tape could be read into the memory of the MCA via a tally reader. A tektronix oscilloscope, type RM 503, connected to the MCA, was used for displaying the spectra. Furthermore, a direct visual comparison of different spectra could be accomplished by simultaneous displaying of the spectra, stored in different parts of the memory, on the oscilloscope.

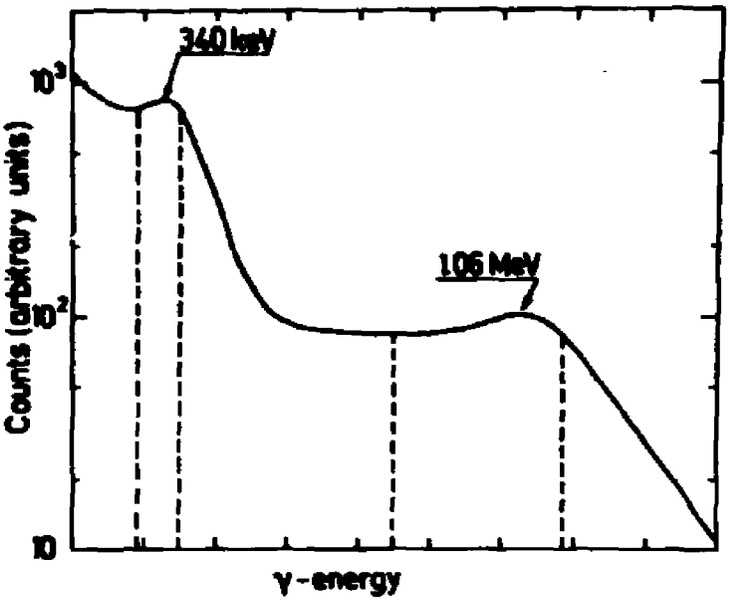

Fig. 6. γ-spectrum from a Na^{22}-source. The setting of the windows of the two single-channel analysers are shown by the broken lines. 340 keV and 1.06 MeV correspond to the Compton-edges for 0.511 MeV and 1.28 MeV respectively.

2.3. Discussion of the Measuring System

2.3.1. Time Resolution

As mentioned in section 2.1, the most important factors determining the time resolution of the system, once the scintillator and the PM are chosen, are the triggering level of the fast discriminators and the width of the windows of the single channel analysers. Any increase in high voltage of the detectors may in some cases increase the time resolution on account of the smaller time spread of the stronger accelerated electrons in the PM-tube. However, no such effect was found for voltages in a wide region (2 kV - 3 kV). Also the variation of the FD discriminator levels did not have any appreciable effect on the width of the prompt curve (FWHM), which shows that this width exhibits a rather flat minimum as a function of that level.

However, the setting of the SCA windows strongly affects the FWHM. With both windows placed at the Compton edge (around 930 keV) of the two γ-energies characteristic for Co^{60} (1.17 MeV and 1.33 MeV) with a width of approx. 20%, a FWHM of 315 psec was obtained. However, with the setting actually used for the Na^{22} source shown in fig. 6, the FWHM obtained was 427 psec. By decreasing the width of the windows, this number could have been somewhat reduced, but this would entail a reduction of the number of coincidences. The chosen widths are thus a compromise between these

two factors. The measured prompt curve is shown in fig. 7.

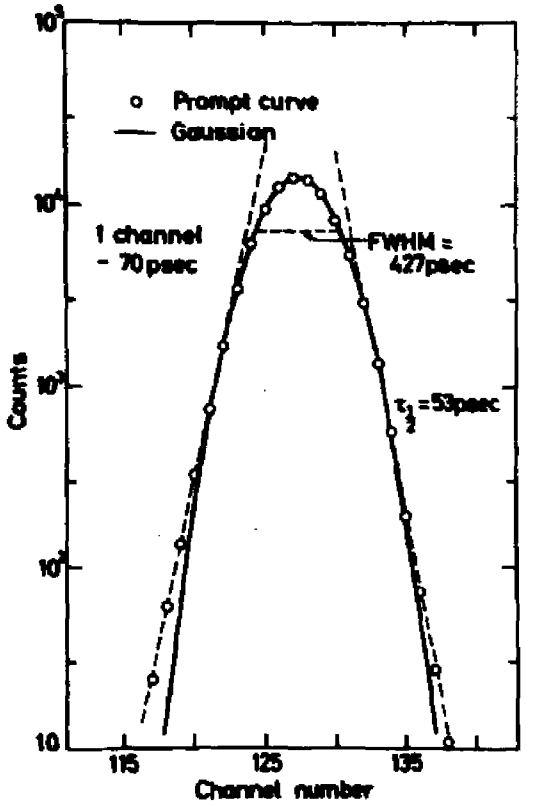

Fig. 7. A measured prompt curve. The full width at half maximum and the slope of the sides are given. Also the Gaussian used in the data analysis as an approximation to the prompt is shown.

2.3.2. Time Calibration

Time calibration, determination of the time equivalent to the width of one channel in the MCA, was done in two different ways. In one case was used the Ortec delay unit model 425, which makes it possible to insert delays from 1 to 32 nsec. The other method was based upon a special electronic unit that - controlled by a precision 200 MHz sinewave generator - produced pulses to the start and stop input of the TAC with time intervals that were multiples of 5 nsec.

Regarding the first method, two outputs from the same FD were connected to the TAC: one directly to the start input, the other via the delay to the stop input. By relating the channel number, in which the very narrow peak thus obtained (width around one channel) is positioned, to the delay inserted, calibration is performed. The result found was that for a delay of less than seven nsec the TAC gave no output at all, for delays up to around 12 nsec the relation between time and channel No. was nonlinear, whereas a linear relationship existed for larger delays. With the uncertainties for the delays quoted by Ortec, the time per channel found by this

method is 69.6 ± 1 psec. During measurements, in order to get the spectrum in the linear range, a 3 meter cable was inserted between the FD and the stop input of the TAC. Together with delays in other cables, a total delay of approx. 19 nsec between the start and stop pulses for a prompt event was obtained. By the second method a spectrum is produced consisting of peaks 5 nsec apart. The time per channel found in this way was 69.5 ± 1 psec. So throughout this work, one channel has been put equal to 70 psec.

The linearity can be checked in another way. If a radioactive source is placed at each detector, and the two detectors with sources are shielded against each other (e.g. by lead bricks), the spectrum recorded is only a a random background. Within the statistical uncertainty, the number of counts in each channel should be the same. Deviations from this are due to a nonlinear relationship between time and channel number. A plot of such a random background shows that the integral nonlinearity is around ± 1% for the whole range of channels used for spectrum analysis (Nos. 122 to 511). Since the essential part of the lifetime spectra in the present work is always contained in 200 channels or less, the effect of nonlinearity on the spectrum is less than ± 0.5%. Hence the time calibration used is believed to be correct to within ± 1.5%.

2.3.3. Stability

The stability of the system has been checked frequently during the period of measurements (approx. one year). Around every two weeks (at the beginning more frequently, later on when confidence in the stability had been gained less frequently) the γ-spectra from the detectors, the SCA windows, and the shape and position of the prompt curve were controlled. Corrections of the windows were only necessary two or three times.

One of the results of the spectrum analysis is the channel number equivalent to time equal zero (T_o) (the peak of the prompt curve). The number from the analysis always agreed with the figure found by direct measurement of the prompt curve. The drift of T_o was typically one tenth of a channel per day, and during the whole measuring period the drift never changed the number by more than 1 from channel number 127. The small variation of T_o directly demonstrates time calibration stability, since T_o is determined by the constant delay of 19 nsecs between the start and stop pulses. Calibration was directly checked a few times and found to agree with the first measurement. Furthermore, the spectrum of a saturated aqueous solution of $KMnO_4$ was recorded several times during the measuring period. It exhibited a single lifetime the value of which, as deter-

mined from the different spectra, agreed within 1%. This is further discussed in the next section and in appendix III. The high stability of the equipment was partly achieved by keeping the laboratory room temperature constant to within $\pm$ 1°C by a thermostat system.

2.3.4. Detector Positions

A deterioration of the spectra may take place if source and detectors are arranged co-linearly. In that case a "tail" will be added to the spectrum as sketched out in fig. 8. The reason is probably the following: since the

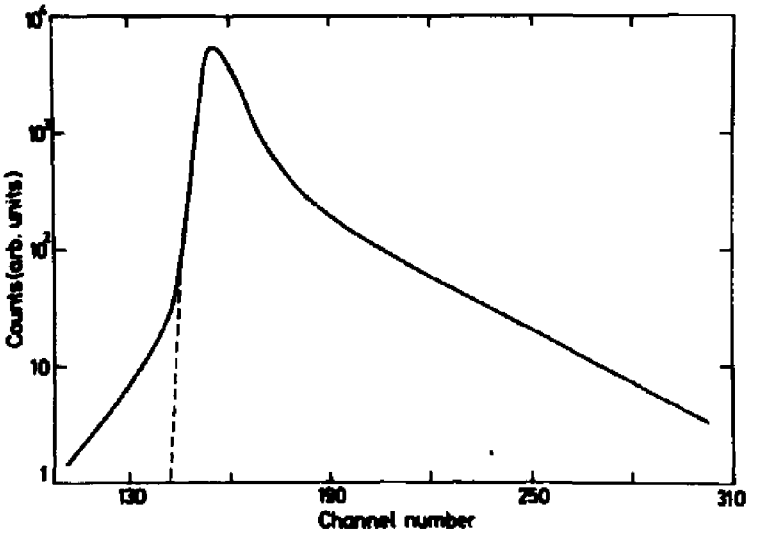

Fig. 8. Deterioration of a lifetime spectrum by a "tail" for "negative times" as obtained when source and detectors are arranged co-linearly.

two annihilation quanta are emitted in opposite directions and if one is detected by detector 2, there is a great probability that the other will be detected by detector 1 together with the Y-quantum of 1.28 MeV. Thus the pulse height condition determined by the SCA1 is not satisfied correctly, and this fact will result in a broadening of the lifetime spectrum. In order to avoid this effect, both detectors were placed somewhat above the source (fig. 12).

2.4. Positron Sources

As the source of positrons, the isotope Na^{22} was used in the form of NaCl sealed between two foils of Melinex (Mylar) in a so-called "sandwich-source". It was prepared in the following way: one or two drops of a $Na^{22}Cl$-solution were placed on the Melinex foil and the water then evaporated. The salt was surrounded by a layer of contact glue (ECC 776 from 3M was among

several others found to be the most suitable for the purpose), and similarly another piece of foil was glued leaving a circle free. After 20 minutes the two foils were assembled, and a square of approx. 1 x 1 cm^2 was cut around the source material. The thicknesses of the foils used were 6μ (approx. 0.8 mg/cm^2) or 9μ (approx. 1.2 mg/cm^2). These sources proved to be very stable mechanically. Several were made, and only one leaked after having been used for some time. The number of positrons annihilating in the foils (source annihilation) was found to be from 7 to 10 per cent of the total number annihilating. The source annihilation was determined by measuring the lifetime spectrum of a saturated aqueous solution of $KMnO_4$, which is known to exhibit only one lifetime of approx. 0.4 nsec. Since the spectrum of Melinex shows a long lifetime, that of the $KMnO_4$ solution will have a longlived component too with a relative intensity of a few per cent caused by source annihilation. Since the spectrum of the Melinex is known, the total source annihilation can be determined from this longlived component. This will be further discussed in appendix III. Since the source annihilation depends upon the material surrounding the source[34], the amount of source annihilation found is only fully correct for the $KMnO_4$ solution. However, as water molecules constitute nearly the whole of the solution (more than 99% of all molecules), it has been assumed that the source annihilation is the same in pure water and in ice. Furthermore, it is also reasonable to assume that the amount is independent of the temperature. On these assumptions, all the spectra analysed have been corrected for source annihilation ("source correction") as described in the following chapter. The Melinex spectrum was measured at different temperatures and resolved into two components, the temperature dependence of which is shown in fig. 9. All the sources employed had a strength of approx. 50 μ Curie. This strength was found suitable considering the uncertainties caused by counting statistics involved in the determination of the lifetimes and intensities and the effects of high counting rates in the electronic equipment. This is discussed in appendix I. A typical counting rate was four coincidences per second which made it possible to record a spectrum with a reasonably good counting statistic in one or two days.

For the determination of the resolution curve, a Co^{60} source was used in the form of a small needle with a strength of approx. 50 μCi.

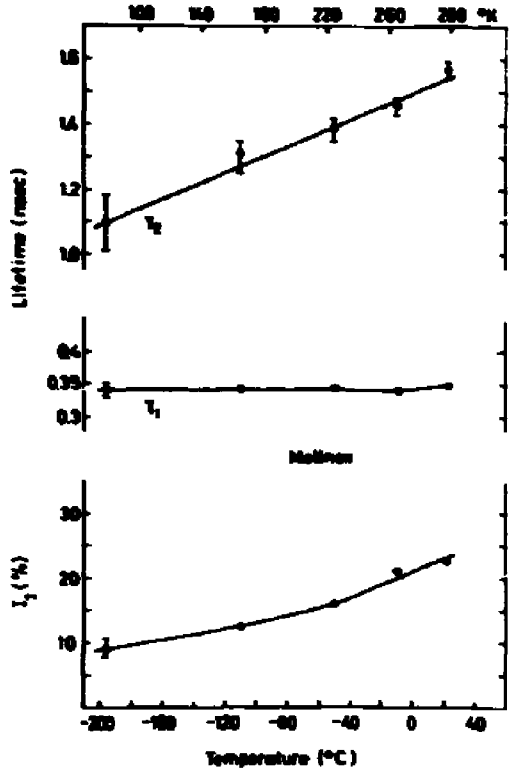

Fig. 9. Parameters obtained by two-term fits of lifetime spectra for Melinex as function of temperature.

2.5. Description of the Cryostat System

The different temperatures of the samples were obtained by means of a system in which the samples were cooled with liquid nitrogen (LN_2) and heated by an electric current in a heating coil. The cryostat system consisted of four main parts: the cryostat, the "cold finger", the sample holder, and the thermostat.

2.5.1. Cooling System

The cold finger connected the cryostat to the sample holder. The cryostat (from The Oxford Instrument Company Ltd.), containing 10 liters of LN_2, was in the bottom provided with a tube that lead the LN_2 to the cold finger. Its connection to the tube was made via a thick copper-block. Cold fingers of different thermal conductivities could be used, such as a brass tube (10 mm diameter, walls 1 mm thick), a brass rod (10 mm diameter) and two copper rods of 10 and 30 mm diameter respectively. The length of the cold fingers was 85 mm. At the end of the cold finger the sample holder was fixed tightly with a screw to secure good thermal contact. Two different sample holders were used, both made of copper, the one for polycrystalline samples contained in cylindrical brass containers, the other for

monocrystalline samples with rectangular shape. They are shown in fig. 10. In the sample holders the heating coil was placed, fixed between two

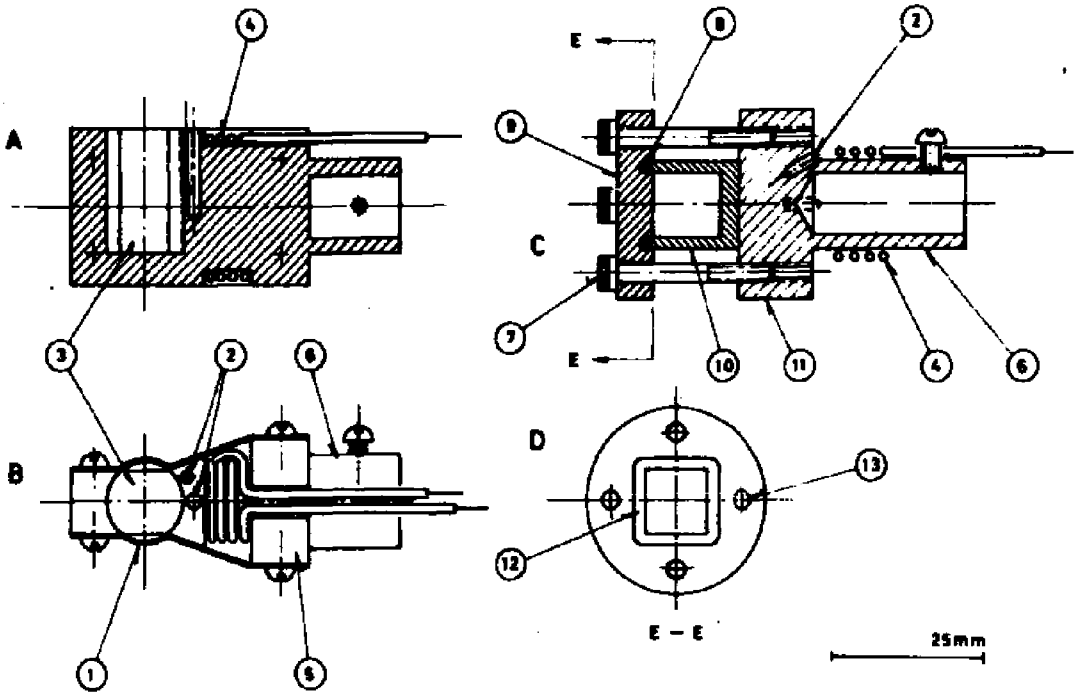

Fig. 10. Sample holders; for polycrystalline samples,(A) cross section, and (B) seen from above; for monocrystalline samples,(C) cross section, and (D) cover for sample container. 1) Cupper foil, 2) holes for thermistors, 3) hole for sample container, 4) heating coil, 5) cupper block, 6) cylindrical tube for cold finger, 7) screws for fixing sample container with cover, 8) o-ring, 9) cover for sample container, 10) sample container, 11) cylindrical cupper block, 12) recess for o-ring, 13) holes for screws.

layers of Plastic Padding, which was found to give the best thermal contact between heating coil and sample holder, at the same time being able to withstand the large variations in temperature. The sample holders further contained holes for thermistors. All parts of the system that were cooled were contained in a vacuum chamber to secure good thermal insulation against their surroundings.

2.5.2. Control and Measurement of Temperature

The temperature was controlled by a thermostat, which is described in ref. 35. It is based on the principle that a thermistor in contact with the sample holder forms one branch of a bridge. The difference voltage of the bridge is amplified and controls the current in the heating coil. The temperature of the sample holder could be changed by changing the resistance of a variable resistor in the bridge. The sample holder would then be

heated (or cooled) until the resistance of the thermistor was close to that of the variable resistor. With two thermistors, covering two different temperature regions and mounted at the sample holder, the whole interval from liquid nitrogen (-196°C) to room temperature was covered. If the thick copper rod was used as cold finger, temperatures from LN_2-temperature to approx. -165°C were possible; if the brass tube was used, the range from -165°C to room temperature was covered.

The temperature was measured with two copper-constantan thermocouples. If the sample holder for polycrystalline samples was used, one thermosouple was pressed between the sample container and the copper foils surrounding it. The other thermocouple was either mounted in a similar way on the other side of the sample container or taken through the top of the container sticking directly into the ice sample (see fig. 11). The hole in the container cover was sealed with Araldit to make it air-tight. If the monocrystal sample holder was used, the thermocouples were placed in small holes between the bottom of the sample container and the copper block with the heating coil. For the improvement of thermal contact between a

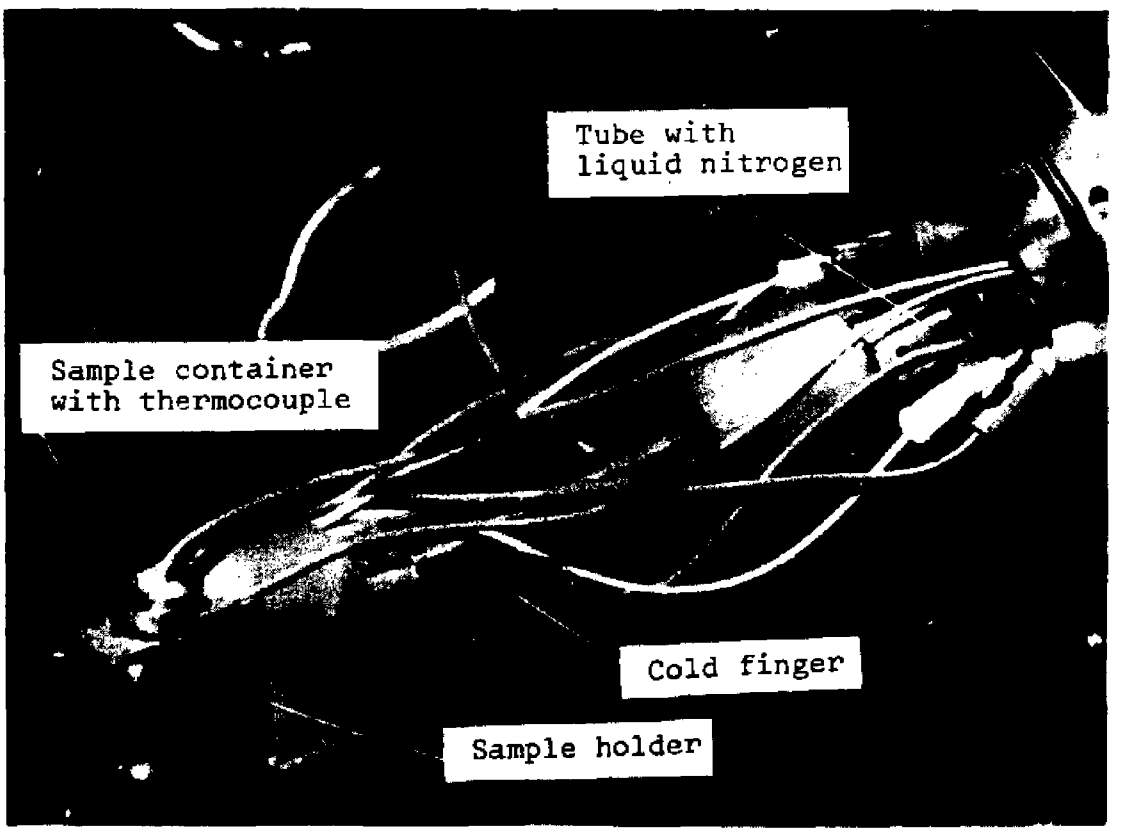

Fig. 11. Part of the cryostat system with vacuum chamber removed. The wires are for the heating coil, the two thermistors, and the two thermocouples.

sample holder and the thermistors and thermocouples, they were embedded in silicone grease (with the exception of the thermocouple directly positioned in the sample naturally).

To provide a reference temperature, a mixing of ice and water was used, and the voltages of the thermocouples were measured on a DC micro voltmeter. The voltmeter was checked as against a precision potentiometer several times during the measuring period, and no deviations were found. However, although the temperature control system was able to keep the temperature of the sample holder (or more correct: the thermistor) constant to within one or two tenths of a degree, the temperatures of the two thermocouples sometimes deviated slightly. This was probably due to temperature gradients in the sample or reduced thermal contact to the thermocouple. Therefore, the temperatures measured are only believed to be correct to within $\pm$ 1% of the temperature in degrees centigrade or within $\pm$ 0.5°C, whichever is the greater.

Fig. 11 shows part of the cryostat system with the vacuum chamber removed, and fig. 12 gives an overall impression of the experimental apparatus.

Fig. 12. Overall view of the experimental equipment.

2.6. Samples

All ice samples, except the monocrystalline ones, were prepared by freezing the liquid in a cylindrical brass container whose inner dimensions were 10 mm in diameter and 15 mm high. A brass cover with an O-ring was screwed into the container to seal it tightly. In some cases a thermocouple was led through the cover directly into the sample. The source was inserted in the middle of the container along a diameter thus dividing it into two half-cylinders.

Before the freezing of a new sample, the source and container were carefully rinsed, first in distilled water and then several times in the liquid to be frozen. Freezing took place immediately after the liquid was poured into the container in order to prevent impurities from the container walls to be dissolved in the liquid. All the aqueous solutions were frozen by putting the container into liquid nitrogen that cooled the sample to -196°C in approx. one minute (referred to as "fast freezing"). The results for pure ice did not depend on the freezing rate, so these samples were cooled more slowly in most cases.

The light water used to prepare the polycrystalline samples was distilled twice; the water had a specific conductivity of approx. 10^{-6} (ohm cm)$^{-1}$. It contained an equilibrium amount of air. The purest heavy water used had a specific conductivity of around 10^{-5} (ohm cm)$^{-1}$, and contained less than 0.1% H_2O.

The solutions to be frozen were made from concentrated solutions of high purity (for chemical analyses) by dilution with water distilled twice or by dissolving a salt in the water. The concentrations of some of the solutions were checked analytically, and based on this an uncertainty was estimated at $\pm$20% on the figures given for the concentrations.

The monocrystalline samples were prepared by cutting two pieces of crystal from a larger monocrystal, each of the dimensions 10 x 10 x 4 mm^3. The crystals were ground with fine emery paper and polished with a piece of silk. The two crystals were then placed in the sample container (a cube of 1 cm^3) with the source between them and pressed slightly against each other by packing around them small pieces of tissue. The sample holder was then assembled, thus making the container tight against the outer vacuum.

3. ANALYSIS OF THE MEASURED SPECTRA

3.1. Basis of the Analysis

The numerical analysis of the recorded spectra was based mainly on two important assumptions:

a) In a measured spectrum the numbers in the channels fluctuate around a curve that is the sum of a constant background and a number of decaying exponential functions somewhat smeared on account of the finite time resolution. The smeared functions are determined by folding the exponentials with the resolution function of the measuring system. The fluctuations around this curve are distributed in accordance with Poisson distributions.

b) The resolution function of the system can be measured as the time spectrum for two γ-quanta emitted simultaneously (for instance from a Co^{60}-source). It is to a good approximation a Gaussian curve.

Since the spectra are recorded in channels in a MCA, they are not continuous curves, but the number in each channel is the average of the curve mentioned in a) over the width of one channel. In a careful analysis this has to be taken into account. Furthermore, a correction for the positrons annihilating in the source material should be made (source correction). The lifetime spectrum of the source material (in this work mostly Melinex) should be subtracted from the measured spectrum, the area of the former being a proper fraction of that of the latter.

The mathematical expressions assumed for a measured curve are found in appendix II.

3.2. Manual Analysis

All measurements made at the Laboratory of Applied Physics II[36] were analysed manually in the following way: A measured spectrum consisted of 400 numbers (as recorded in a Laben 400 channels MCA). The

lifetime spectrum was contained in less than 100 of the channels, the rest of them exhibiting only the random background. The latter was determined as the average of the numbers in the last 30 channels and subtracted from the recorded number in each channel. The total area of the spectrum was then determined as the sum of the numbers in all channels, and the correction for source annihilation performed by subtracting channel by channel the spectrum of the source foil material (or the material of the sample container walls). The area of the correction spectrum amounted to a fraction, viz. 5% or 23%, of the lifetime spectrum area (determined as described in section 2.4.). The spectrum thus obtained was subsequently analysed in a semilogarithmic plot to extract lifetimes and their intensities. First, among the points corresponding to the highest channel numbers a straight line was drawn which gave the best visual fit to the points. The slope of this line determined the longest lifetime. If the position and slope of the line and the position and width of the prompt curve are known it is possible, by means of formula (II 1) in appendix II, to draw the rest of the curve representing the long-lived component. This was done and the component subtracted from the spectrum. The same procedure was then used on the long-lived component of the spectrum thus obtained. By this method it was possible to separate, in the spectra for ice, three, and in the spectra for water, two different lifetime components. An example of a manual analysis is shown in fig. 13.

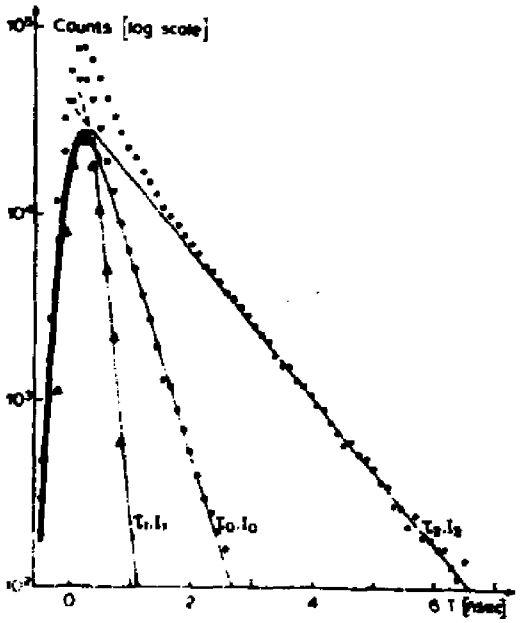

Fig. 13. A lifetime spectrum for D_2O at -22°C manually resolved into three components. (The indices characterizing each component in this figure and in fig. 14 are different from those used in the rest of the report).

3.3. Computer Analysis

All spectra obtained through the measurements at Risö were analysed on the Burroughs 6500 computer at Risö, and the program POSITRONFIT was used. The main features of this program are the following: A curve consisting of a constant term and a sum of exponentials folded with a Gaussian and integrated over intervals equivalent to one channel (formula (II 3) in appendix II) is fitted to the experimentally determined spectrum in the least-squares sense, i.e. the parameters of the curve are so chosen as to minimize $\Phi = \sum_1^n w_i \Delta_i^2$, the sum being extended over n measuring points. Δ_i are the differences between the measured count numbers and those predicted by the model. The weights w_i are, in principle, arbitrary. Several advantages are gained, however, by taking $\frac{1}{w_i} = \sigma_i^2$ (the variance of the count number at the i'th data point, which in our case equals the mean of that count number due to the Poisson statistics). First, this weighting seems quite reasonable in virtually ruling out those data points associated with large variances. Second, on certain assumptions (small fluctuations and an ideal model) it permits a relatively simple statistical analysis resulting in an estimate of the variance-covariance matrix of the least-squares estimate of the parameters, including in particular their variances. The quantity $\Phi_{min} = \text{Min} \sum_1^n (\Delta_i/\sigma_i)^2$ obeys approximately the χ^2-distribution with n-k degrees of freedom, where k is the number of free parameters to be estimated. When n-k is large, as is the case in our applications, it can be shown that $(\Phi_{min}/(n-k))$ is normally distributed with mean 1 and standard deviation $\frac{1}{\sqrt{2(n-k)}}$. We shall refer to that ratio as "the variance of the fit". It serves as an indicator of the validity of the mathematical model: large deviations from unity suggest that the assumed model is no good representation of the measured spectrum.

From a measured prompt curve can be determined its width, as given by σ, and the channel number at the position of its peak, T_o (representing time equal zero). However, it was found that the result of the analysis was very sensitive to the value used for T_o. Furthermore, an exact exterimental determination of T_o is very difficult, and in addition it is subject to changes by drift in the electronic equipment and to changes in the position of the sample. Therefore it was included as one of the fitting parameters.

The parameters to be fitted in our model are thus annihilation rates, λ_j, channel number equivalent to time equal zero, T_o, intensities, $\frac{I_{oj}}{\lambda_j}$, and background, B (see appendix II). The model is linear in the intensities and background, but nonlinear in the λ_j and T_o. The nonlinearity calls for

an iterative method of finding the least-squares estimate of the parameters: In POSITRONFIT, Marquardt's technique is used [38]; it combines in an almost optimal fashion the method of Gauss-Newton and the method of steepest descent. Contrary to most other fitting programs, POSITRONFIT takes advantage of the fact that the model is only partially nonlinear. According to this, the iterations take place in the subspace of the nonlinear parameters, and conditional solutions for the linear parameters are calculated after each iteration. This device results as a rule in a considerable saving of iterations at the expense of a slight increase in the cost per iteration. The iterations start from a guessed initial set of the λ_j and T_o and are terminated when Φ proves to be stationary. POSITRONFIT is described in detail in refs. 39, 40, 41.

POSITRONFIT allows a spectrum to be fitted with any number of exponential functions from one to four. Furthermore, it is possible to give any combination of lifetimes and intensities fixed values. The fitting will then take place subject to the constraints thus imposed. Also correction for the annihilation in the source can be made by the program.

The procedure followed by the program when analysing a spectrum is as follows: First the recorded spectrum is fitted with the desired number of exponential terms and constraints and the parameters for this spectrum are determined. With T_o from this procedure, the source correction spectrum is generated, formula (II 4) in appendix II being used, and is subtracted from the measured spectrum. The corrected spectrum is then fitted, the procedure starting from the parameters determined from the first iteration cycle. This correction procedure presupposes that the values from the two iteration cycles for T_o should be very close. This applies to all the spectra analysed.

The final results of the analysis are estimates for the corrected spectrum of lifetimes and relative intensities as well as background and channel number equivalent to time equal zero, all with standard deviations. Further more, a matrix describing the correlation between the fitted parameters is given.

In appendix III the input and output data are described in more detail, and some examples of the application of the program are given.

3.4. Discussion of the Analysis

3.4.1. Basic Assumptions

Of the assumptions that form the basis of the analysis (see 3.1.), the

first one - that a lifetime spectrum consists of a sum of exponential terms - is generally accepted for positron lifetimes in all ordinary, condensed materials. To account for the smearing, by folding the prompt curve into the spectrum is the logical mathematical way of doing it. To assume the prompt curve to be a Gaussian is not generally correct since it depends upon the characteristics of the measuring system, but in many cases it is a good approximation [37]. That this is so in the present work is seen in fig. 7, where a measured prompt curve is compared with the Gaussian used in the analysis. The two curves coincide down to around 2% of the peak value, the Gaussian correctly representing all important parts of the prompt curve. This is further confirmed through the analysis of a spectrum of a saturated solution of $KMnO_4$, for which the variance of the fit exhibits a minimum as function of the FWHM for the value of FWHM determined from the prompt curve, as described in appendix III.

3.4.2. Manual and Computerized Analysis

The manual analysis of spectra described in 3.2. suffers from the difficulties involved in visual determination of what straight line gives the best fit to a certain number of experimental points (see fig. 13). Furthermore, it is a tedious job to do the fitting, the result of which to some extent depends on the judgment of the person performing the fitting. On the other hand the difficulties, the possibilities, and the limitations of extracting information from a measured spectrum are easily apprehended.

This is not quite true in the case of computer fittings. But many advantages are gained: The different spectra are analysed in a consistent way in accordance with the statistical distribution of the measured numbers in a spectrum. The fitted parameters are given with statistical uncertainties. The variance of a fit and a graphical representation of measured and fitted spectra give a good impression of the goodness of a fit. Different methods of analysis (i.e. different number of exponential terms and constraints) make it possible to extract as much information from a measured spectrum as it contains. And not unimportant, the analysing procedure is fast.

3.4.3. Experience from Analyses

The experience gained from the use of POSITRONFIT indicates that not more than 3 terms can be resolved directly in any spectrum, since the variance of the fit will not be decreased by using 4 terms (unless long life-

times of the order of several nseconds are involved). The number of iterations used to obtain convergence were normally of the order of 15 including the iterations both before and after source correction was performed. A number of spectra were analysed several times with different initial guesses of the lifetimes for the purpose of testing the unambiguity of the final result. Except for a few cases, where the background was strongly mixed with one of the exponential terms resulting in an extremely long lifetime (e.g. 184 nsec) which is easily discoverable, the result of an analysis was always the same for the same spectrum.

Sometimes analysis with 3 terms of a spectrum resulted in very large uncertainties on the fitted parameters, while fitting with 2 terms gave a rather poor fit (i.e. large variance). This means that the spectrum contained more information than can be determined through the number of parameters involved in a two-term fit but not enough to determine all parameters in a three-term fit. In such cases a physically meaningful constraint may be imposed on one of the parameters (lifetime or intensity) and a three-term fit performed under this constraint, thus reducing by one the number of parameters to be determined. The results presented in chapter 4 show many examples of this. Another example of the use of constraints is the case where from physical reasons a spectrum is believed to contain say 4 lifetime components. If the parameters of a sufficient number of them are known, they can be used as constraints and the unknown parameters determined by the fitting procedure.

From what is said above it is obvious that the number of components contained in a certain spectrum is very often difficult to determine. Furthermore, if a spectrum does not contain enough information to determine all parameters in, say, a three-term fit, there will be several sets of parameters for 3 terms that will fit the spectrum almost equally well (the variances of the different fits will be nearly identical). And in appendix III it is demonstrated that rather small width variations of the prompt curve used in the analysis may cause large changes in the fitted parameters. All this leads to the conclusion that the parameters determined from a certain spectrum by different methods of analysis may very well differ significantly unless special care is taken with respect to the amount of information contained in the spectrum. This fact also makes it difficult to establish a direct connection between the parameters determined from a spectrum and the different annihilation processes of the positrons (such as the statement: The longest lifetime determined is that of ortho-Ps and its relative intensity

the relative amount of ortho-Ps formed). The results obtained for ice presented in the next chapter are good examples of this.

3.4.4. Analysis Uncertainties

Apart from the above-mentioned difficulties involved in the analysing procedure, a number of uncertainties are connected with the final results of an analysis:

The statistical counting statistics uncertainties (estimated by the program).

The time calibration uncertainty of the measuring system. As mentioned in 2.3. this factor is $\pm 1.5\%$.

The uncertainty caused by the uncertainty of the prompt curve width, which typically is $\pm 5 \cdot 10^{-3}$ nsec (from the uncertainty in its determination and drift in electronic equipment). This results in uncertainties which are comparable to or - in most cases - appreciably smaller than the standard deviations estimated by the computer. These uncertainties depend very much on the individual spectrum and the number of terms used in the fit. (See appendix III).

The uncertainties caused by the difference between the actual prompt curve and the Gaussian used in the fitting procedure are believed to be of the order of one or two per cent.

The source correction also implies uncertainties. Firstly, the fraction of positrons annihilating in the source is only determined to within about 2% (of the total number). Secondly, the spectrum of the source annihilation is determined by letting all positrons annihilate in Melinex. However, since many of the positrons annihilating in the source are scattered into it from the surrounding material [34], the number that annihilates from a Ps state in the source will probably depend upon the Ps formation probability of this material. This means that the spectrum of the source annihilation will depend upon the surrounding material. It was not possible to determine the real source spectrum, so the spectra used for source correction were the Melinex ones. This introduces an uncertainty in the corrected spectrum. Furthermore, the source foils may change their spectrum due to the constant irradiation they suffer. However, these changes were found to be very small for Melinex.

Apart from the statistical standard deviations estimated by the program, all the mentioned uncertainties have the effect of biasing the results of the analysis in a certain direction. Thus, when measurements within the

same series are compared, only computed standard deviations should be considered uncertainties, while the rest of the uncertainties should be included when comparisons are made with other experiments.

3.4.5. Analysis of a $KMnO_4$-Solution

Finally attention should be drawn to the utility of a measured spectrum of a saturated aqueous solution of $KMnO_4$. The analysis of this spectrum will, as described in appendix III, provide the following information: The width of the resolution function, the amount of source annihilation, and with a very small uncertainty the lifetime of free positrons in the solution. If various laboratories could agree upon the value of this lifetime, it could serve as a standard for time calibration of equipments. The solution is very easy to make, impurities do not play any role, the exact temperature is not important, and the measurement is very easy to make.

4. EXPERIMENTAL RESULTS

4.1. Positron Lifetimes in H_2O and D_2O as Function of Temperature

4.1.1. The Ice Water Phase Transition and Water

The results published in ref. 36 are shown in fig. 14. They demonstrate for H_2O and D_2O that at the ice water phase transition a discontinuity exists

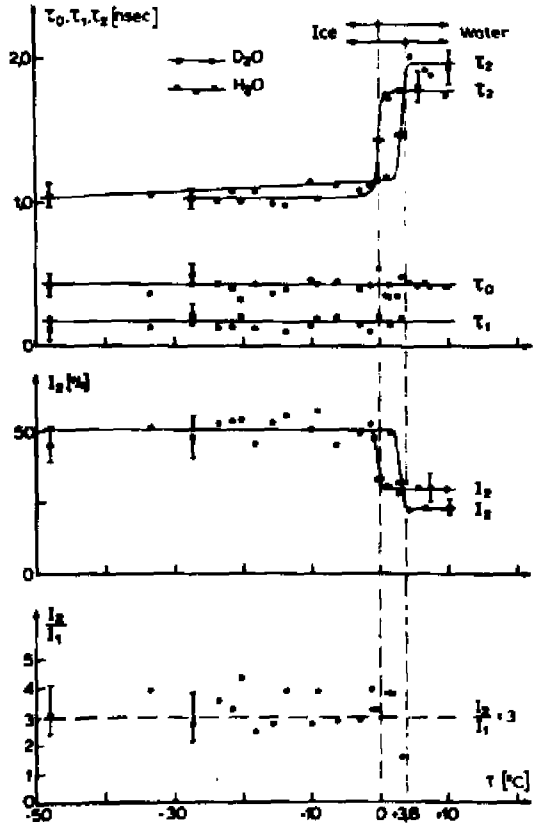

Fig. 14. Parameters resulting from manual analysis of lifetime spectra in H_2O and D_2O as functions of temperature. The analysis included correction for annihilation in source and container walls. (The indices characterizing each component in this figure and in fig. 13 are different from those used in the rest of the report).

in the lifetime and relative intensity of o-Ps. In order to be able to use the more refined method of analysis provided by POSITRONFIT, the spectra were re-measured and the temperature region extended down to liquid nitrogen temperature.

The numerical results from 3-term fits of spectra for light and heavy water at 20°C are given in table 1. Here and in the following the lifetimes and relative intensities are numbered from shortest to longest lifetime. This is done since no common convention has been adeopted by those authors who have published results analysed for more than two lifetimes. In addition it is in several cases difficult to establish a well-defined relationship between a lifetime, resulting from an analysis, and a specific physical process.

Table 1

Lifetimes and relative intensities from 3-term fits of spectra for H_2O and D_2O at 20°C. The uncertainties are standard deviations as estimated by the computer

	$\tau_1 \pm \Delta\tau_1$ (nsec)	$\tau_2 \pm \Delta\tau_2$ (nsec)	$\tau_3 \pm \Delta\tau_3$ (nsec)	$I_1 \pm \Delta I_1$ (%)	$I_2 \pm \Delta I_2$ (%)	$I_3 \pm \Delta I_3$ (%)
H_2O	0.22±0.02	0.46±0.02	1.86±0.02	25.0±5.1	48.2±4.7	26.9±0.5
D_2O	0.31±0.03	0.53±0.06	2.01±0.03	44.6±12.6	33.2±12.1	22.2±0.6

4.1.2. Pure Ice

In figs. 15 and 16 lifetime spectra measured for H_2O at -182°C and -2°C are shown. The curves resulting from 2- and 3-term fits are also drawn. The results for H_2O and D_2O ice as analysed by 2-term fits are shown in fig. 17. The longer lifetime is constant (around 0.61 nsec) for temperatures below -100°C. Above -100°C it increases with increasing temperature. The relative intensity of the longer lifetime is constant (around 74%) for low temperatures, but is decreased for temperatures above -100°C. Furthermore, the results for mono- and polycrystalline H_2O and for D_2O agree closely. In the figure is indicated the differences between the variances of the 2-term and the corresponding 3-term fits ($\Delta_{2,3}$). The variance of a 3-term fit is the smallest one that can be obtained for a particular spectrum (section 3.4.3.). Therefore $\Delta_{2,3}$ more

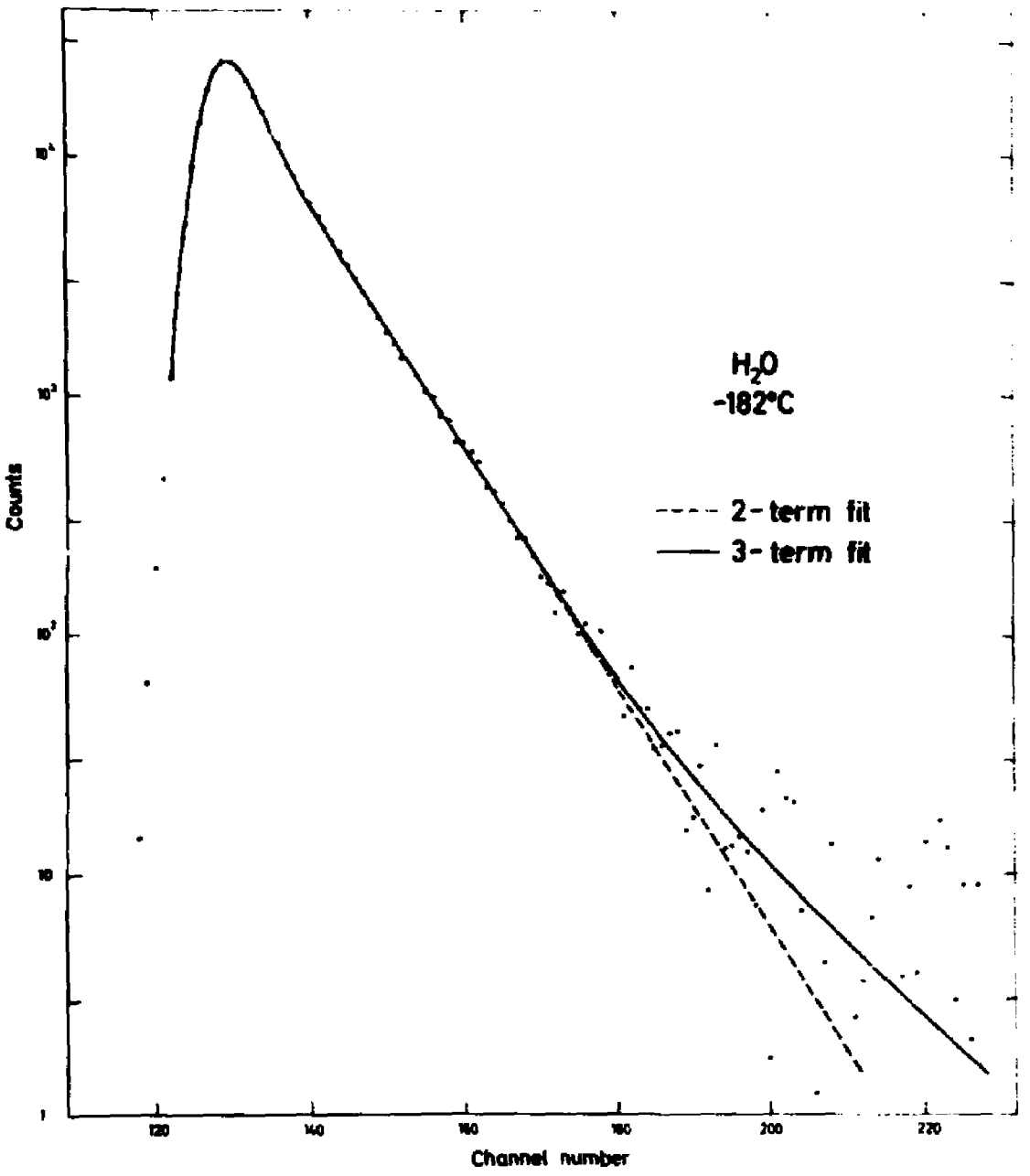

Fig. 15. Measured lifetime spectrum for H_2O at -182°C, corrected for 7% source annihilation and for background. The curves resulting from a 2-term and a 3-term analysis are also shown. One channel equals 70 psec.

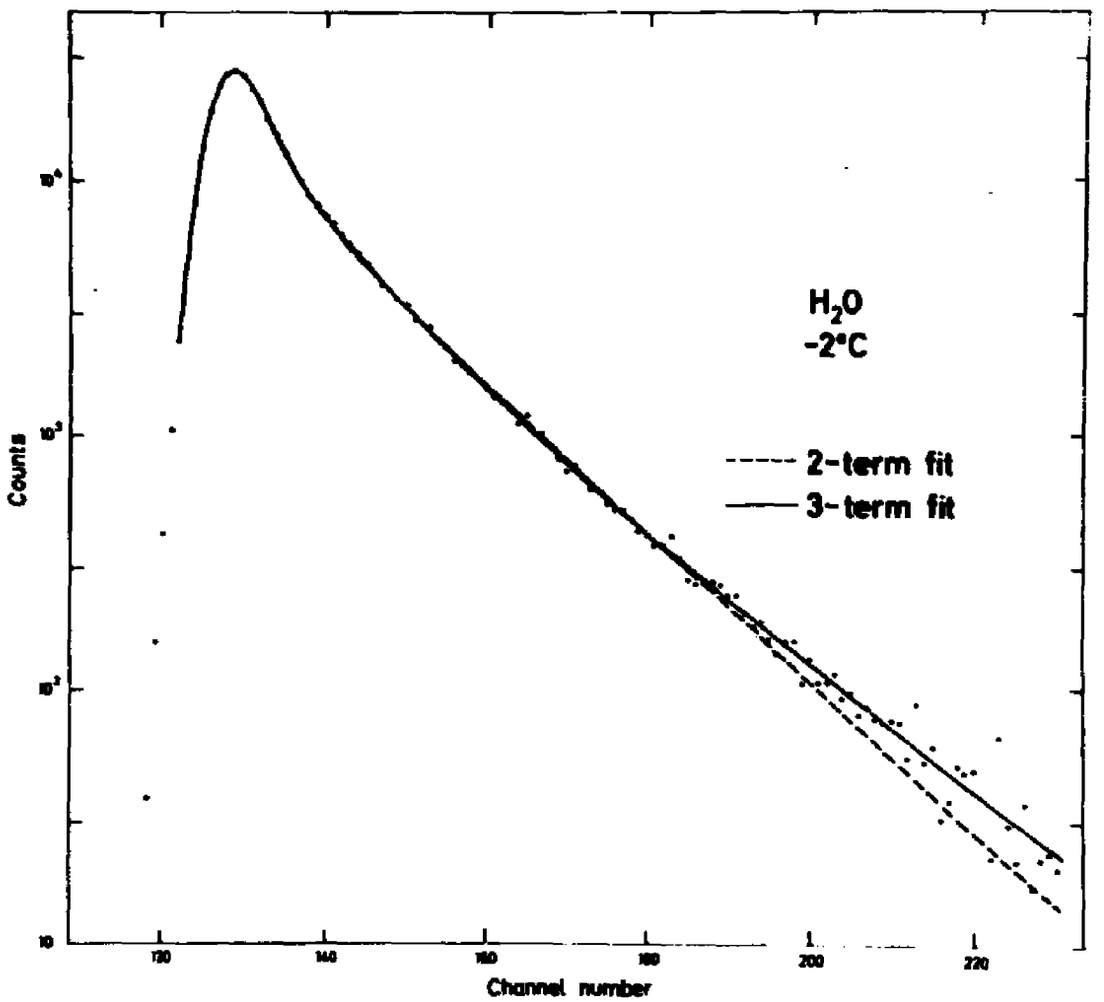

Fig. 16. Measured lifetime spectrum for H_2O at -2°C, corrected for 7% source annihilation and for background. The curves resulting from a 2-term and a 3-term analysis are also shown. One channel equals 70 psec.

directly shows the goodness of a 2-term fit than does the variance of the fit itself, since the value of the variance from one spectrum to another is subject to statistical fluctuations which are almost eliminated in $\Delta_{2,3}$. Since the values of $\Delta_{2,3}$ in fig. 17, except for a few points, are several times larger than the expected statistical standard deviation of the variance (shown by the black bar), the fits are rather poor. This is also illustrated in figs. 15 and 16. Thus although the curves in fig. 17 naturally contain essential information about the temperature dependence of the measured spec-

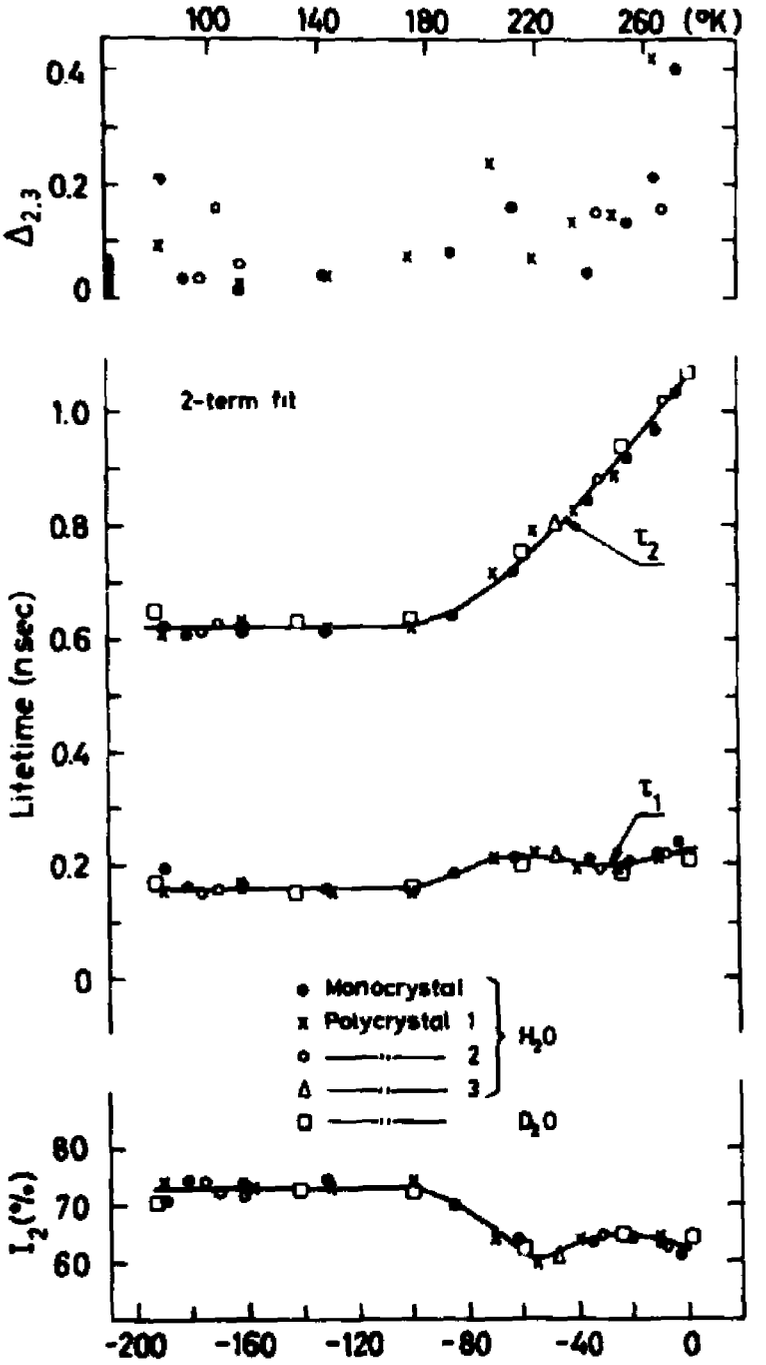

Fig. 17. Lifetimes and relative intensities from a 2-term analysis of lifetime spectra for light and heavy ice as function of temperature. The analysis includes correction for source annihilation. $\Delta_{2,3}$ is the difference between the variances of a 2-term and the corresponding 3-term fit. The magnitude of the statistically determined standard deviation of the variance is shown by the black bar.

tra, they do not correctly represent these spectra.

In order to improve the fit, an analysis with 3 terms was performed. The results for H_2O are shown in fig. 18. The uncertainties (i.e. the bars, which on some of the experimental points indicate the standard deviations as estimated by the computer) are greatly increased. For the sake of clarity the experimental points for I_1 and I_2 have been omitted, and only typical uncertainties are indicated. Furthermore, a few points with extremely large uncertainties have been omitted.

The tendency of the longest lifetime is the same as for the 2-term fit except at the lowest temperatures, where a long-lived component is revealed. Also a short lifetime (of approx. 0.12 nsec) has been resolved. It is almost independent of temperature, and so is its intensity I_1. On the other hand, I_3 increases from a few per cent at low temperatures to around 40% at the melting point. Very often the intensity of a long-lived component with a lifetime longer than approx. 0.5 nsec is directly associated with the relative amount of o-Ps. However, such an association is in this case contradicted by several facts:

a) From angular correlation measurements a total relative area of narrow components associated with p-Ps is found equal to 15.2% at -148°C. Taking into account pick-off of p-Ps a total number of $18 \pm 0.5\%$ p-Ps is found [42]. This is also true in the whole temperature range from -182°C to 0°C [89]. This entails an o-Ps intensity of $54 \pm 1.5\%$, if the reasonable assumption is made that no ortho-para conversion takes place.

b) In angular correlation magnetic quenching measurements on ice at -100°C and -5°C a Ps formation probability is found of $65 \pm 4\%$ [43], which gives an o-Ps intensity of $49 \pm 3\%$, if no conversion takes place.

c) In the measurements on HF-doped ice described in the following section, a longlived component of intensity $52 \pm 2\%$ is found at -160°C. It is ascribed to o-Ps.

d) Measurements on HF-doped ice (10^{-3} mole fraction) in the temperature interval between -196°C and -20°C exhibit a longlived component of intensity varying between 42% and 54%.

e) The Ps-formation probability is expected to depend only slightly on the temperature from 0°C and down, since the energies in-

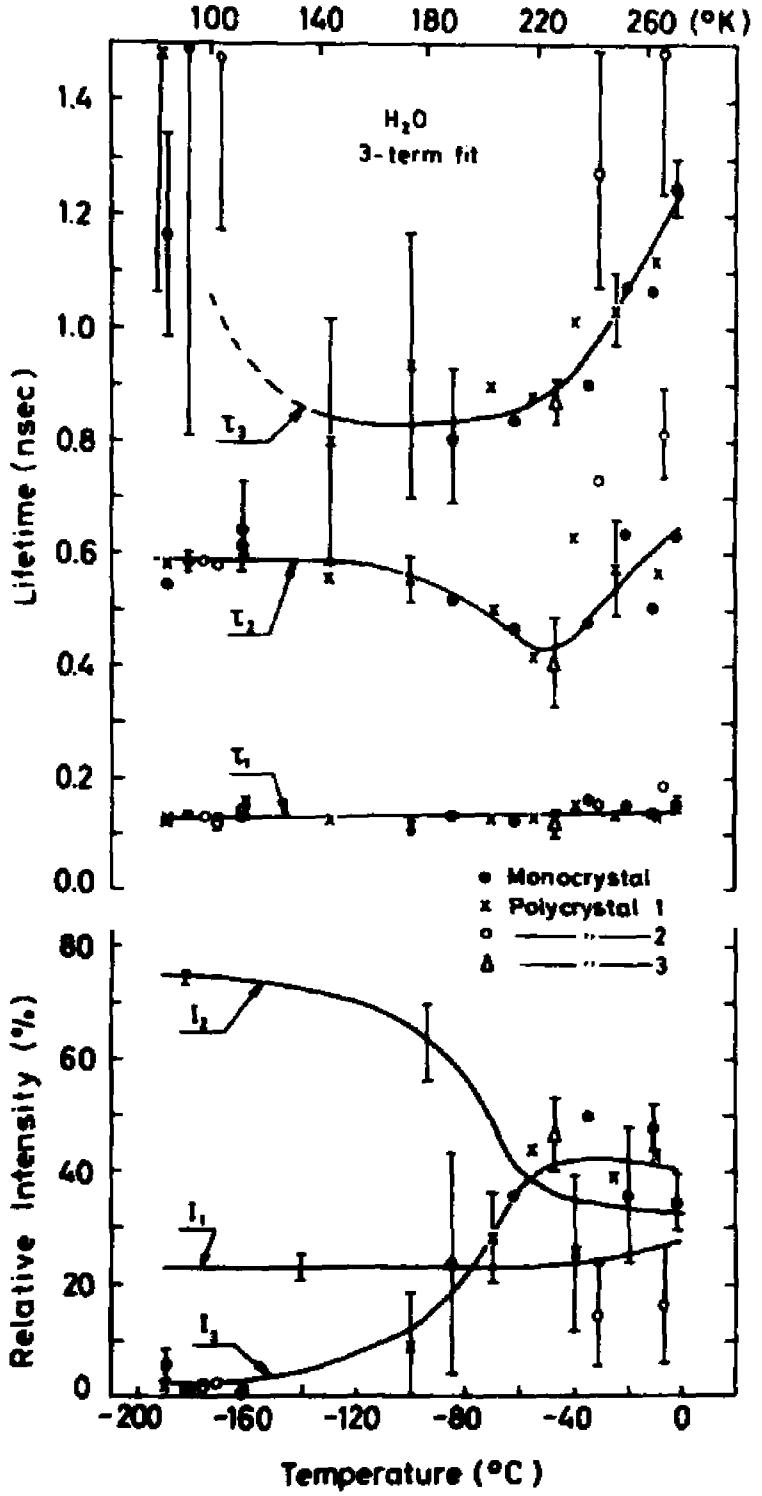

Fig. 18. Lifetimes and relative intensities from a 3-term analysis of lifetime spectra for H_2O as function of temperature. The analysis includes correction for source annihilation. Experimental points for I_1 and I_2 have been omitted for the sake of clarity. Typical uncertainties indicated on the curves for I_1 and I_2 and on some of the experimental points are standard deviations as estimated by the computer.

volved in temperature changes are of the order of one or two per cent of an electron volt, while energies involved in the determination of the Ore gap are of the order of one to ten eV [44] (see also appendix VI).

f) It is easy to show that the 3γ-annihilation rate is proportional to the product of the o-Ps lifetime and its intensity:

$$R_{3\gamma} \propto I_{o\text{-}Ps} \cdot \tau_{o\text{-}Ps}$$

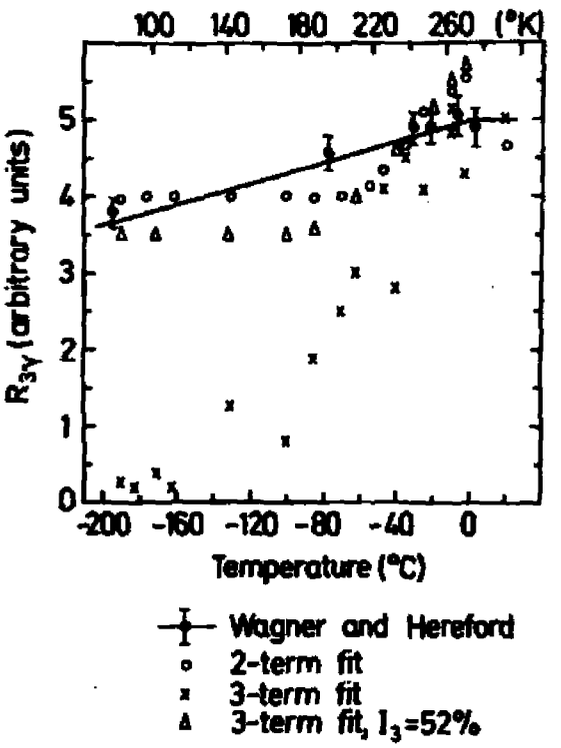

Fig. 19. Rate of 3γ - annihilations measured by Wagner and Hereford [19] compared with the product of the longest lifetime and its relative intensity for the present measurements. Results are shown for different fitting procedures. Normalisation was made to give the best visual fit to the results of Wagner and Hereford, for the open circles and triangles over the whole temperature range and for the crosses around 0°C.

In fig. 19 the measurements of Wagner and Hereford [19] are compared with the products of the longest lifetimes and their corresponding intensities determined by 2- and 3-term fits of the present measurements. From fig. 19 it is evident that the longest lifetime of the 3-term fit cannot directly be associated with o-Ps.

These points taken together have lead to the conclusion that the total

amount of o-Ps formed in ice must be $52 \pm 2\%$, independent of temperature. Since I_1 in fig. 18 is nearly temperature independent it is likely that in the two resolved longlived components the decay of o-Ps (which may very well take place through different processes) is mixed with other annihilation processes. In order to extract from the measured spectra the long lifetime component with a relative intensity of 52%, which may be associated with o-Ps, the spectra were finally fitted, 3 terms being used, but subject to the constraint that $I_3 = 52\%$. The results are shown in fig. 20. Below $-100^{\circ}C$ average values of the three resolved lifetimes are 0.675 nsec, 0.435 nsec and 0.120 nsec. The average relative intensity of the shortest lifetime is 20%, leaving 28% to the medium lifetime component. Above $-100^{\circ}C$ the longest lifetime increases with temperature to 1.1 nsec at $0^{\circ}C$. The curve is almost identical with that for τ_2 in fig. 17, it is only shifted 0.05 nsec upwards. The medium lifetime shows a complex behaviour, while the shortest is almost constant above $-100^{\circ}C$. The intensity of the latter also has an irregular behaviour. The curve termed "free volume model" will be discussed in section 5.3.2.

Except for a few points, the values of $\Delta_{3,3}$ (the difference between a 3-term fit with $I_3 = 52\%$ and a 3-term fit without constraints) lie well within the statistical standard deviation of the variance, which is shown by the black bar. Hence the results in fig. 20 correspond to fits of the measured spectra that are almost as good as those corresponding to fig. 18.

The product $I_3 \cdot \tau_3$ taken from fig. 20 is also shown in fig. 19. It does not follow the curve of Wagner and Hereford in detail, but is much closer to it than that for a 3-term fit without constraints.

4.2. Positron Lifetimes in Frozen Aqueous Solutions of HF

4.2.1. Fast Frozen HF-Solutions

In many areas of ice physics, ice is doped with hydrogen flouride and ammonia in order to create defects (so-called L- and D-defects, and ionic defects)[45)46)47)] (see also section 5.1.2.). With the purpose of investigating the influence of HF doping on the lifetime of positrons, aqueous solutions of different HF concentrations were fast frozen. The measurements were made at $-160^{\circ}C$.

For HF concentrations larger than $5 \cdot 10^{-5}$ mole fraction, the results of 3-term analyses of the spectra are given in table 2.

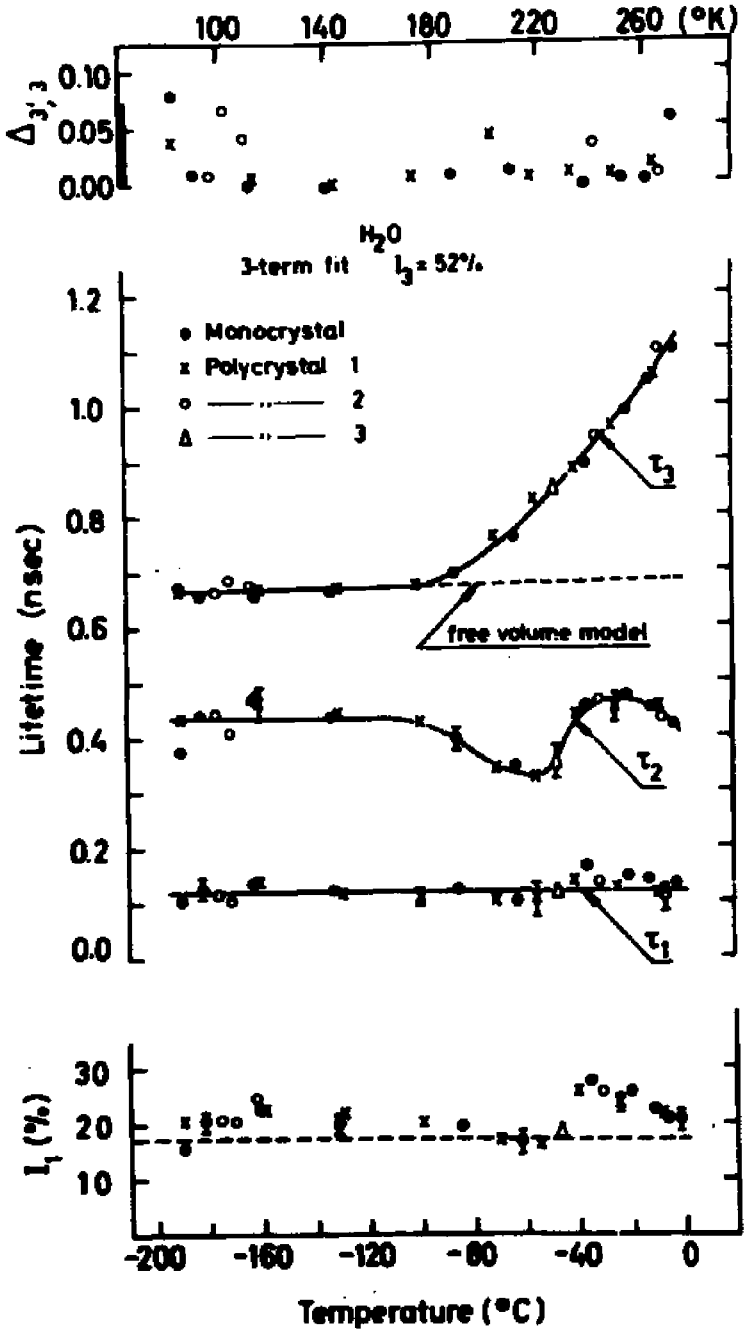

Fig. 20. Lifetimes and relative intensities from a 3-term analysis of lifetime spectra for light ice subject to the constraint I_3 = 52%. The indicated typical uncertainties are the standard deviations as estimated by the computer. $\Delta s'_{,3}$ is the difference between the variances of these analyses and the corresponding 3-term fits without constraints. The magnitude of the statistically determined standard deviation of the variance is shown by the black bar. The curve calculated for the free volume model is fitted to experiments at -190°C.

Table 2

Lifetimes and relative intensities from 3-term fits of spectra for fast frozen solutions of HF at -160°C. The uncertainties on lifetimes and relative intensities are standard deviations as estimated by the computer. The uncertainties on the concentrations are estimated at ± 20%.

Concentration (mole fract.)	$\tau_1 \pm \Delta\tau_1$ (nsec)	$\tau_2 \pm \Delta\tau_2$ (nsec)	$\tau_3 \pm \Delta\tau_3$ (nsec)	$I_1 \pm \Delta I_1$ (%)	$I_2 \pm \Delta I_2$ (%)	$I_3 \pm \Delta I_3$ (%)
$5.5\ 10^{-5}$	0.12±0.01	0.49±0.07	1.25±0.03	27.0±2.3	23.7±1.8	49.4±2.8
$5.5\ 10^{-5}$	0.11±0.01	0.48±0.05	1.24±0.02	26.8±1.6	23.2±1.3	50.1±2.0
$5.5\ 10^{-4}$	0.10±0.01	0.41±0.05	1.23±0.02	24.7±2.0	21.9±1.4	53.5±1.6
$5.5\ 10^{-3}$	0.13±0.01	0.53±0.09	1.25±0.03	28.5±2.2	21.1±2.4	50.4±3.6
$5.5\ 10^{-2}$	0.11±0.03	0.34±0.05	1.18±0.02	21.1±4.9	24.9±4.1	54.0±1.4

From table 2 the averages of τ_3 and I_3 are 1.23 nsec and 52% respectively. In section 4.1.2. it was argued (points a) and b)) that in pure ice around 52% o-Ps is formed. Hence it is most probable that all annihilation of o-Ps contributes to the longlived component.

Trapping of positrons in defects which causes an increase in positron lifetime is known both in metals and ionic crystals for sufficiently high defect concentration[48) 49) 50)]. A reasonable assumption seems to be that the lengthening of the o-Ps lifetime in the fast frozen solutions of HF is due to trapping of o-Ps in some sort of defects created by the HF impurities during freezing. Probably due to more empty space between the molecules in the defect region, the o-Ps lifetime against pick-off is nearly doubled. A simple model that takes into account the processes involved in the trapping of positrons and Ps[49) 50)] is reviewed in appendix IV.

The formulas given in appendix IV show that two characteristic rates govern the decay of the Ps; one is the annihilation rate in the trap, the other the sum of the bulk annihilation rate and the trapping rate. The intensity of the component with lifetime characteristic of the trap increases with the number of traps (formula (IV 1) in appendix IV). Relating this model

to experiments, we find that the o-Ps lifetime in a trap is 1.23 nsec (table 2). In accordance with this, the measured spectra were analysed by fitting them with 3 terms, keeping one of the lifetimes fixed at 1.23 nsec. The relative intensity of this component as a function of HF concentration is shown in fig. 21. A curve derived from the trapping model (I_2 in (IV 1) in appendix IV) on the assumption that the total amount of o-Ps is 52% is also shown. It was fitted to experiments at the concentration $1.9 \cdot 10^{-6}$ mole fraction.

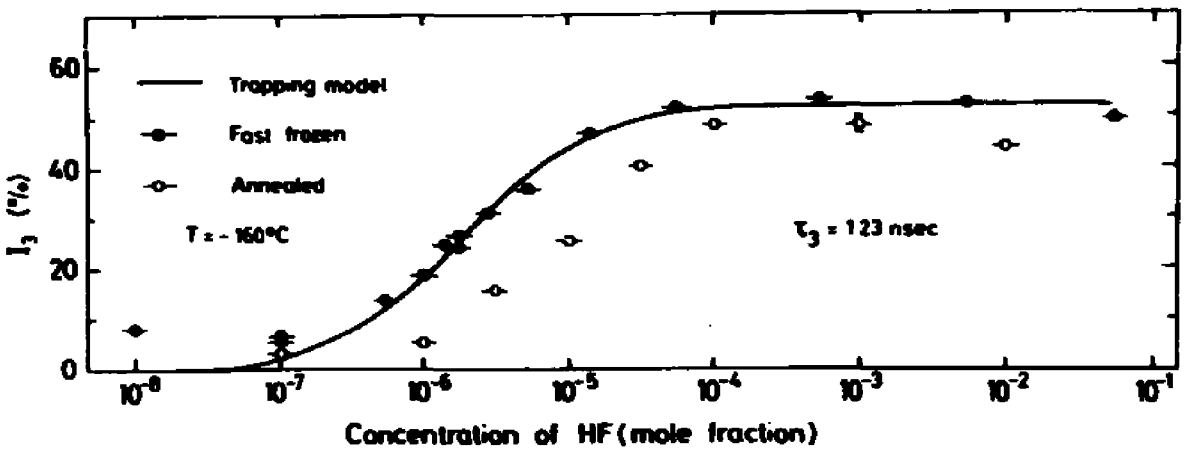

Fig. 21. The relative intensity of the component with lifetime 1.23 nsec as function of HF concentration for fast frozen solutions, and for fast frozen solutions that were annealed 20 hours at -18°C and subsequently cooled at a rate of around 1°C/minute. The horizontal bars at each point indicate the estimated uncertainties in the HF concentrations. The uncertainties in I_3 as estimated by the computer are in most cases within the size of the circles. The results are compared with the trapping model (appendix IV).

With the results of fig. 21 combined with the trapping model (appendix IV), the cross section for Ps trapping can be calculated from the formula:

$$v \cdot C_{HF} \cdot \sigma = \varkappa$$

where v is the velocity of Ps (assumed thermal, $4.7 \cdot 10^6$ cm/sec at 113°K), C_{HF} the concentration of HF which is proportional to the trapping rate $\varkappa$. σ is the trapping cross section. From fig. 21 we get for $C_{HF} = 1.9 \cdot 10^{-6}$ mole fraction ($\approx 6.4 \cdot 10^{16}$ cm^{-3}) $I_3 = 26\%$ which is equivalent to $\varkappa = \lambda_b - \lambda_t = 0.67 \cdot 10^9$ sec^{-1} (appendix IV, (IV 1). $\lambda_b = \frac{10^9}{0.67}$ sec^{-1}, $\lambda_t = \frac{10^9}{1.23}$ sec^{-1}). Hence we find:

$$\sigma = 2.2\ 10^{-15}\ \text{cm}^2 = 22\ \text{A}^2.$$

Another quantity often used to characterize a reaction rate is the reaction constant, $K = \varkappa / C_{HF}$. We find:

$$K = 6.3 \cdot 10^{12} \frac{1}{\text{mol sec}} = 1.05 \cdot 10^{-8} \frac{\text{cm}^3}{\text{sec}}$$

This is about one hundred times larger than the biggest reaction constants known from o-Ps reactions in aqueous solutions [7].

4.2.2. Annealed Frozen HF-Solutions

The fast freezing procedure is likely to leave the frozen samples in a non-equilibrium state. As an attempt to approach equilibrium conditions, fast frozen samples were annealed at -18°C for 20 hours and subsequently cooled to -160°C with a rate of around 1°C/min. Their lifetime spectra were then measured at -160°C. The spectra were analysed in the same way as those for fast frozen samples. The results are also shown in fig. 21. At low HF-concentrations, the points show the same variation as those for fast freezing, but they are shifted about a factor of 4.6 towards higher HF-concentrations. For high HF-concentrations, larger deviations occur between the two sets of measurements. Some fast frozen and consequently annealed samples were cooled to -160°C with a rather high rate (10 - 15°C/min). The analysis of the measured spectra gave results close to those of fast frozen samples.

4.2.3. The Transition from Fast Frozen to Annealed State

In order to further investigate the transition from fast frozen to annealed state which is indicated by fig. 21, fast frozen samples were heated to different temperatures. They were then re-cooled slowly to -160°C and their lifetime spectra recorded. The results showed that the transition takes place below -100°C since no further change of the spectra occurred by heating the samples to higher temperatures. The temperature region up to -100°C was subsequently investigated in more detail for a HF-concentration of 10^{-6} mole fraction. The result of this is shown in fig. 22 as the relative intensity of the component with lifetime 1.23 nsec as a function of temperature. The points were measured in the order indicated by the arrows. The intervals between consecutive measurements were one day and one night, the cooling rate approx. 1°C/minute. An irreversible transition is clearly seen to take place in the interval between approximately -130°C and -120°C.

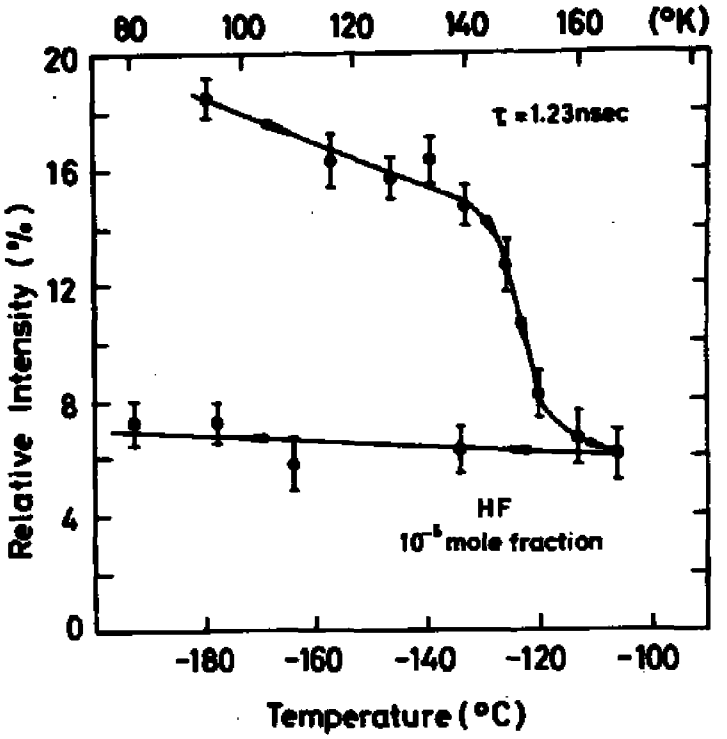

Fig. 22. Change of lifetime spectrum for a fast frozen 10^{-6} mole fraction HF solution upon heating (and re-cooling) as indicated by the relative intensity of a component with lifetime 1.23 nsec. The intervals between successive measurements were one day, the cooling rate approximately 1°C/minute. The indicated uncertainties are the standard deviations as estimated by the computer.

4.3. Positron Lifetimes in Frozen Aqueous Solutions of Various Acids, Bases, and Salts

Some measurements were made on frozen NH_3 solutions at different temperatures. Only small differences from the results of pure ice were found. The most important results are given in table 3.

Table 3

Relative intensities of component with lifetime 1.23 nsec at -160°C and lifetime and intensity of longlived component at -9°C for frozen aqueous solutions of NH_3. The uncertainties on τ_3 and I_3 are standard deviations as estimated by the computer. The uncertainties on the concentrations are estimated at $\pm$ 20%. The sequence of the measurements on 10^{-3} mole fraction was the one used in the table.

Concentration (mole fract.)	Temperature (°C)	$\tau_3 \pm \Delta\tau_3$ (nsec)	$I_3 \pm \Delta I_3$ (%)	Treatment
$4 \cdot 10^{-2}$	-160	1.23	9.1 ± 0.9	fast frozen
10^{-3}	-160	1.23	5.0 ± 1.1	fast frozen
10^{-3}	- 9	1.22 ± 0.07	34.5 ± 7.6	
10^{-3}	-160	1.23	5.7 ± 0.5	annealed

A number of other fast frozen salt and acid solutions have been investigated at one or two different concentrations in order to compare with the HF results. None of them influenced the lifetime as strongly as HF. The results, indicated by the relative intensity of a 1.23 nsec lifetime component, are listed in table 4.

Table 4

Relative intensity of component with lifetime 1.23 nsec for fast frozen solutions measured at -160°C. The uncertainties are standard deviations as estimated by the computer. For comparison, values for pure ice and HF are included. The uncertainties on the concentrations are estimated at ±20%.

	Concentration (mole fract.)	$I_3 \pm \Delta I_3$ (%)
Pure ice	0	1.5 ± 0.5
HF	10^{-4}	52 ± 2
LiF	10^{-4}	11.9 ± 0.8
NH_4F	$1.3 \cdot 10^{-4}$	6.5 ± 0.7
CsF	10^{-4}	8.2 ± 0.7
HCl	10^{-4}	31.2 ± 0.6
HCl	10^{-2}	50.3 ± 0.7
HBr	10^{-4}	37.2 ± 0.8
HJ	10^{-4}	23.3 ± 1.4
H_2SO_4	$1.1 \cdot 10^{-4}$	3.2 ± 0.6
NaCl	10^{-5}	5.9 ± 0.8

4.4. Experimental Experiences and Difficulties

From the preceding sections of this chapter one may get the impression that all the measured spectra were obtained in a smooth way without any difficulties. This is, however, not quite true. In this section will be discussed some of the problems involved in obtaining reproducible results.

In the first results measured for heavy ice, the long lifetime as a function of temperature followed the shape of the curve shown in fig. 17,

but the whole curve was shifted upwards by about 50 psec. Also τ_1 and I_2 deviated from those in fig. 17. When it was realized from the measurements on frozen aqueous solutions that very small amounts of impurities might lengthen the positron lifetimes appreciably, the curve was re-measured with heavy ice frozen from the purest heavy water available (specific conductivity less than 10^{-5} (ohm cm)$^{-1}$). Now the results agreed with those of light ice (fig. 17), but still a very small shift towards longer lifetimes was revealed. Measurements on ten times cleaner D_2O would probably show no shift at all (the light water used had a specific conductivity of less than 10^{-6} (ohm cm)$^{-1}$).

The measurements on monocrystals gave no unambiguous results either. The first measured pair of monocrystals studied also gave longer lifetimes than those for polycrystalline samples. Moreover, the long lifetime from a 2-term fit increased for temperatures below around -170°C. An analysis keeping one lifetime in a 3-term fit fixed at 1.2 nsec showed that the intensity of this component was around 5% for temperatures of -166°C and above and around 10% for temperatures of -174°C and below. A close examination of the two pieces of monocrystal showed some small unclear spots in the bulk of the ice. They were likely to be caused by impurities segregated out during growth of the crystal. Hence, probably also other parts of the crystal contained considerable amounts of impurities. Consequently two pieces were cut from another monocrystal that was perfectly transparent. The results of measurements on these samples are those presented in figs. 17, 18 and 20. Attempts were made to check the impurity content of the monocrystals by measuring the specific conductivity of the melt water from them. The conductivities were quite large, but they could not unambiguously be ascribed to impurities in the bulk of the ice. Only small pieces of monocrystal (approx. 1 cm^3) were available for the check, so that unavoidable impurities on the surface may have contributed considerably to the total impurity concentration in the melt water.

Also the light ice measurements were checked for the possible influence of impurities, in particular the influence of dissolved oxygen. This was done by freezing four times distilled, oxygen-free water in a nitrogen atmosphere. The measurements on this sample were within experimental uncertainty in agreement with the other light ice results, although there was a tendency towards a small increase in the long lifetime.

The measurements on light and heavy water were also performed two or three times to check the results, some of the measurements being on

oxygen-free water. They all agreed within experimental uncertainties with those of table 1.

Quite a few difficulties arose from the annealed fast frozen HF solutions, until it was realized that a number of large disagreements between results were caused by the use of too old solutions. All HF-solutions were stored in polyethylene bottles. It was realized that solutions one or two months old were useless, since they all gave a long lifetime of around 1.3 nsec, when fast frozen. Probably after this period of time a high concentration (in this connection) of impurities from the walls of the bottle had been dissolved in the water.

Because of the possible influence of these extra impurities and a suspicion about an uncontrolled heating of the first sample, the transition around -125°C (fig. 22) in a fast frozen HF solution was measured twice. In the two cases the transition was found in the same temperature interval.

Finally the indication of a transition around -170°C given by the impure monocrystal was pursued with a fast frozen 10^{-6} mole fraction HF solution that was annealed at -18°C for 20 hours. It was subsequently slowly cooled to the temperature region of interest and measured at a number of temperatures around -170°C. The results showed with a high probability that differences do exist between spectra taken at temperatures above and below approx. -170°C. However the results were not unambiguous, and lack of time prevented a further investigation of the phenomenon within the framework of the present report.

The examples of experimental difficulties given in this section show that great care must be taken to eliminate the influence on the positron lifetimes of impurities in ice. Recent publications [64) 65) 49)] show that also in other solid materials than ice, the results of positron annihilation measurements will be strongly influenced by the presence of even small concentrations of impurities or defects.

5. DISCUSSION

5.1. Properties of Ice and Water

5.1.1. The Water Molecule

The distances from an oxygen atom to the two hydrogen atoms in a water molecule are 0.96 A, and the angle between two straight lines connecting the oxygen nucleus with the hydrogen nuclei is $104.^{\circ}5$ [46]. The electron density distribution in the molecule has been the subject of several theoretical calculations. They lead to the result that in the plane of the three atoms the electrons are not distributed symmetrically around lines drawn from the oxygen nucleus toward the hydrogen nuclei, but have a higher density in the angle between these lines than outside, i.e. the bonds between oxygen and hydrogens are somewhat bent towards each other. Furthermore, two lobes of charge project away from the molecular plane, one above and one below. They are the so-called lone-pair electrons and to some extent they probably project away from the hydrogen atoms [46]. A visualization of the water molecule is thus an oxygen atom with four electron clouds pointing out from it in a somewhat distorted tetrahedral fashion. Two of the electron clouds also each contain a proton.

5.1.2. Ice

When water molecules are built together to form an ice lattice the tetrahedral configuration is retained. Each oxygen atom is bound to four neighbour oxygens by hydrogen bonds, each formed of a lone pair and a hydrogen-oxygen bond. The water molecules still, to some extent, exist as individual molecules in the ice lattice, since two of the four protons surrounding an oxygen atom are closer to the oxygen (1.0 A) and two farther from it (1.76 A). This lattice arrangement is seen in fig. 23, which shows the crystal structure of ordinary ice, the so-called hexagonal ice I (ice Ih).

The tetrahedrally bonding of the oxygen atoms and the fact that two protons are positioned close to and two far from each oxygen do not com-

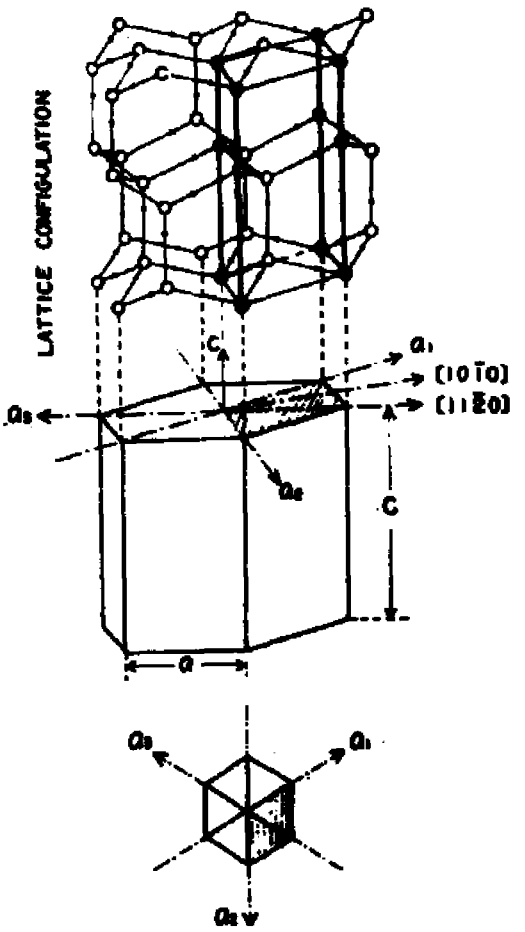

Fig. 23. Crystal structure of hexagonal ice I (ice Ih). The thicker lines show a lattice unit cell (from ref. 51).

pletely define the ice structure. The oxygens may theoretically be arranged in a number of different crystalline and amorphous structures, and for each structure the protons may be distributed in the bonds in many different ways. In crystalline structures some of these distributions will be ordered (i. e. in two different un'. cells equivalent protons are always positioned in the same way with respect to the oxygens), while others will be disordered.

Actually, at least ten different forms of ice are known at present. Most of them only exist at high pressures (several kbar) or in a metastable form at low temperatures [47]. At normal pressure two crystalline forms of ice can exist: the ordinary one of a hexagonal crystal structure, ice Ih (fig. 23), and another of a cubic structure, ice Ic, which may exist at low temperatures. Ice Ic can be made by heating some of the high pressure forms of ice. It can also be made from a non-crystalline form of ice, the so-called vitreous, glassy, or amorphous ice that transforms irreversibly

to ice Ic when heated to temperatures above approx. 135°K [52].

Both Ice Ih and Ic are disordered in the hydrogens. However it has been suggested [66] that an ordering of the hydrogen atoms may take place at low temperatures, so that the entropy vanishes at 0°K. Indications of irregularities in physical properties around 100°K have been found in several experiments [67] [68] [69] [70], but none of them has given an unambiguous answer to the question whether an ordering of the hydrogens takes place. The difficulties of observing a clear effect have been explained by the slowness of the transition if the latter is taking place at all [71].

Ice Ih has been the subject of numerous experiments. Based on them, a model of the microscopic structure of ice has been developed. It contains different structural defects, the so-called orientational (or Bjerrum) defects [53], ionic defects, vacancies, and interstitials. A Bjerrum L-defect exists when the proton is missing in a hydrogen bond, and a D-defect when two protons are contained in the same hydrogen bond. An H_3O^+-ionic defect exists when three protons are situated close to the same oxygen, and an HO^--ionic defect when an oxygen atom has only one proton close to it. The model further assumes that HF and NH_3 can be incorporated substitutionally in the lattice thus creating L- and H_3O^+-defects and D- and HO^--defects respectively. This model explains a number of experimental observations, especially regarding the electrical properties of ice. A detailed discussion of the model is found in ref. 45.

Some experimental observations, however, seem to be inconsistent with this model. In refs. 54 and 55 is described a hexagonal microstructure observed in ice monocrystals. According to the references, the microstructure consists of coordinated, hexagonal, prismatic units of a width ranging from approx. 0.5 to 10 microns and a length from about 1 to 10 microns. Such a microstructure is not incorporated in the model described above. Furthermore, many older measurements have been questioned by recent experimental results, in particular on electrical properties, and many people still find values of the same physical quantity which may differ by orders of magnitude. Most of the discrepancies are probably due to small uncontrolled amounts of impurities, surface effects and different measuring techniques [47] [56] [58]. Recent studies of the HF solubility in ice monocrystals [59] indicate that the interpretation of older experiments [60], which provided strong support of the defect model described above, may be challenged. Also from theoretical considerations the model has been questioned [57]. Hence, at present a rather unclear picture exists of the microscopic proc-

esses causing the observed macroscopic properties of ice.

5.1.3. Water

As regards water the picture is even more confusing. The well-known experimental facts that water at the melting point is around 10% more dense than ice and that it has a density maximum at 4°C are two properties among several that differ from those of other liquids and which make water a unique substance. Radial distribution functions obtained by X-ray diffraction suggest that the tetrahedral bonding of oxygen atoms known from ice also exists in water. This fact has been used in many of the models proposed for water as an argument in favour of the conception of water having some ice-like structure. Most of the models are so-called mixture models in which the water is assumed to be composed of a mixture of two or more individual species, of which one is generally assumed to be ice-like and the other closer packed water molecules with broken hydrogen bonds. The closer packing accounts for the higher density of water compared with ice, and a shift with temperatures of the equilibrium amounts of the different species combined with the usual thermal expansion reproduces for example the density maximum at 4°C. Other thermodynamic properties as well as the radial distribution functions are reproduced quite well by most of the mixture models. Another model, the so-called "distorted hydrogen-bond" model in which the hydrogen bonds are assumed not to be broken but only bent to some extent, also accounts reasonably well for most of the experimentally observed properties of water. This model as well as all the others, however, contain approximately ten adjustable parameters. A detailed discussion of the different models is given in ref. 46.

Regardless of which models are used, however, two main differences certainly exist between ice and water, namely the long range order of ice, which water does not possess, and the reorientational and translational frequencies for the molecules which are 10^5-10^6 sec^{-1} in ice and 10^{11}-10^{12} sec^{-1} in water [46].

5.2. The Ice Water Phase Transition and Water

5.2.1. The Phase Transition

The change in the long positron lifetime and its intensity was found to take place at the melting point for both H_2O and D_2O (fig. 14). This seems

to be in good agreement with the results for H_2O in ref. 21*. Also for other molecular substances, an abrupt increase in the long lifetime upon melting has been reported (viz. napthalene [78], teflon [44], methanol [62]). For a few other molecular materials, values of the long lifetime in both the solid and liquid phase have been published (phenol [79], octanol [80], ammonia [63], methane [82], cyclohexane [82], benzene [82], glycerol [44], polyethylene [44]). In all cases the long lifetime is longer in the liquid than in the solid. In some cases the increase can be correlated directly to an increase in free volume (i. e. the "empty" space between the molecules of the substance) upon melting (naphthalene [21], teflon [44], glycerol [44], polyethylene [44], benzene [23]) while in others such a correlation is not possible, and the lifetime in the liquid is longer than predicted by the volume change (water [21], ammonia [63]).

The intensity of the longlived component does not vary in a regular way from solid to liquid phase for the various substances mentioned above. In some of them the liquid value is the largest (naphthalene [78], cyclohexane [82], benzene [82], teflon [44]) and in others the smallest (phenol [79], methanol [62]) while in some it is unchanged over the phase transition (ammonia [63], methane [82]). These results show that no simple rules exist which govern the changes in the long lifetime and its intensity at a solid - liquid phase transition, and hence no general pattern exists into which water and ice may be fitted.

5.2.2. Water Compared with Other Molecular Liquids

The values for light water of the long lifetime and its relative intensity (table 1, section 4.1.1.) agree very well with most of the published data on these quantities [79]. The longlived component is attributed to annihilation of o-Ps. Its relative intensity also agrees closely with the value of $36 \pm 1\%$ for the total Ps formation as determined by angular correlation magnetic quenching experiments [43] if the reasonable assumption is made that no ortho-para conversion takes place. (The effect of conversion is discussed in appendix V).

Gray, Cook and Sturm [83] have measured positron lifetimes in close to 200 organic liquids, including light and heavy water. Although their results and those of table 1 do not agree in detail (ref. 83: $\tau_3 = 2.07 \pm 0.05$ nsec in

---

* Although some inconsistency seems to exist in the temperature axis of the figure in ref. 21.

H_2O; 1.93 ± 0.09 nsec in D_2O) they also find the intensity of the longlived component in H_2O a few per cent larger than in D_2O. (20.3% and 16.8%). They find the same lifetime for normal and deuterated benzene, but around 5% smaller intensity for the latter (35.8% and 30.4%).

Singh, Singru and Rao [84] measured among other organic substances lifetimes in normal and deuterated acetone. They found a slightly longer lifetime in the latter (within uncertainty) and a few per cent lower intensity (17.3% and 13.6%). Normal and deuterated methanol were investigated by Chuang and Tao [62]. They found the same lifetime in the two liquids, but one or two per cent smaller intensity in the deuterated methanol. So it seems to be a general feature of a liquid whose molecules contain hydrogen that deuteration will decrease the Ps yield.

Gray, Cook and Sturm [83] have been able to ascribe empirically a quenching cross section to each structural group in the organic molecules they have treated. The cross section accounts for the amount of quenching (pick-off) a certain group will cause to the o-Ps lifetime. The o-Ps lifetime for a certain molecular liquid can then be found by summing the quenching effects of the different structural groups of the molecule. This empirical rule can account for the long lifetime in nearly all the liquids investigated by Gray et al. However, an exception is water in which it predicts a lifetime around 65% too long. The authors ascribe the discrepancy to the hydrogen bonding of water. Bisi, Gambarini, and Zappa [85] have made a similar empirical rule for a number of molecular liquids by ascribing to each atom an effective number of electrons with which pick-off annihilation takes place. They also find good agreement between calculations and experiments for most of the liquids they have studied. An exception is water, for which their model predicts a 30% shorter lifetime than measured. So it is evident that water reacts in an abnormal way with Ps when compared to other molecular liquids, although the nature of the deviation is difficult to define.

5.2.3. Water Compared with Ice

A satisfactory explanation of the differences in Ps formation probabilities between ice and water and between liquid H_2O and D_2O will probably require a detailed knowledge of the slowing-down processes of positron and Ps in the substances. Since very little is at present known about these processes, it is not possible to give this explanation. A discussion within the framework of the Ore gap model (section 1.2.) has been attempted (see appendix VI). Although it gives some indication of a narrower gap for water

than for ice and hence a smaller Ps formation probability for water, its main conclusion is that too many uncertain factors are involved in the determination of the Ps yield to give but a rough qualitative agreement with experiment. The model gives no explanation of the difference between liquid H_2O and D_2O.

Regarding lifetimes, the problem is to explain why o-Ps has a longer lifetime in water than in ice, in spite of water being more dense than ice. A qualitative discussion of this is given below.

In angular correlation curves for water, the width of the narrow component which is attributed to p-Ps is considerably larger than for ice at low temperatures [27)42)43)]. A simple explanation for this is that while Ps is delocalized in ice at low temperatures [42)] it is localized in water. If p-Ps is localized by a harmonic potential and has a spherical spacial distribution with a typical diameter of 3 A, a spread in its momentum will result on account of the uncertainty principle, and the corresponding width of the angular correlation curve will be approx. 3.6 mrads. (appendix VII)). In section 4.2.1. it was shown that very small amounts of defects in ice would trap Ps. In the very irregular structure of water it is therefore likely that Ps becomes trapped in a hole within a very short time, i.e. becomes localized.

In several liquefied gases positron lifetimes of the order of tens of nsec have been observed [8)]. This phenomenon is caused by a bubble which Ps by exchange forces creates around itself in the liquid. Because of the strongly reduced electron density in the bubble the o-Ps lifetime against pick-off will be greatly increased. An analogous picture has been used for some ordinary liquids in which o-Ps is believed to create a cage where it stays localized with a longer lifetime than would be expected from the average electron density of the liquid. Lee and Celitans [61)] used this model to explain the relationship between the quenching constants of oxygen and nitric oxide dissolved in various liquids and the viscosity of these liquids. They assumed that the cage moves as a whole through the liquid and that a reaction occurs, in one of many collisions, every time a cage and a quencher molecule meet. Also in some aliphatic compounds and their derivatives the bubble model gives a fair description of the o-Ps pick-off annihilation [72)].

In the light of this and the above-mentioned results from angular correlation measurements, it is reasonable to assume that the longer o-Ps lifetime in water compared to ice is caused by the formation of a cage around the Ps atom in water. The forces stabilizing the cage are the ex-

change force between the Ps electron and the electrons of the surrounding water molecules, and the bonding between the water molecules. The former tends to increase the size of the cage, while the latter tends to make the cage collapse. A similar model has been used to explain the solution of non-polar molecules in water: first a cavity is formed and then the non-polar molecule is transferred into it [86]. Since water is a very open structure it is easy for a molecule (or Ps) to find a region where sufficient space is available for it [86].

The difference in o-Ps lifetime between H_2O and D_2O is probably caused by the slower movement of the D_2O molecules at a given temperature (the translational and rotational frequencies of D_2O are of the order of 20% lower than for H_2O [46] because of the higher mass). This gives fewer collisions between the water molecules and the cage surrounding the Ps atom and hence a more stable cage, which is likely to increase the o-Ps lifetime. Measurements of the lifetime in light and heavy water as a function of the temperature will give more information about this problem.

In ice the rigid structure will probably prevent formation of cages (at least at low temperatures), and since no difference exists between the lattice parameters for H_2O and D_2O [46] no difference in lifetime should be expected.

5.3. Pure Ice

5.3.1. Analysis of Spectra

In the analysis of the ice data it is striking that the results shown in fig. 18 and fig. 20 are so different. The main reason is that the spectra corrected for source annihilation contain more than three exponential terms. And when a spectrum, which contains more terms than can be resolved, is fitted with a smaller number of terms, the fitted parameters are strictly speaking only mathematical numbers that describe a curve which is a good approximation to the measured spectrum. If in an analysis weight is attached to one part of the spectrum, and in another analysis of the same spectrum to another part, the parameters resulting from the analyses are likely to be different in the two cases. The weight can be changed for example by changing the numerical weight ascribed to each point in a least-square fitting procedure or by imposing some sort of constraint on the parameters to be fitted. A method of analysis, which has often been used, is the one by which the component with the longest lifetime

is determined and subtracted from the spectrum, and the difference then considered as an unresolvable mixture of shorter lifetimes. This method attaches great weight to the longlived component and more or less ignores the detailed shapes of the shortlived ones. It cannot be said in general what particular method of analysis is the most correct to use; the only requirement is that the resulting parameters must represent a curve that fits the measured one reasonably well. The method to be chosen for a certain problem should be the one that most efficiently extract the wanted physical information from the measured spectrum. The above considerations only apply if a spectrum contains a larger number of components than can be resolved. If a spectrum is known to contain only a resolvable number of components (normally 1, 2 or 3) the correct way of analysis is naturally to fit with the relevant number of terms without any constraints. Following these considerations, the parameters in fig. 18 are mathematical figures each of which need not be directly associable with a single well-defined physical quantity, while in fig. 20 the parameters are the results of an attempt to associate the longlived component with o-Ps.

As seen in fig. 18 a longlived component of a relative intensity of one or two per cent can be resolved at low temperatures. The influence of this component on the fitted parameters is greatly reduced in the 2-term fit (fig. 17) and in the 3-term fit with an intensity fixed at 52% (fig. 20). However, it strongly influences the results of the 3-term fit without constraints (fig. 18). The origin of the component is not known, but various possibilities exist. It may be an inherent part of a true ice spectrum and is then probably caused by the annihilation of a small fraction of the total amount of o-Ps under special conditions. The component could also be due to small uncontrolled amounts of impurities (it is likely that the deviating results of run 2 for polycrystalline samples are caused by this), or it may be caused by insufficient correction for annihilation in the source. The uncertainties involved in the source correction procedure are discussed in section 3.4.4. Souder [87] has shown that in metals the positron lifetime is dependent upon whether the source is external or "deeply embedded" in the metal. A similar effect of the surface of the material may influence the lifetime of Ps in ice, in particular since Ps is delocalized in ice as is the positron in a metal.

5.3.2. Free Volume Model

It seems reasonable for temperatures below -100°C to ascribe the three lifetime components in fig. 20 to annihilation of o-Ps (τ_3, I_3, the basis of

the analysis), "free" positrons (τ_2, I_2), and p-Ps (τ_1, I_1). The value of τ_2 (0.44 nsec) is close to the "free" positron lifetime in water (0.40 nsec, section 3.4.5.), and τ_1 (0.12 nsec) is in good agreement with the lifetime of free p-Ps (which becomes 0.105 nsec when pick-off is taken into account). Furthermore, I_1 is fairly close to 1/3 I_3 (the broken line).

The rather small increase occurring in the volume of ice when its temperature increases from -200°C to near the melting point is not sufficient to explain the large increase in the longest lifetime above -100°C as only being a volume effect. The thermal expansion coefficient of ice is zero around 75°K and increases almost linearly with temperature above 75°K and reaches the value $5 \cdot 10^{-5}$ $(^{\circ}K)^{-1}$ at the melting point [45]. Hence the volume increases approximately as:

$$V = V_o (1 + 4 \cdot 10^{-7} \cdot (T - 75)^2)$$

where T is the temperature in Kelvin. At the melting point the volume is around 1.6% larger than at 75°K. Since the volume in ice not occupied by the molecules (the "free volume") amounts to around 66% [86], a change of only 1.6% cannot give so much more space for Ps that the pick-off rate will decrease to nearly half the original value. To get an approximate quantitative expression of this, the simple "free volume model" of Wilson et al. [23] can be used. They calculate the o-Ps lifetime to be:

$$\tau = k V_f^{0.87} ,$$

where k is a constant and V_f is the volume of the hole in which the o-Ps atom is assumed to be. If the free volume amounts to around 66% as in ice, a relative increase of the total volume of $(\Delta V_t/V_t)$ will entail a relative increase in free volume of approx. 1.5 $(\Delta V_t/V_t)$. From the expressions for τ and V above we find:

$$\tau = \tau_o (1 + 0.87 \cdot 1.5 \cdot (\Delta V_t/V_t))$$

$$= \tau_o (1 + 5.2 \cdot 10^{-7} \cdot (T - 75)^2) .$$

The change in lifetime with change in temperature as given by this expression is shown in fig. 20 by the broken line termed "free volume model". It was fitted to experiment at -190°C, and agrees well with the measurements up to -100°C, but not above since the relative change in lifetime caused by changes in free volume over the whole investigated temperature range should

amount to only around 2%. This order of magnitude also agrees with the results of the more elaborate free volume model of Brandt et al.[21)44)88)]. The latter gives for spherical geometry values that range from a little less than 2% to around 5.5% depending upon a scattering parameter S[21)88)].

5.3.3. Trapping of Ps and Positrons

A more reasonable explanation of the large increase of the long lifetime is that trapping of o-Ps takes place in defects, the number of which increases with temperature. This explanation is supported by the temperature dependence of angular correlation curves for ice single crystals[89)]. With increasing temperature, the area of the side peaks and the narrow central peak (see fig. 3) decrease and a component with a width of around 3.2 mrad emerges. This strongly suggests that with increasing temperature an increasing number of p-Ps atoms becomes localized within a few Angstrom (i.e. becomes trapped). Hence, also o-Ps must be trapped and, at a certain temperature, with a higher probability than is p-Ps, since the o-Ps lifetime is longer than that of p-Ps. This involves two characteristic decay rates of o-Ps (appendix IV).

In pulse radiolysis experiments on ice, the absorption of light by irradiation-produced solvated electrons has been measured[90)91)]. The results indicate that there is a high probability for an electron, moving quasi-freely around in the ice lattice, to be trapped[90)91)]. Although the timescales over which the pulseradiolysis and positron lifetime measurements are carried out are different (μsec and nsec, respectively) these results suggest that also positrons will be trapped in ice. Defects are involved in the trapping process. Since their number increases with temperature, the trapping probability is likely to increase too. Hence it is likely that the decay of the positrons not forming Ps will also be governed by two different rates (appendix IV), and consequently that the lifetime spectra for higher temperatures contain at least five components.

Therefore, τ_3 in fig. 20 is an average of the longest lifetimes in a spectrum (mainly due to o-Ps), and the peculiar behaviour of τ_2 and I_1 is caused by the mixing of the shorter lifetime components in the analysis.

If the traps for o-Ps are one kind of temperature-created defects, the number of traps, N, should depend upon temperature, T, as[92)]:

$$N = N_o \exp(-E_a/kT) ,$$

where N_o is a constant, E_a is the activation energy for the creation of a

defect and k is Boltzmann's constant. Experimentally the relative variation of the number of traps can be determined if the o-Ps lifetime in the traps, τ_t, is known. Keeping one lifetime fixed at τ_t in the analysis of the spectra gives the relative intensity, I_t, of this lifetime component. The number of traps will then be proportional to $N' = [I_t/(0.52 - I_t)]$ if the total o-Ps yield is 52% (appendix IV). Hence, a plot of log N' against 1/T (Arrhenius plot) will show a straight line if the above-mentioned exponential dependence exists. From the slope of the line, E_a can be determined.

This analysis has been carried out for different values of τ_t, ranging from 1.1 nsec to 1.7 nsec. The plot is shown in fig. 24 for the values 1.1 and 1.23 nsec. (The value 1.23 nsec was taken from the results for frozen solutions of HF. However, since the nature of the traps is probably different

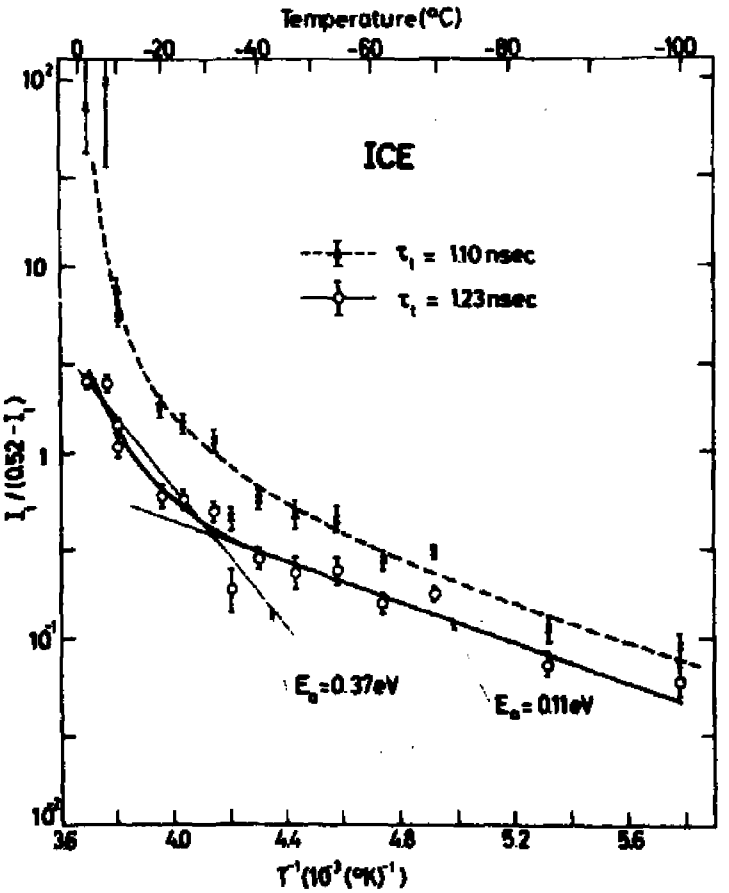

Fig. 24. The quantity (I_t/ (0.52 - I_t)), which from a simple trapping model is proportional to the number of traps, plotted against T^{-1} (Ahrrenius plot) for two different τ_t, the o-Ps lifetime in the traps. I_t is the relative intensity of the component with lifetime τ_t. The slopes of the two straight lines determine activation energies for possible temperature-created defects, that trap o-Ps.

in the two cases, the lifetimes in the traps need not be the same. Actually, fig. 18 suggests that it is larger than 1.23 nsec in pure ice.) For bigger values of τ_t the plot looks essentially like the one for τ_t = 1.23 nsec, only the curve which can be drawn through the points is lowered, the more the bigger τ_t is. The important point is that it is not possible to fit the points to a single straight line in a reasonable way, whatever value is used for τ_t. To determine the order of magnitude of the activation energies involved, the points for τ_t = 1.23 nsec was fitted with two straight lines. The associated energies are 0.11 eV and 0.37 eV. The same magnitudes or slightly smaller values will be found for larger τ_t-values.

The nonlinearity of the Arrhenius plot indicates that the increase of lifetime with temperature is not simply caused by the trapping of o-Ps in one kind of thermally created defects in which o-Ps has one well-defined lifetime. Another explanation might be that trapping takes place in two different types of defects with different activation energies (and possibly also different τ_t). A linear plot can be obtained, though, with only one kind of trap, if the lifetime in the trap increases strongly with temperature (around 15% from -100°C to 0°C). Such a large increase, however, seems unrealistic in the light of the previous discussion of the effect of thermal expansion. Since any physically reasonable model which increases the number of "fitting parameters" is likely to be in agreement with the points in fig. 24, probably also other explanations can be thought out.

5.3.4. Possible Trapping Centres

The different sorts of defects which are generally believed to exist in ice were shortly described in section 5.1.2. None of them, however, can be correlated satisfactorily to the trapping of o-Ps. An estimated vacancy concentration at -10°C is approx. 10^{-10} mole fraction[45] (in ref. 93 it is suggested that it may be as high as 10^{-5} mole fraction near the melting point, but no arguments are given for the figure). The concentrations of interstitials and ionic defects are around 10^{-11} mole fraction[45]. Since it seems to be quite common that defect concentrations have to be of the order of parts per million to be detected by positrons or Ps (section 4.2.1. and refs. 49, 64, 65), these defect concentrations in ice are too small to act as efficient trapping centres. Also the effect of dislocations on Ps must be too small to be observable. A typical density is 10^6 cm^{-2} [51) 55] which roughly speaking is equivalent to at most 10^{-9} mole fraction of point defects. It is likely that the number of dislocations is different for the different samples,

in particular between the mono- and polycrystalline samples. The fact that the results are the same for the different ice samples supports the assumption that dislocations have no influence on the positron lifetimes. Neither has any annealing effect been observed, although of two subsequent measurements one was normally carried out at a high temperature, the other at a low temperature. The only defects of sufficient concentrations are L- and D-defects, of which around 10^{-6} mole fraction exist at $-10^{\circ}C$. The energy required to form a pair of these defects is 0.68 eV [45)46)]. The apparent activation energy for the formation of one of these defects will then be $\frac{1}{2}$ 0.68 eV = 0.34 eV [45)92)], close to the 0.37 eV found from fig. 24. The concentration of L-defects is generally believed to be increased by HF doping and decreased by NH_3 doping (for D-defects vice versa). However both of these dopings tend to increase the long positron lifetime (see fig. 21 and table 3), thus indicating that neither L- nor D-defects are responsible for the trapping of Ps.

Grain boundaries in ice may provide trapping centres for Ps, in particular since Ps is delocalized before trapping takes place. However, as the results for poly- and monocrystalline samples are identical the only grain boundaries which may have an influence are those of the hexagonal microstructure [54)]. Nothing is known, however, about the change of this microstructure with temperature that might be correlated to the present measurements.

Proton magnetic resonance measurements [94)] in the temperature range from $-20^{\circ}C$ to $0^{\circ}C$ indicate that more than 10^{-3} mole fraction of the molecules in pure ice are in a liquid-like state. If regions really exist in the crystalline structure where water molecules are loosely bound as in the liquid they will almost certainly trap Ps atoms. The number of such regions and their volume are likely to depend upon temperature, a dependence which might result in the observed change in positron lifetime with temperature.

The above discussion shows that although different possible mechanisms are conceivable which may explain the measured temperature dependence of the positron lifetimes, a detailed model will at present be based mainly on guessing. Angular correlation measurements on ice single crystals over the whole temperature interval treated here are likely to give more information about the annihilation mechanisms. A more detailed determination than that given in ref. 19 of the $3\dot{\gamma}$ annihilation rate as function of temperature is also desirable.

The sudden change in dependence on temperature of the long lifetime

from a slow to a rapid variation above a certain temperature takes probably also place in ammonia [63]. As in ice the "free volume model" accounts for the slow variation, but not for the rapid one. In quartz, which has a hexagonal crystal structure like ice, Ps is also delocalized [64]. At room temperature and at liquid nitrogen temperature only one [95] or two [96] [97] short (~ 0.3 nsec) lifetime components have been observed. The very short o-Ps lifetime is explained as being caused by a smaller free volume compared with ice [95]. It would be interesting to see whether the lifetime shows a behaviour similar to that in ice and ammonia at higher temperatures.

5.4. Frozen Aqueous Solutions

The very good agreement (except for the lowest HF concentrations) between the trapping model and the measurements on fast frozen HF solutions (fig. 21) strongly supports the assumption that o-Ps (and hence also p-Ps) becomes trapped in defects created by HF in the ice matrix during fast freezing. As discussed in appendix VII, the localization of p-Ps that occurs on trapping will cause a broadening of the narrow component of the angular correlation curve. A small broadening is actually observed [98], and this fact further supports the assumption that trapping of Ps takes place, although detailed quantitative agreement between angular correlation and lifetime measurements on the basis of a simple trapping model (appendix IV) could not be established. The large reaction constant for the trapping of o-Ps must probably be related to the delocalization of Ps.

5.4.1. Other Measurements on Frozen Aqueous Solutions

In an attempt to understand the processes leading to the present experimental results for the frozen aqueous solutions, some experimental results obtained by other methods will be discussed below.

Generally speaking, the solubility of any atom, molecule and ion in ice is very small (in particular compared with normal solubilities in liquid water). The strong hydrogen bonds make ice very reluctant to include foreign atoms, ions or molecules, and the relatively high solubility (compared with other molecules) of HF, NH_3 and NH_4F (for HF $4 \cdot 10^{-6}$ to $4 \cdot 10^{-5}$ mole fraction; see further below) has been considered as being caused by their ability to substitute water molecules in the ice lattice [45]. However, in particular the measurements by Bilgram [59] of the amount of HF incorporated in ice single crystals grown from a solution of HF make it unlikely that all HF goes substitutionally into the crystal. Bilgram proposes that HF is in-

corporated preferentially in the grain boundaries of the hexagonal microstructure [54]. An explanation of the diffusion of HF through an ice single crystal must also include these grain boundaries as strongly influencing the diffusion process [100].

The composition of the matrix resulting from a freezing through states of equilibrium of aqueous solutions of hydrogen fluoride, as well as other acids, bases, and salts in higher concentrations can be found from ordinary two-component phase diagrams [101]. By slow cooling, pure ice will crystallize and regions with increasing concentration of the solute will be segregated from the crystalline phase. When the eutectic temperature has been reached, the segregated regions will freeze as a whole, normally to a crystalline structure of hydrates.

When the cooling rate becomes faster so that freezing does not take place under equilibrium conditions, the picture becomes more complicated. Different methods (i.e. differential thermal analysis (DTA), electron paramagnetic resonance (EPR), nuclear magnetic resonance (NMR), perturbed angular correlation (PAC), and Mössbauer effect) have been applied to investigate the structure of fast frozen aqueous solutions. A number of questions have not yet been solved, but from the references 101 - 110 some conclusions can be drawn.

Vuillard [101] has by DTA investigated a number of fast frozen aqueous solutions of bases, acids and salts for concentrations larger than about 1%. For all of them he finds that a glassy state exists at low temperatures. Upon heating, it is transformed into a supercooled liquid, the so-called glass transition. It takes place within a few degrees around a characteristic temperature, the transition temperature. For a certain solute, the transition temperature is independent of the concentration, at least up to 25%. The transition temperatures range from -145°C up to -109°C for the solutions described in ref. 101. When the supercooled liquids are further heated, they crystallize at a higher temperature. Since crystallization requires first the formation of a nucleus from which it can start, the crystallization temperature depends upon the amount of impurities present and on the heating rate [101] [102].

Mössbauer experiments [104] - [108] on fast frozen solutions of especially salts of iron and tin indicate that at low temperatures the Mössbauer atom exists as a hydrated ion (e.g. $Fe(H_2O)_6^{+2}$) segregated in amorphous regions, which may be surrounded by crystalline ice depending upon the concentration of the solution. When the frozen solution is heated to around

-85°C, the Mössbauer effect disappears completely for some hours and then returns (in most cases with the characteristic spectrum parameters changed). This is associated with the glass transition and subsequent crystallization. When the solution is in the supercooled liquid state, no Mössbauer effect is observed. Also NMR and PAC [109] measurements have shown "a lively motion of water molecules" in frozen aqueous solutions in this temperature region. The relatively high temperature for the glass transition compared with those found by Vuillard [101] shows that it depends strongly on the solute. In addition, the concentration influences the details of the transition [105]. Also EPR spectra [110] for low temperature fast frozen aqueous solutions of Mn- and Gd-salts indicate that hydrated metal ions are segregated into amorphous regions.

5.4.2. Frozen Aqueous Solutions of HF

In the light of the above discussion the following explanation is suggested for the results of the measurements on the frozen HF solutions.

By fast freezing, a glassy region of H_2O molecules is formed around each impurity, the detailed structure of which is not known (could be F^-, HF, HF_2^- or more complex. This is further discussed below). In the amorphous region exist "holes" of empty space, both smaller and larger than those between the molecules of the surrounding crystalline lattice. The delocalized Ps will stand a certain chance of being trapped in one of the larger holes, and thus, owing to more space, it will obtain a longer lifetime against pick-off. When the amorphous regions are heated above approx. -130°C, a glass transition takes place and when the heating is very slow (as was the case for the measurements reported in fig. 22) the supercooled liquid will crystallize at a temperature a few degrees higher. On account of the presence of the impurities, the lattice is distorted and will still cause trapping of Ps, although with smaller probability than do the amorphous regions.

A problem exists in the above-mentioned model, viz. that for the higher HF concentrations apparently only one longlived positron lifetime component exists. If Ps had a possibility of being trapped in holes of different sizes in the amorphous regions, this would result in the appearance of a number of longlived components in the positron lifetime spectrum, each with a lifetime characteristic of a certain hole size. One possibility is that the sizes of the holes which are potential trapping centres do not differ very much, so that the resulting lifetime differences are too small to be resolved experimentally. Localization of Ps within a diameter of e.g. 5 A increases

its zero point energy by around 0.6 eV (appendix VII). So, if Ps becomes trapped in a hole of that diameter, the Ps "potential" energy (mainly repulsion due to exchange forces between electrons) must be at least 0.6 eV lower in the trap than in the bulk. Since both zero point and "potential" energy increase with decrasing hole size, such energy conditions set lower limits to the sizes of the holes in which Ps can be trapped. If these sizes are close to the maximum size of the created holes, only little spread in the pick-off lifetimes of the trapped Ps will result.

Another mechanism that could ensure a single long life time would be a high escape probability for the Ps from the trap (see appendix IV). For high trapping rates an atom would in its lifetime sample all possible trap sizes which would result in one single mean lifetime for all o-Ps. Since the trapping energies, however, are probably of the order of several tenths of an eV and thermal energy is around a hundredth of an eV, the probability for thermally assisted escape is low. One more possible explanation for the single long lifetime would be that Ps is not trapped in a single hole in an amorphous region, but by the region as a whole. It will then sample all different hole sizes at one time, and hence have one single mean lifetime. The width of the narrow component in angular correlation curves for frozen HF solutions [98] indicates that this may be the case.

The maximum solubility of HF in ice monocrystal is reported to be $4 \cdot 10^{-6}$ mole fraction [59] when incorporated during crystal growing (10^{-3} mole fraction in polycrystalline ice grown from solution), and $4 \cdot 10^{-5}$ when introduced into an ice monocrystal by diffusion [99) 100]. These concentrations are close to those at which the biggest change of the positron lifetime spectrum takes place (fig. 21). However, this is probably fortuitous, since for instance the solubility in ice of HCl is around $1.4 \cdot 10^{-7}$ mole fraction [103], while the largest changes in the lifetime spectrum take place around 10^{-4} mole fraction (table 4).

5.4.3. Comparison between Various Frozen Aqueous Solutions

Among the investigated frozen aqueous solutions, that of HF has the strongest effect on the positron lifetime spectrum (tables 3 and 4, section 4.3.). The effects of the other hydrogen halides are also considerable, but they decrease with increasing size of the cation. The solutions of LiF and CsF were measured to find out whether simply the presence of the F^- ion in the solution before freezing would cause the observed effect. That was not the case and furthermore, the size of the metal ion in the fluoride salt was relatively unimportant for the amount of Ps trapping. As one might ex-

pect, neither an excess number of protons in the aqueous solution could themselves be responsible for the change (H_2SO_4 and the other acids). As already mentioned HF together with NH_3 and NH_4F are considered the species which have the highest solubility in ice [45], but as shown in the tables, the high solubility has nothing directly to do with the large effect of HF.

The general picture of the effect of different solutes is further complicated by the fact that in angular correlation measurements [98] the largest effect is found for HCl and the smallest for HF. The measurements furthermore showed that the halides, and among them the acids, broadened the narrow component much more effectively than did the other impurities.

Having the discussion in section 5.4.1. in mind, the reason for the difference between the effects of HF and the other fluorides might be the following: During freezing, metal ions (and NH_4^+) will segregate as hydrated ions in relatively few and large amorphous regions where also F^- ions are likely to be incorporated to preserve charge neutrality. Since the proton will not be segregated during freezing, the tendency of hydrogen fluoride to cluster is much smaller and hence the number of atoms in each cluster will be smaller resulting in a larger number of clusters in the ice. As the trapping probability per impurity atom must be smaller the more atoms each cluster contains, the effect will be that frozen aqueous solutions of acids will trap Ps more efficiently than do frozen solutions of salts of the acid in the same concentration. The smaller effect of the other hydrogen halides compared with HF should then be caused by their larger anions whose segregation tendency is larger. This suggestion can be tested by investigating the influence of freezing rate on trapping of Ps. If the suggestion is correct, the trapping probability must increase with increasing freezing rate since a larger rate must reduce the cluster size. The differences between the effects of HF and HCl in lifetime and angular correlation experiments might be caused by differences in freezing rates.

If the different solutes produce essentially different amorphous structures, a simple explanation of their different trapping capabilities would be that HF for some reason produces a more open structure which will trap Ps with larger probability. At least it is a fact that an amorphous ice structure does not necessarily cause a longer Ps lifetime than crystalline ice [111].

As appears from the preceding discussion, relatively little knowledge has been gained about the structure and the effect on positrons and Ps of

impurities in ice. More extensive investigations in the field of doped monocrystals and frozen aqueous solutions are necessary to arrive at a detailed understanding of these phenomena.

5.5. Conclusion

The present work has centred on an experimental investigation of positron lifetimes in the solid and liquid forms of light and heavy water, and in frozen aqueous solutions. The temperature region which was investigated ranged from -190°C to +20°C. All spectra were resolved in three lifetime components. The following major results were obtained.

It was established that an abrupt change in o-Ps yield and lifetime takes place at the solid-liquid phase transition for both light and heavy water. In the liquid the lifetime is longer and the yield smaller in heavy (2.01 ± 0.06 nsec, $22.2 \pm 1.2\%$) than in light water (1.86 ± 0.04 nsec, $26.9 \pm 1.0\%$) while in ice no difference was found. Also mono- and polycrystalline samples gave identical results. In the temperature range from -190°C to -100°C essentially no change of the lifetime spectrum takes place as a function of temperature, which is in agreement with a "free volume model". From -100°C to the melting point the longest lifetime increased from 0.68 ± 0.02 nsec to 1.12 ± 0.02 nsec, its intensity in both intervals being 52%. The increase in lifetime was ascribed to trapping of o-Ps in temperature-created defects although no direct correlation with already known defects could be established. The large Ps yield of $70 \pm 3\%$ found in ice is probably the biggest one observed in any substance.

In frozen aqueous solutions of HF, trapping of Ps was found to occur even for concentrations less than parts per million. The trapping was in very good agreement with theory, thus serving as a first clear demonstration of Ps trapping in defects. At -160°C the o-Ps lifetime in the traps was 1.23 nsec. The very high reaction constant associated with the trapping process in fast frozen solutions (around hundred times larger than the biggest known from aqueous solutions) was ascribed to the delocalization of Ps in ice. An irreversible transition was observed around -125°C by heating a fast frozen HF solution of a concentration of one part per million. It was ascribed to a phase transition from an amorphous to a crystalline state of a region around each impurity. Several other frozen aqueous solutions were investigated, but none of them showed as strong an influence on the lifetime spectrum as did HF.

The present work and corresponding measurements by the angular cor-

relation technique probably make ice the substance which has been investigated in most detail by positron annihilation. The results obtained for ice may therefore (although ice in some respects is a rather special substance) serve as a starting point in the interpretation of measurements on other materials. To serve this aim better, however, more measurements on ice would be desirable. They might comprise an extension of the temperature interval down to liquid helium temperature, lifetime magnetic quenching measurements, and angular correlation magnetic quenching experiments on monocrystals. Also a detailed determination of the temperature dependence of the 3 γ-annihilation rate, the effect of irradiation and of doping of monocrystals with for example HF would be desirable.

6. ACKNOWLEDGEMENTS

The work presented in this report was carried out in partial fulfilment of the requirements for obtaining the licentiate degree (Ph.D.). The work was carried out at the Laboratory of Applied Physics II, Technical University of Denmark, from February to December 1969, and at the Chemistry Department, Danish Atomic Energy Commission Research Establishment Risø, from January 1970 to November 1971, under the supervision of professor, dr. philos. Georg Trumpy.

I would like to thank professor Trumpy for his continuous interest and support, and for a number of discussions from which I have benefitted during the progress of the work. I very much appreciate the help Kurt Petersen gave me in teaching me a lot during the year I worked with him. Also I want to thank for the assistance from a number of colleagues at the Laboratory of Applied Physics II and at the workshop.

During my work at Risø I have greatly profited from an inspiring collaboration with O.E. Mogensen. His large knowledge of physics, his enthusiasm, and his constructive criticism have been of great importance to me, and I am very grateful to him for numerous discussions regarding the present work. P. Kirkegaard has developed the very efficient computer program which was used for data analysis. I am much indepted to him for this invaluable help. Also I want to thank E. Mose Christiansen and A. Sloth for their assistance in building up and testing the electronic equipment, and P. Gosler for language correction of the manuscript. The kind and efficient assistance of many people from the Chemistry Department and from the departments of Reactor Physics, Electronics, Service, Construction, and from the Library and Workshop is greatly acknowledged.

I am grateful to G. Kvajić for supplying the ice single crystals.

APPENDIX I

DETERMINATION OF SOURCE STRENGTH

As mentioned in section 2.1.3. an increase in source strength will increase the random background relative to the lifetime spectrum, thus mixing to a larger extent these two components of the measured spectrum. On the other hand, with a stronger source the number of counts will increase resulting in a reduction of the statistical uncertainty of the measured spectrum. So the question may arise whether a strong or weak source should be used in order to get the smallest uncertainties in the parameters (intensities, lifetimes) extracted from the lifetime spectrum (i. e. the measured spectrum after subtraction of the background). These uncertainties naturally decrease when the relative uncertainty of the number of counts in each channel of the lifetime spectrum decreases. So, using the following symbols (deadtime of the electronics has been disregarded since its effect is small in this respect), we find the relative uncertainty of a count number.

Period of measurement: T

Time pr. channel: τ

Source strength: N_o

Efficiency of detector 1 (2): $\varepsilon_1 (\varepsilon_2)$

Mean value of number of counts in channel

No. i due to the lifetime spectrum: $N_o \varepsilon_1 \varepsilon_2 T f_i$ $(\sum_i f_i = 1)$

Random background in each channel: $\tau \varepsilon_1 \varepsilon_2 N_o^2$

Relative uncertainty in number of counts in

channel No. i after subtraction of the background: Δ_i.

It is a well-known fact that in ordinary counting statistics, the number of counts are distributed around a mean value with the standard deviation equal to the square root of the mean value. So Δ_i equals the square root of the total number of counts in channel No. i divided by the number after subtraction of the background:

$$\Delta_i = \frac{\sqrt{N_o \varepsilon_1 \varepsilon_2 T f_i + N_o^2 \varepsilon_1 \varepsilon_2 T \tau}}{N_o \varepsilon_1 \varepsilon_2 T f_i} = \frac{1}{\sqrt{\varepsilon_1 \varepsilon_2 T}} \frac{\sqrt{1 + \frac{\tau N_o}{f_i}}}{\sqrt{N_o f_i}}$$

By differentiation it can readily be seen that Δ_i will decrease with increasing N_o. However, from the above expression it follows that for large source strength, Δ_i will become constant. In a channel where, for a certain N_o, $f_i = \tau N_o$ (the lifetime spectrum and the background are equal in magnitude), a quadruple increase in source strength will decrease Δ_i by 20% only. Those parts of a lifetime spectrum that determine the longest living component normally have f_i's of the order of magnitude of $10^{-4} - 10^{-3}$. If τ is taken as $7 \cdot 10^{-11}$ sec, one finds a source strength of 50 to 500 μ Curie from the relation $N_o = f_i/\tau$. Any increase of the source strength above this order of magnitude will not decrease the uncertainties in the values found for the long lifetime and its intensity. And since the parameters determined for the shorter living components are dependent on those found for the longer ones, no great decrease in uncertainty can be gained for them either. Furthermore high counting rates in the electronic equipment always tend to produce different pile-up phenomena that will deteriorate the spectra obtained [30].

Accordingly sources of around 50 μ Ci were chosen for the measurements. Once this choice is made, the only methods of reducing counting statistics uncertainties are to increase the measuring time or the efficiency of the detectors (by for instance reducing the source detector distance or widen the windows of the SCA's).

APPENDIX II

MATHEMATICAL MODEL FOR A MEASURED SPECTRUM

The ideal lifetime spectrum of a number of positrons annihilating at the rate λ_j ($=\tau_j^{-1}$, τ_j is the mean lifetime) is described by a decaying exponential function:

$$I_j(t) = I_{oj}\exp(-\lambda_j t) \quad t \geq 0$$

$$I_j(t) = 0, \quad t < 0$$

where t is the channel number (equivalent to time). I_{oj} is a constant.

If the measuring system has a time resolution function which is a Gaussian with the standard deviation $\frac{\sigma}{\sqrt{2}}$ and centred around channel No. T_o:

$$P(t) = \frac{1}{\sigma\sqrt{\pi}} \exp\left[-(t-T_o)^2/\sigma^2\right]$$

the ideal spectrum will be smeared as determined by the folding of I_j with P:

$$F_j(t) = \frac{I_{oj}}{\sigma\sqrt{\pi}} \int_o^\infty \exp(-(t-T_o-t')^2/\sigma^2) \cdot \exp(-\lambda_j t')\, dt'$$

Evaluating the integral, we have:

$$F_j(t) = \frac{1}{2} I_{oj}\left[\exp(-\lambda_j(t-T_o-(1/4)\lambda_j\sigma^2))\right]\left[1-\mathrm{erf}\left(\tfrac{1}{2}\lambda_j\sigma - \frac{t-T_o}{\sigma}\right)\right], \qquad (\text{II } 1)$$

where erf(x) stands for the error function

$$\mathrm{erf}(x) = 2\pi^{-1/2} \int_o^x e^{-t^2}\, dt$$

σ is related to the Full Width at Half Maximum of the prompt curve by:

$$\mathrm{FWHM} = 2\sqrt{\ln 2}\cdot\sigma$$

In order to find the number in channel No. i, F(t) should, since the numbers recorded in the measured spectrum are averages over the width of one channel, be integrated over this width. The result is:

$$F_{j,i} = \frac{I_{oj}}{2\lambda_j} \left[Y_{j,i} - Y_{j,i+1} - \operatorname{erf}\left(\frac{t_i - T_o}{\sigma}\right) + \operatorname{erf}\left(\frac{t_{i+1} - T_o}{\sigma}\right) \right], \qquad \text{(II 2)}$$

$$\text{with } Y_{j,i} = \exp\left[-\lambda_j (t_i - T_o) + (1/4)\,\lambda_j^2 \sigma^2\right] \cdot \left[1 - \operatorname{erf}\left(\tfrac{1}{2}\lambda_j \sigma - \frac{t_i - T_o}{\sigma}\right)\right]$$

where t_i is the value of the variable t at the common limit of channels No. i-1 and i.

So the mathematical expression taken to describe a measured spectrum with p lifetimes and the background B is:

$$N_i = B + \sum_{j=1}^{p} F_{j,i} . \qquad \text{(II 3)}$$

The source correction can be made by subtracting from the measured spectrum a source correction spectrum given by:

$$N_i^s = C \sum_{l=1}^{m} F_{l,i} \qquad \text{(II 4)}$$

This has m terms of type (II 2) with I_{oj} and λ_j replaced by I_{ol}^s and λ_l^s, the parameters for the spectrum of the source material. The normalization constant C can be written:

$$C = \alpha \left[\sum_{j=1}^{p} \frac{I_{oj}}{\lambda_j} \right] \left[\sum_{l=1}^{m} \frac{I_{ol}^s}{\lambda_l^s} \right]^{-1}$$

Source annihilation is the fraction termed α of the total number of annihilations.

APPENDIX III

INPUT AND OUTPUT DATA, AND EXAMPLES OF APPLICATION OF POSITRONFIT

Apart from the spectrum to be analysed the input data required by the program POSITRONFIT are:

a) A figure to indicate whether the results of each iteration should be printed out and whether a table of the fitted and experimental points together with a graphical representation of these points should be printed out.

b) The FWHM of the prompt curve in nsec.

c) The time equivalent to one MCA channel in nsec.

d) A guess of T_o, the channel number corresponding to zero time.

e) The number of exponential terms to be used in the fit and the number of fixed lifetimes and relative intensities.

f) Guesses of the lifetimes to be determined (in nsec) together with the values of the fixed lifetimes (in nsec) and relative intensities (in per cent).

g) Finally the number of exponential terms (up to 4) in the source correction spectrum and their lifetimes (in nsec) and relative intensities (in per cent) together with the fraction (in per cent) the area of the correction spectrum shall amount to of the area of the lifetime spectrum.

The output data are:

a) As determined by the input the results of each iteration and tables and graphs of the measured and the fitted points may be printed out.

b) The analysed spectrum and the guessed and fixed values of the lifetimes and T_o.

c) Identification number of the spectrum (in the version used, the number in the second channel of the spectrum, which can be determined manually by use of the multi-channel analyser).

d) The number of iterations used by the computer to make the iterations converge (i.e. find the minimum value of Φ).

e) The FWHM of the prompt curve, the time pr channel, and the parameters determining the source correction as fixed by the input data.

f) The variance of the fit.

g) The fitted and fixed parameters (lifetimes, relative intensities, background and T_o), all with standard deviations.

h) The areas of the fitted curve (calculated as the sum of the absolute intensities) and the measured one (calculated by summing the numbers in all channels), the extent of agreement between which, together with the variance show the goodness of the fit.

i) The variance, the parameters and the areas for the fit before source correction are also printed out for comparison.

j) Finally a matrix showing the total correlations between the fitted parameters is printed out.

In fig. III 1 is shown the most important part of a typical output with one intensity constraint.

A spectrum of a saturated aqueous solution of $KMnO_4$ provides a good example of some of the capabilities of the POSITRONFIT program. Since $KMnO_4$ is a strong oxidiser all Ps is oxidised to free positrons. The spectrum of the solution therefore contains one single lifetime only. However, as the fraction α of the positrons annihilates in the source material (Melinex), which exhibits a longlived component, the spectrum actually measured will also comprise a long lifetime with an intensity of a few per cent. The results of the fitting of such a spectrum are shown in fig. III 2. The analysis has been carried out for different values of FWHM close to the one found from the prompt curve (0.427 nsec). Firstly, it is seen that the variance has a minimum very close to the FWHM determined from the prompt curve. Secondly, the long lifetime at the minimum is very close the one determined directly for Melinex at room temperature (1.54 nsec, see fig. 9). These two facts strongly support the assumptions on which the analysis is based (section 3.1.). Since the intensity I_2 of the Melinex spectrum is 23% and the one found here $2.4 \pm 0.4\%$, the fraction of positron annihilating in the source must be

$$\alpha = \frac{2 \cdot 4}{23} \cdot 100 = 10.4 \pm 1.7\%$$

```
CONVERGENCE OBTAINED AFTER  8 + 5 ITERATIONS

          PARAMETERS FOR SPECTRUM NO    1254
          ************************************
          MONOCRYSTALLINE ICE -182 DEGREES C
          ************************************

     TIME SCALE = 0.070 NSEC/CHANNEL    FWHM = 0.425 NSEC

     NUMBER OF TERMS = 3     NUMBER OF LIFETIME CONSTRAINTS = 0

     NUMBER OF CONSTRAINTS FOR RELATIVE INTENSITIES = 1
     TERM INDICES FOR INTENSITY CONSTRAINTS       3
     FIXED RELATIVE INTENSITIES                52.00

     SOURCE CORRECTION   7.0 PCT
     SOURCE LIFETIMES IN NSEC      0.342   1.150
     SOURCE INTENSITIES IN PCT     90.00   11.00

     VARIANCE OF THE FIT =    0.987
     ITS DISTRIBUTION SHOULD BE APPROXIMATELY NORMAL (1.0.072)
     EXCESS PROBABILITY =  57.27 PCT


     LIFETIMES IN NSEC             0.124   0.440   0.657
     STANDARD DEVIATIONS           0.015   0.026   0.007

     RELATIVE INTENSITIES IN PCT  20.36   27.64   52.00
     STANDARD DEVIATIONS           1.80    1.80    0.00

     BACKGROUND                   70.36
     STANDARD DEVIATION            0.47


     TIME-ZERO    CHANNEL NUMBER  127.628
     STANDARD DEVIATION            0.037


     AREA CHECK     AREA FROM FIT   = 0.34152E 06
                    AREA FROM TABLE = 0.34188E 06


MATRIX OF TOTAL CORRELATIONS
(RELATIVE INTENSITIES,BACKGROUND,FREE LIFETIMES,TO)

 1.000 -1.000 -0.000  0.110  0.871  0.952 -0.746 -0.530
-1.000  1.000 -0.000 -0.110 -0.871 -0.952  0.746  0.530
 0.000 -0.000  0.000  0.000 -0.000 -0.000  0.000  0.000
 0.110 -0.110  0.000  1.000  0.075  0.141 -0.206 -0.034
 0.871 -0.871 -0.000  0.075  1.000  0.825 -0.554 -0.851
 0.952 -0.952 -0.000  0.141  0.825  1.000 -0.874 -0.546
-0.746  0.746  0.000 -0.206 -0.554 -0.874  1.000  0.298
-0.530  0.530  0.000 -0.034 -0.851 -0.546  0.298  1.000

EXECUTION TIME =     76.62 SEC.
```

Fig. III 1. The most important part of a typical output from a fitting with three terms and one intensity constraint.

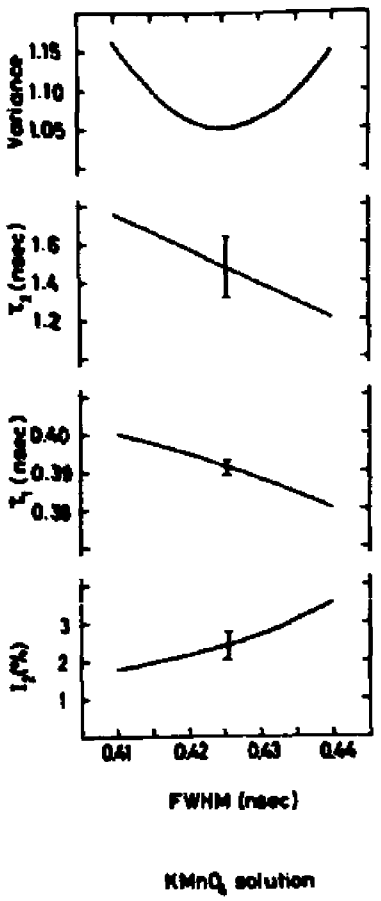

Fig. III 2. Variations of parameters estimated by a two-term analysis of a spectrum of a saturated aqueous solution of $KMnO_4$. The variations are shown as functions of the full width at half maximum (FWHM) of the Gaussian resolution curve used in the analysis. The experimentally determined value of FWHM was 0.427 nsec.

Thirdly, the short lifetime is very well determined and varies only slightly with the width of the prompt curve used in the analysis. (It should be mentioned that the same value was found for the short lifetime in a saturated solution of $KMnO_4$ in heavy water and of $K_2Cr_2O_7$ in light water). When correction for the 10% source annihilation is made and the two exponential terms are fitted, the results obtained are

$$\tau_1 = 0.395 \pm 0.002 \text{ nsec} \qquad \tau_2 = 1.8 \pm 23.2 \text{ nsec}$$

$$I_1 = 100.02 \pm 0.3\% \qquad I_2 = -0.02 \pm 0.3\%$$

These results clearly show that the corrected spectrum contains only one lifetime.

In fig. III 3 the variations of parameters with the FWHM used in the analysis are shown for more complex spectra. The uncertainties in the parameters caused by a typical uncertainty of the prompt curve width ($\pm$ 5.10^{-3} nsec) are comparable to or - in most cases - appreciably smaller than the standard deviations estimated by the computer. Since the spectra analysed may consist of more than three lifetime components, but only three have been resolved, the variances need not necessarily have a minimum at the FWHM value determined from the prompt curve.

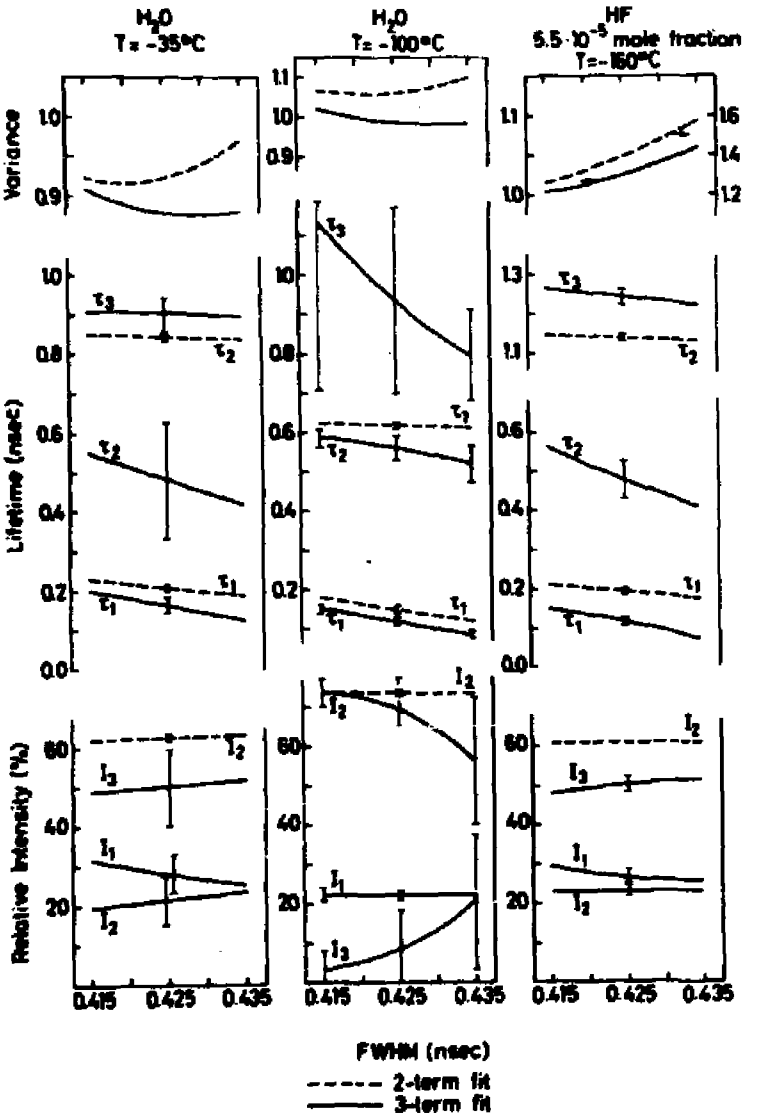

Fig. III 3. Variations of estimated parameters for two- and three-term fits of different spectra as function of FWHM of the Gaussian resolution curve used in the analysis.

APPENDIX IV

TRAPPING MODEL

The following symbols are used:

Time	:	T
Number of (or probability of finding) Ps atoms (or positrons) in bulk	:	$P_b(T)$
and in trap	:	$P_t(T)$
Annihilation rate in bulk	:	λ_b
Annihilation rate in trap	:	λ_t
Concentration of traps	:	C_t
Trapping rate	:	$\varkappa (\propto C_t)$
Escape rate from trap	:	δ

The following equations are assumed to govern the numbers P_b and P_t:

$$\frac{dP_b}{dT} = -\lambda_b P_b - \varkappa P_b + \delta P_t$$

$$\frac{dP_t}{dT} = -\lambda_t P_t + \varkappa P_b - \delta P_t$$

On the condition that all the Ps is in the bulk at the time zero (i.e. $P_b(0) = 1$, $P_t(0) = 0$), the solutions to the equations are

$$P_b(T) = \frac{\lambda_b + \varkappa - \Lambda_2}{\Lambda_1 - \Lambda_2} \exp(-\Lambda_1 T) + \frac{\Lambda_1 - \lambda_b - \varkappa}{\Lambda_1 - \Lambda_2} \exp(-\Lambda_2 T)$$

$$P_t(T) = \frac{-\varkappa}{\Lambda_1 - \Lambda_2} \exp(-\Lambda_1 T) + \frac{\varkappa}{\Lambda_1 - \Lambda_2} \exp(-\Lambda_2 T)$$

Λ_1 and Λ_2 are determined as the two roots of the equation:

$$(\Lambda - \lambda_b - \varkappa)(\Lambda - \lambda_t - \delta) - \delta\varkappa = 0 .$$

For small values of δ, the roots are:

$$\Lambda_1 \simeq \lambda_b + \varkappa - \frac{\varkappa\delta}{\lambda_t + \delta - \lambda_b - \varkappa}$$

and

$$\Lambda_2 \simeq \lambda_t + \delta + \frac{\kappa\delta}{\lambda_t + \delta - \lambda_b - \kappa}$$

The curve measured in a lifetime experiment will be:

$$-\frac{d}{dT}(P_b + P_t) = \Lambda_1 \frac{\lambda_b - \Lambda_2}{\Lambda_1 - \Lambda_2} \exp(-\Lambda_1 T) + \Lambda_2 \frac{\Lambda_1 - \lambda_b}{\Lambda_1 - \Lambda_2} \exp(-\Lambda_2 T)$$

$$= f_1 + f_2$$

Hence the lifetimes and intensities determined from the lifetime curve are:

$$\tau_1 = \frac{1}{\Lambda_1} \; ; \; I_1 = \int_0^\infty f_1 \, dT = \frac{\lambda_b - \Lambda_2}{\Lambda_1 - \Lambda_2}$$

$$\tau_2 = \frac{1}{\Lambda_2} \; ; \; I_2 = \int_0^\infty f_2 \, dT = \frac{\Lambda_1 - \lambda_b}{\Lambda_1 - \Lambda_2} \; .$$

If trapped Ps cannot escape ($\delta = 0$), simple expressions are found:

$$\tau_1 = (\lambda_b + \kappa)^{-1} \; ; \; I_1 = 1/(1 + \frac{\kappa}{\lambda_b - \lambda_t})$$

(IV 1)

$$\tau_2 = \lambda_t^{-1} \; ; \; I_2 = (\frac{\kappa}{\lambda_b - \lambda_t}) / (1 + \frac{\kappa}{\lambda_b - \lambda_t})$$

Thus, one lifetime which is independent of trapping rate is the Ps lifetime in the trap; the other lifetime which decreases with increasing trapping rate refers to the bulk.

Positrons annihilating in a trap will often have an angular correlation curve, which is more narrow than the one for positrons annihilating in the bulk. The intensity of the narrow component will be:

$$N = \int_0^\infty \lambda_t P_t dT = \frac{\kappa \lambda_t}{\Lambda_1 \Lambda_2}$$

For $\delta = 0$ we have:

$$N = \left(\frac{\varkappa}{\lambda_b}\right) / \left(1 + \frac{\varkappa}{\lambda_b}\right) \qquad \text{(IV 2)}$$

N follows the same curve as function of $\frac{\varkappa}{\lambda_b}$ as does I_2 as function of $\frac{\varkappa}{\lambda_b - \lambda_t}$. This curve is shown in section 4.2. fig. 21. It reaches half the maximum value for $\varkappa = \lambda_b - \lambda_t$ for a lifetime experiment, but for $\varkappa = \lambda_b$ in an angular correlation experiment.

The number of traps will be proportional to $\frac{I_2}{I_1} = \frac{I_2}{1-I_2}$ in a lifetime experiment, and to $\frac{N}{1-N}$ in an angular correlation experiment.

APPENDIX V

INFLUENCE OF ORTHO-PARA CONVERSION ON LIFETIME AND ANGULAR CORRELATION SPECTRA

The following symbols are used:

Time	t
Number of (or probability of Ps being) triplet Ps atoms	$P_T(t)$
and singlet Ps atoms	$P_S(t)$
Annihilation rate (pick-off) from triplet state	λ_T
and from singlet state	λ_S
Vacuum annihilation rate from singlet state	λ_S^o
Conversion rate	K

Following ref. 7, p. 28, the equations for annihilation with conversion are assumed to be:

$$\frac{dP_T}{dt} = 3KP_S - (K + \lambda_T) P_T$$

$$\frac{dP_S}{dt} = KP_T - (3K + \lambda_S) P_S$$

In ref. 7 these equations have been solved in the general case. If no strong conversion takes place, i.e. if $K \ll \lambda_S^o \approx \lambda_S - \lambda_T$, we can expand the solutions to first power in K/λ_S^o:

$$P_T(t) = -\frac{3}{4}(K/\lambda_S^o)\exp(-(\lambda_S + 3K)t) + \frac{3}{4}(1 + K/\lambda_S^o)\exp(-(\lambda_T + K)t)$$

$$P_\sigma(t) = \frac{1}{4}(1 - 3K/\lambda_S^o)\exp(-(\lambda_S + 3K)t) + \frac{1}{4}(3K/\lambda_S^o)\exp(-(\lambda_T + K)t)$$

A lifetime experiment will measure a spectrum given by:

$$N(t) = \lambda_T P_T(t) + \lambda_S P_S(t) \quad .$$

Hence, the intensity, I_1 , of the shortlived component (lifetime: $(\lambda_S + 3K)^{-1}$ and of the longlived one, I_2 , (lifetime: $(\lambda_T + K)^{-1}$) will be:

$$I_1 = \frac{1}{4} \left(1 - \frac{6K}{\lambda_S^o} \right) ; \; I_2 = \frac{3}{4} \left(1 + \frac{2K}{\lambda_S^o} \right) \quad .$$

Thus, the influence of conversion on the longlived component will be a decrease in lifetime, but an increase in intensity.

If self-annihilation from the singlet state gives a narrow angular correlation component, and pick-off from both singlet and triplet a broad component (3 γ annihilation from the triplet state is ignored) , we find for the intensity, I_N , of the first one:

$$I_N = \int_o^\infty \lambda_S^o \; P_S (t) \, dt$$

$$I_N = \frac{1}{4} \; \frac{\lambda_S^o}{\lambda_S} \; \left(1 + 3K \frac{\lambda_S^o}{\lambda_S (\lambda_T + K)} \right) ,$$

i.e. the intensity of the narrow component will increase with increasing conversion.

Hence we also have:

$$I_2/I_N = 3 \frac{\lambda_T + \lambda_S^o}{\lambda_S^o} \left[1 + K \left(\frac{2}{\lambda_S^o} - \frac{3 \lambda_S^o}{\lambda_S (\lambda_T + K)} \right) \right]$$

If $K \ll \lambda_T \ll \lambda_S^o$ this can further be approximated to :

$$I_2/I_N = 3 \frac{\lambda_T + \lambda_S^o}{\lambda_S^o} \left[1 - K \left(\frac{3}{\lambda_T} - \frac{5}{\lambda_S^o} \right) \right]$$

So, while both I_2 and I_N increase with increasing conversion, I_2/I_N will decrease. With $K = 0.01 \; \lambda_S^o$ and $\lambda_T = 0.2 \; \lambda_S^o$ (ice at low temperature) we find:

$$I_2/I_N = 3 \cdot 1.2 \cdot [0.9]$$

i.e. I_N is increased relative to I_2 by 10% due to conversion.

APPENDIX VI

ORE GAP MODEL FOR WATER AND ICE

As mentioned in section 1.2. the lower limit of the Ore gap in a gas is E_L = V-6.8 eV, where V is the ionisation energy of the gas. A positron with a kinetic energy less than E_L will not be able to provide sufficient energy to overcome the binding of an electron and hence will not be able to form Ps. In a condensed material the affinities of positron and Ps to the material have to be taken into account when E_L is determined. This can be done by considering the energies involved in the following imaginary process: A positron with kinetic energy E_+ and affinity Q_+ and an electron with ionisation energy V are taken out of the material, a Ps atom is formed by which 6.8 eV is gained, and the Ps atom with affinity Q_{Ps} is put back into the material. The kinetic energy of the Ps atom in the material will then be:

$$E_{Ps} = E_+ - Q_+ - V + 6.8\ eV + Q_{Ps} \ .$$

Since E_{Ps} must be positive or zero, E_L is determined as the value of E_+ for which $E_{Ps} = 0$:

$$E_L = V - 6.8\ eV + Q_+ - Q_{Ps}$$

The upper limit of the Ore gap must be the lowest excitation energy, E^*, as in the gas case.

The limiting energies of the Ore gap derived here are higher than those given by Ferrell [12] by the amount Q_+. This is because he refers the kinetic energy of the positron to the outside of the material, which does not seem to be an appropriate way of doing it.

In the following, estimates of the energies V, Q_+ and Q_{Ps} will be given for ice and water. For ice, V has been measured directly by ESCA [73] to 6.6 eV. The value for water is less well determined. The best determination seems to be made with flash photolysis by Boyle et al. [74] who find it close to 6.5 eV. Since a positron before it forms Ps is in a "free" state, Q_+ must be estimated on the basis of the average bulk properties of the substance and must not include affinities due to, for instance, trapping of a positron. Hence, the positron affinity originates from the polarisation of the medium by the positron. Therefore, Q_+ can be calculated as the loss of energy in

the electric field around the positron, when it is taken from vacuum into the medium. The energy, W, of the field, E, is [75]

$$W = \int_V \tfrac{1}{2} \epsilon E^2 dv$$

where ϵ is the dielectric constant, and the integration is over all space. Taking E to be spherical symmetric outside a sphere of radius r_1 and

$$E(r) = \frac{e}{4\pi \epsilon r^2}$$

(e is the positron charge, and r the distance from the centre of the sphere) and carrying out the integration for $r > r_1$ we have:

$$W_1 = \frac{1}{\epsilon_r \, r_1}$$

where ϵ_r is the relative dielectric constant, W_1 is in units of the Rydberg energy (13.6 eV), and r_1 is in Bohr radii (0.53 A). Hence, Q_+ will be:

$$Q_+ = \frac{1}{r_1} \left(1 - \frac{1}{\epsilon_r} \right),$$

if the field is assumed to be unchanged within r_1 when the positron is taken from vacuum into ice or water.

Since a positron has a large velocity even at thermal energies ($\sim 5 \cdot 10^6$ cm/sec or around 10^{14} intermolecular distances pr. sec for temperatures relevant here) the value to be used for ϵ_r should be somewhere between the high frequency and the optical value for the dielectric constant (for ice 3.2 and 1.72 respectively, for water a few per cent larger) in the case of the slowest positrons [45]. For positrons moving faster than around 10^{16} intermolecular distances pr. sec, ϵ_r should be put equal to 1.0 [45].

A typical intermolecular distance in ice and water is 3 A [46], but for the temperatures relevant here, thermal positrons will have de Broglie wave lengths of the order of 100 A.

So for a rough estimate of Q_+ we can take r_1 equal to 10. With $\epsilon_r = 2$ we find for both water and ice the order of magnitude: $Q_+ \sim 1/20$ Rydberg = 0.7 eV, the value being a few per cent larger for water than for ice.

To estimate Q_{Ps} the following assumption is made about the formation and behaviour of a Ps atom: It is formed in a localized state. By subsequent collisions with molecules it becomes more and more delocalized with time. In water it will be trapped relatively fast in a localized state, while in ice

it may stay delocalized until it annihilates or it may become trapped. In the delocalized state Ps will have a "potential" energy with respect to vacuum outside the substance. It is due to exchange repulsion between the Ps electron and the molecular electrons. Both in water [43] and ice [89] trapping of p-Ps gives a narrow component of a width 3.0 - 3.5 mrads. From the discussion in appendix VII this is equivalent to a localization within around 3.3 Angstrom and a zero point energy of about 1.5 eV. Since trapping does take place the potential energy mentioned above must be at least 1.5 eV.

In water the space available for Ps formation will be holes with a typical diameter of 3 A. A Ps atom which is localized by a harmonic potential and has a spherical spacial distribution with a typical diameter of 3 A will have a zero point energy of around 1.8 eV (appendix VII). In ice which is 9% less dense, there exist long "shafts" of open space due to the regular structure [46]. Therefore the space available for Ps formation is larger by more than ten per cent compared with water, and the zero point energy of Ps at the moment of formation will be smaller by more than the twenty per cent which arise from the density difference. Hence we can as a rough estimate take the Ps affinity to be -3.3 eV for water and -2.8 eV for ice. This leaves us with an estimate of E_L for water at 3.7 eV and for ice at 3.3 eV.

Since no appreciable absorption of photons with energies less than around 6 eV takes place in either water or ice [74, 76, 77], the lowest electronic exitation energy must be about this value. Hence we find an Ore gap of 2.7 eV for ice and 2.3 eV for water. According to the simple model, the amount of Ps should be equal to $(E^* - E_L) / E^*$. This expression gives a value (45%) rather far from the one actually found in ice (approx. 70%), but a value (38%) for water very close to the experimental one (36%). If the possibility exists that Ps can be formed in a delocalized state, Q_{Ps}, will be approximately -1.5 eV and E_L for ice 2.0 eV. This value gives a theoretical Ps yield of 67%, quite close to the experimental result. However, the agreements should not be taken too seriously considering the quite large uncertainties involved in the estimates of the different affinities. Furthermore, some of the simple assumptions used in the Ore gap model, e.g. that all positrons in the gap form Ps and that the positron energy spectrum is rectangular from zero to E, can not generally be expected to prove fully correct. As discussed in ref. 7 the possibility exists that a fraction of the positrons in the Ore gap will be slowed down below its lower limit without having formed Ps. The amount will be determined by the competition between slowing down and Ps formation processes. Hence the Ps yield will only to some unknown

approximation be given by the previously mentioned simple expression.

An estimate, made as above, of the width of the Ore gap for liquid D_2O will give the same result as for H_2O. An attempt has been made to correlate properties which differ for H_2O and D_2O [46] with the difference in Ps yield for the two substances. However, no convincing correlation has been found.

In conclusion, the discussion in this appendix shows that a number of factors are involved in a theoretical treatment of the Ps formation probability in a condensed material within the framework of the Ore gap model. The exact influence of several of these factors, which may even not be well defined, is difficult or impossible to estimate for a particular substance. Hence, any agreement between theory and experiment can only be expected to be a rough qualitative one in favorable cases.

APPENDIX VII

Ps TRAPPED IN A HARMONIC POTENTIAL

To illustrate the relation between the width of the narrow component in angular correlation experiments and the width of the Ps wave function, these quantities are calculated for a harmonic potential well for the Ps centre-of-mass:

$$V = - \tfrac{1}{2} M \omega^2 (x^2 + y^2 + z^2),$$

where M is the mass of Ps, ω the parameter (the classical frequency of the harmonic oscillator) that determines the width of the potential, and (x, y, z) the co-ordinates of the Ps centre-of-mass.

The Schrödinger equation separates into three independent, one-dimensional equations for the harmonic oscillator. Hence, only the solution for the z-co-ordinate is of interest. In the ground state, the energy is [112]:

$$E_o = (3/2) \hbar \omega ,$$

where $\hbar$ is Plancks constant divided by 2π . The ground state wave function is [112]:

$$\psi (z) = N_z \exp (- \frac{M \omega}{2\hbar} z^2),$$

where N_z is a normalization factor.

Hence, the probability distribution for the Ps atom along the z-direction is:

$$| \psi (z) |^2 = | N_z |^2 \exp (- \frac{M \omega}{\hbar} z^2) .$$

Its full width at half maximum is:

$$\Gamma_z = 2 (\hbar \ln 2 / M \omega)^{\frac{1}{2}} .$$

The Fourier transform of $\psi (z)$ determines the distribution of p_z , the z-component of the momentum. It is:

$$\Phi (p_z) = N' \int_{-\infty}^{\infty} \psi (z) \exp (- i \frac{p_z \cdot z}{\hbar}) dz = N_p \exp (- \frac{p_z^2}{2M\hbar\omega}),$$

where N_p is a normalization factor.

The probability distribution for p_z is then:

$$|\Phi(p_z)|^2 = |N_p|^2 \exp\left(-\frac{p_z^2}{M\hbar\omega}\right),$$

which has a full width at half maximum, Γ_p :

$$\Gamma_p = 2\,(M\hbar\omega\ \ln 2)^{\frac{1}{2}}.$$

In an angular correlation experiment this momentum is equivalent to an angle:

$$\Gamma_\theta = \Gamma_p / m_o c \qquad \text{(radians)}$$

where m_o is the electron rest mass and c the velocity of light.

We then have:

$$\Gamma_\theta \cdot \Gamma_z = (4h \cdot \ln 2)/(m_o c) = 10.7,$$

when Γ_θ is in mrad and Γ_z in Angstrom. E_o is related to Γ_z by:

$$E_o = (3/2)\,\hbar\omega = (3/2)\,h\,(4h \cdot \ln 2/M\Gamma_z^2).$$

With $M = 2m_o$ we find:

$$E_o = 16/\Gamma_z^2,$$

when E_o is in eV and Γ_z in Angstrom.

REFERENCES

1) N. R. Hanson, The Concept of the Positron. Cambridge University Press (1963) 236 pp.

2) W. Gordon, Der Comptoneffekt nach der Schrödingerschen Theorie. Z. Phys. 40, 117-133 (1926).

3) P. A. M. Dirac, On the Annihilation of Electrons and Protons. Proc. Camb. Phil. Soc. 26, 361-375 (1929-30).

4) P. A. M. Dirac, A Theory of Electrons and Protons. Proc. Roy. Soc. A 126, 360-365 (1930).

5) C. D. Anderson, The Apparent Existence of Easily Deflectable Positives. Science, New Series 76, 238-239 (1932).
C. D. Anderson, The Positive Electron, Phys. Rev. 43, 491-494 (1933).

6) P. M. S. Blackett and G. P. S. Occhialini, Some Photographs of the Tracks of Penetrating Radiation. Proc. Roy. Soc. A 139, 699-726 (1933).

7) V. I. Goldanskii, Physical Chemistry of the Positron and Positronium. Atomic Energy Review 6, 1-148 (1968).

8) A. T. Stewart and L. O. Roellig (editors), Positron Annihilation, Proceedings of the Conference Held at Wayne State University, 1965. Academic Press, New York - London, 1967. 438 pp.

9) J. D. McGervey, Positronium Reactions in Solutions. In ref. 8, p. 143-154.

10) A. I. Akhiezer and V. B. Berestetskii, Quantum Electrodynamics, Interscience Publ., New York, 1965, 868 pp.

11) A. Ore, Annihilation of Positrons in Gases. Univ. Bergen Årbok, Naturvitenskap. Rekke No. 9, 1949. Bergen 1950. 16 pp.

12) R. A. Ferrell, Theory of Positron Annihilation in Solids. Rev. of Mod. Phys. 28, 308-337 (1956).

13) J. Green and J. Lee, Positronium Chemistry, Academic Press, New York, 1964, 105 pp.

14) O. E. Morgensen, Electron Properties in Tin and Bismuth by Angular Correlation of Annihilation Photons. Thesis (1968). Laboratory

of Applied Physics II, Technical University of Denmark, Lyngby, Denmark. 139 pp.

15) P. R. Wallace, Positron Annihilation in Solids and Liquids, in Solid State Physics, Vol. 10, 1-69, Academic Press, New York, 1960.

16) A. R. Mackintosh, Positron Annihilation in Solids, AEC-Report IS-299, 1962. 34 pp.

17) K. Siegbahn, ed., Alpha-, Beta- and Gamma-Ray Spectroscopy, North Holland Publ. Company, Amsterdam 1965. 1742 pp. in 2 vols.

18) R. E. Bell and R. L. Graham, Time Distribution of Positron Annihilation in Liquids and Solids, Phys. Rev. 90, 644-654 (1953).

19) R. T. Wagner and F. L. Hereford, Temperature Effects in the Annihilation of Positrons, Phys. Rev. 99, 593-594 (1955).

20) R. L. de Zafra and W. T. Joyner, Temperature Effect on Positron Annihilation in Condensed Matter, Phys. Rev. 112, 19-29 (1958).

21) W. Brandt, S. Berko, and W. W. Walker, Positronium Decay in Molecular Substances, Phys. Rev. 120, 1289-1295 (1960).

22) G. Iaci, I. F. Quercia, and E. Turrisi, Positrons Annihilation in Water and Ice with an External Magnetic Field, Nuovo Cim. 24, 746-756 (1962).

23) R. K. Wilson, P. O. Johnson, and R. Stump, Variation in Positron Lifetime with Pressure, Phys. Rev. 129, 2091-2095 (1963).

24) G. Fabri, E. Germagnoli, I. F. Quercia, and E. Turrisi, Positronium Decay in the Ice-Water System, Nuovo Cim. 30, 21-27 (1963).

25) G. Fabri, G. Poletti, and G. Randone, Magnetic Quenching of Positronium Decay in Water, Phys. Rev. 135A, 80-82 (1964).

26) G. Iaci, M. LoSavio, and E. Turrisi, Hyperfine Energy Splitting of Positronium Measured in Water, Can. J. Phys. 46, 2033-2038 (1968).

27) P. Colombino, B. Fiscella, and L. Trossi, Study of Positronium in Water and Ice from 22 to -144°C by Annihilation Quanta Measurements, Nuovo Cim. 38, 707-723 (1965).

28) P. Jauho and M. Virnes, Temperature Dependence of Positron Lifetime in Water, Phys. Letters 26A, 208-209 (1968).

29) P. Colombino and B. Fiscella, Positronium Annihilation in Magnetic

Fields up to 21 kG, Nuovo Cim. 3B, 1-14 (1971).

30) A. Schwarzschild, A Survey of the Latest Developments in Delayed Coincidence Measurements, Nucl. Instr. and Meth. 21, 1-16 (1963).

31) E. Gatti and V. Svelto, Review of Theories and Experiments of Resolving Time with Scintillation Counters, Nucl. Instr. and Meth. 43, 248-268 (1966).

32) L.G. Hyman, Time Resolution of Photomultiplier Systems, Rev. Sci. Instr. 36, 193-196 (1965).

33) B. Bengtson and M. Moszynski, Timing Properties of Scintillation Counters. Nucl. Instr. and Meth. 81, 109-120 (1970).

34) M. Bertolaccini and L. Zappa, Source-Supporting Foil Effect on the Shape of Positron Time Annihilation Spectra, Nuovo Cim. 52 B, 487-494 (1967).

35) M. Eldrup og S. Mørup, Temperaturreguleringssystem. Intern rapport nr. 15, 1969. Laboratory of Applied Physics II, Technical University of Denmark.

36) K. Petersen, M. Eldrup and G. Trumpy, Temperature Dependence of the Positron Lifetime in H_2O and D_2O, Phys. Letters 31A, 109-110 (1970).

37) I. Berkes et al., Analysis of Nuclear Decay Data for Lifetimes of 10^{-9} sec order. Nucl. Instr. and Meth. 27, 355-356 (1964).

38) D.W. Marquardt, An Algorithm for Least-Squares Estimation of Nonlinear Parameters, J. Soc. Ind. Appl. Math. 11, No. 2, 431-441 (1963).

39) P. Kirkegaard and M. Eldrup, POSITRONFIT: A Versatile Program for Analysing Positron Lifetime Spectra. Submitted to Computer Phys. Commun. (1971).

40) P. Kirkegaard, Some Aspects of the General Least-Squares Problem for Data Fitting, Risø-M-1399 (1971) 16 pp.

41) P. Kirkegaard and M. Eldrup, The Least-Squares Fitting Program POSITRONFIT: Principles and Formulas. Risø-M-1400 (1971), 15 pp.

42) O. Mogensen, G. Kvajić, M. Eldrup, and M. Milosević-Kvajić, Angular Correlation of Annihilation Photons in Ice Single Crystals. Phys. Rev. B4, 71-73 (1971).

43) L. Smedskjær and G. Trumpy, Positronium in Ice and Water, Angular Correlation Studies with Magnetic Quenching. In ref. 81, p. 3.145-3.165.

44) W. Brandt and I. Spirn, Positron Lifetime Spectra in Molecular Substances. Phys. Rev. 142, 231-237 (1966).

45) N. H. Fletcher, The Chemical Physics of Ice. Cambridge Monographs on Physics. Cambridge University Press, London 1970. 271 pp.

46) D. Eisenberg and W. Kauzmann, The Structure and Properties of Water. Oxford University Press, London 1969. 296 pp.

47) N. Riehl, B. Bullemer, H. Engelhardt (editors), Physics of Ice. Proceedings of the International Symposium on Physics of Ice, Munich, Germany, 1968. Plenum Press, New York 1969. 642 pp.

48) W. Brandt, Positron Annihilation in Molecular Substances and Ionic Crystals. In ref. 8, p. 155-182.

49) W. Brandt, H.F. Waung, and P.W. Levy, Positron Annihilation Centers in NaCl, Phys. Rev. Letters 26, 496-499 (1971).

50) B. Bergersen and M.J. Stott, The Effect of Vacancy Formation on the Temperature Dependence of the Positron Lifetime. Solid State Comm. 7, 1203-1205 (1969).

51) J. Muguruma and A. Higashi, Observation of Etch Channels on the (0001) Plane of Ice Crystal Produced by Nonbasal Glide. J. Phys. Soc. Jap. 18, 1261-1269 (1963).

52) M. Sugisaki, H. Suga, and S. Seki, Calorimetric Study of Glass Transition of the Amorphous Ice and of the Phase Transformation between the Cubic and the Hexagonal Ices. In ref. 47, p. 329-343.

53) N. Bjerrum, Structure and Properties of Ice. Kgl. Danske Videnskab. Selskab, Mat.-Fys. Medd. 27, 1-56 (1951).

54) F.K. Truby, Hexagonal Microstructure of Ice Crystals Grown from the Melt. J. Appl. Phys. 26, 1416-1420 (1955).

55) W. Drost-Hansen, The Water-Ice Interface as Seen from the Liquid Side. J. Coll. and Interface Sci. 25, 131-160 (1967).

56) A. von Hippel, D.B. Knoll, and W.B. Westphal, Transfer of Protons through "Pure" Ice Ih Single Crystals. I. Polarization Spectra of Ice Ih. J. Chem. Phys. 54, 134-144 (1971).

57) A. von Hippel, Transfer of Protons through "Pure" Ice Ih Single Crystals. II. Molecular Models for Polarization and Conduction. J. Chem. Phys. 54, 145-149 (1971).

58) M.A. Maidique, A. von Hippel, and W.B. Westphal, Transfer of Protons through "Pure" Ice Ih Single Crystals. III. Extrinsic versus Intrinsic Polarization; Surface versus Volume Conduction. J. Chem. Phys. 54, 150-160 (1971).

59) J.H. Bilgram, Segregation of Hydrogen Fluoride in Ice Single Crystals. Phys. Kondens. Materie 10, 317-325 (1970).

60) A. Steinemann, Dielektrische Eigenschaften von Eiskristallen. II. Dielektrische Untersuchungen an Eiskristallen mit Eingelagerten Fremdatomen. Helv. Phys. Acta 30, 581-610 (1957).

61) J. Lee and G.J. Celitans, Oxygen and Nitric Oxide Quenching of Positronium in Liquids. J. Chem. Phys. 44, 2506-2511 (1966).

62) S.Y. Chuang and S.J. Tao, Temperature and Phase Dependence of Positron Lifetimes in CH_3OH and CD_3OD. Phys. Letters 33A, 56-57 (1970).

63) W.H. Holt, S.Y. Chuang, A.M. Cooper, and B.G. Hogg, Positron Annihilation in Condensed Ammonia. J. Chem. Phys. 49, 5147-5149 (1968).

64) G. Coussot, Contribution a l'etude de la structure electronique des isolants par annihilation du positon. Thesis (1970). Orsay, Serie A, No. d'ordre 722.

65) S. Tanigawa, S. Nanao, K. Kuribayashi, and M. Doyama, The Effect of Lattice Vacancies on Positron Annihilation in Copper-Nickel Single Crystals. Phys. Letters 35A, 159-160 (1971).

66) O. Dengel, U. Eckener, H. Plitz, and N. Riehl, Ferroelectric Behaviour of Ice. Phys. Letters 9, 291-292 (1964).

67) D. Helmreich, Elastic Anomalies of Ice at Low Temperatures. In ref. 47, p. 231-238.

68) M.A. Pick, The Specific Heat of Ice Ih. In ref. 47, p. 344-347.

69) S. Mascarenhas, Charge and Polarization Storage in Ice Crystals. In ref. 47, p. 483-491.

70) P.G. Bishop, and J.W. Glen, Electric Polarization Effects in Pure

and Doped Ice at Low Temperatures. Ref. 47, p. 492-501.

71) L. Onsager, Ferroelectricity of Ice? in E.F. Weller (editor), Ferroelectricity. Elsevier Publishing Co., Amsterdam (1967).

72) V.P. Shantarovich and V.I. Goldanskii, Positronium Interaction with Various Organic Molecules. Ref. 81, p. 5.1-5.37.

73) K. Siegbahn et al., ESCA Applied to Free Molecules. North-Holland Publishing Company, Amsterdam - London 1969. 200 pp.

74) J.W. Boyle, J.A. Ghormley, C.J. Hochanadel, and J.F. Riley, Production of Hydrated Electrons by Flash Photolysis of Liquid Water with Light in the First Continuum. J. Phys. Chem. 73 (9) 2886-2890 (1969).

75) J.A. Stratton, Electromagnetic Theory. McGraw-Hill Book Company, Inc., New York and London 1941. 615 pp.

76) R. Onaka and T. Takahashi, Vacuum UV Absorption Spectra of Liquid Water and Ice. J. Phys. Soc. Jap. 24 (3), 548-550 (1968).

77) L.R. Painter, R.D. Birkhoff, and E.T. Arakawa, Optical Measurements of Liquid Water in the Vacuum Ultraviolet. J. Chem. Phys. 51, 243-251 (1969).

78) H.S. Landes, S. Berko, and A.J. Zuchelli, Effect of Melting on Positron Lifetime. Phys. Rev. 103, 828-829 (1956).

79) B.G. Hogg, G.M. Laidlaw, V.I. Goldanskii, and V.P. Shantarovich, Table of Positron Annihilation Data. Atomic Energy Review 6, 149-212 (1968).

80) V.P. Shantarovich, O.E. Mogensen, and V.I. Goldanskii, Positronium Quenching in Liquid and Solid Octanol and Benzene. Phys. Letters 31A, 485-486 (1970).

81) A.T. Stewart, B.T.A. McKee, and C.H. Markham (Committeé). Positron Annihilation, Second International Conference. Queen's University, Kingston, Canada. Aug. 31 - Sept. 2, 1971. Collection of papers presented at the conference. Unpublished.

82) G. de Blonde, B.G. Hogg, D.P. Kerr, and D.M. Miller, Positronium Formation in Several Solid Hydrocarbons? In ref. 81, p. 3.97-3.98.

83) P.R. Gray, C.F. Cook, and G.P. Sturm, Correlation of Triplet Positronium Annihilation Parameters with Structural and Electronic

Properties of Organic Liquids. J. Chem. Phys. 48, 1145-1157 (1968).

84) K. P. Singh, R. M. Singru, and C. N. R. Rao, Positron Lifetime Studies in Organic Media. J. Phys. B, 4, 261-268 (1971).

85) A. Bisi, G. Gambarini, and L. Zappa, Effective Number of Singlet Annihilation Electrons for Positronium in Molecular Liquids. Nuovo Cim. 67B (1), 75-83 (1970).

86) J. Lee Kavanau, Water and Solute-Water Interactions. Holden-Day, Inc., San Francisco, London, Amsterdam. 1964. 101 pp.

87) W. W. Souder, Lifetimes of Deeply Embedded Positrons in Metals. Ph. D. Thesis, May 1969. Iowa State University, Ames, Iowa. IS-T-311, 146 pp.

88) W. Brandt and J. H. Fahs, Positronium Decay in Condensed Matter, Phys. Rev. B2, 1425-1427 (1970).
And Appendix: W. Brandt and J. H. Fahs, Positron Annihilation in Matter: Tables of Electron Pickoff Functions. National Auxiliary Publications Service. 1970. 74 pp.

89) O. Mogensen et al. To be published.

90) K. Eiben, Irradiation-Produced Solvated Electrons in Ice. In ref. 47, p. 184-194.

91) G. Nilsson, H. Christensen, P. Pagsberg, and S. O. Nielsen, Transient Electrons in Pulse-Irradiated Crystalline H_2O and D_2O. Submitted to J. Phys. Chem.

92) C. Kittel, Introduction to Solid State Physics. Second Edition. John Wiley & Sons, Inc., New York, London, 1956. 617 pp.

93) R. G. Seidensticker and R. L. Longini, Impurity Statistics in Ice. In ref. 47, p. 471-482.

94) J. D. Bell, R. W. Myatt, and R. E. Richards, Proton Magnetic Resonance Evidence of a Liquid Phase in Polycrystalline Ice. Nature Phys. Sci. 230, 91-92 (1971).

95) C. H. Hodges, B. T. A. McKee, W. Triftshäuser, and A. T. Stewart, Umklapp Annihilation of Positronium in Crystals. In ref. 81, p. 3.166-3.187.

96) A. Greenberger, A. P. Mills, and S. Berko, Positronium-Like

Block States in Quartz Crystals. In ref. 81, p. 3.140-3.143.

97) A. Bisi, G. Gambarini, and L. Zappa, Positronium State in Quartz Single Crystals. Phys. Letters 35A, 193-194 (1971).

98) M. Milosević-Kvajić, O. Mogensen, G. Kvajić, and M. Eldrup, Angular Correlation of Annihilation Photons in Frozen Aqueous Solutions. To be published in J. Chem. Phys. (1972).

99) M. Kopp, D.E. Barnaal, and I.J. Lowe, Measurement by NMR of the Diffusion Rate of HF in Ice. J. Chem. Phys. 43, 2965-2971 (1965).

100) H. Haltenorth and J. Klinger, Diffusion of Hydrogen Fluoride in Ice. In ref. 47, p. 579-584.

101) G. Vuillard, Contribution a l'étude de l'état vitreux et de la cristallisation des solutions aqueuses. Ann. de Chim. 13^{e} Serie, t. 2, 231-297 (1957).

102) R.W. Douglas, The Chemical Approach to Problems of the Glassy State. In V.D. Frechette (editor), Non-Crystalline Solids. John Wiley & Sons, Inc., New York, London (1960), 374-411.

103) J.G. Paren and J.C.F. Walker, Influence of Limited Solubility on the Electrical and Mechanical Properties of Ice. Nature Phys. Sci. 230, 77-79 (1971).

104) A.J. Nozik and M. Kaplan, Mössbauer Resonance Studies of Ferrous Ions in Ice. J. Chem. Phys. 47, 2960-2977 (1967).

105) J.V. Dilorenzo and M. Kaplan, Phase Transformations in Doped Ice: Concentration Effect in Frozen Ferrous Solutions. Chem. Phys. Letters 3, 216-218 (1969).

106) I. Pelah and S.L. Ruby, Conductivity and Mössbauer Measurements in Doped Ice. J. Chem. Phys. 51, 383-387 (1969).

107) J.A. Cameron, L. Keszthelyi, G. Nagy, and L. Kacsoh, Mössbauer Effect of Ferrous Ions in Cubic Ice. Chem. Phys. Letters 8, 628-630 (1971).

108) R.L. Cohen and K.W. West, Cooling Rate and Glass Formation in Frozen Solutions. Bull. Am. Phys. Soc. 16, 850 (1971).

109) J.A. Cameron, P.R. Gardner, L. Keszthelyi, and W.V. Prestwich, Dynamical Effects on ^{181}Ta Nuclei in Ice. Chem. Phys. Letters 4, 229-230 (1969).

110) R.T. Ross, Dipolar Broadening of EPR Spectra Due to Solute Segregation in Frozen Aqueous Solutions. J. Chem. Phys. 42, 3919-3922 (1965).

111) M. Eldrup, O. Mogensen, and L. Kevan, Positron Annihilation in γ-Irradiated 10 M NaOH Glassy Ice at 85°K. Chem. Phys. Letters 10, 379-380 (1971).

112) E. Merzbacher, Quantum Mechanics. John Wiley & Sons, Inc. New York, London (1961). 544 pp.